



Utrecht University

*Reactivity of 1,3-Dicarbonyl
Compounds with Urea under
Physiological Conditions*

Major Internship Research Report

Gino Prestifilippo
Msc. Drug Innovation
Student number 9675477

I. Acknowledgements

I would like to thank dr. Rene van Nostrum for the opportunity to do my major internship under his guidance as well as for providing a space where I could perform my syntheses within the scope of the thesis, and for taking the role of the first assessor.

I would like to thank prof. dr. ir. Wim Hennink for taking the role of the second assessor and for the valuable input during this project.

I would like to thank dr. Piet Driest for sharing his expertise and his guidance throughout the creation of this thesis. His input has been invaluable.

I would like to thank dr. Karin Gerritsen and Rob Smakman, as well as the other contributors to this project, for the valuable discussions and feedback.

I would like to thank Babette Lentferink for performing the urea reactivity measurements of the synthesized polymeric structures.

I generally would like to express my gratitude for the opportunity to learn from everyone involved, as well as for providing me with my first practical experience in polymer synthesis. The project has proven to be a truly valuable learning experience, and has shaped my aspirations for my future chemistry career.

Finally, I would like to thank my family for their support, as well as Diana Ungureanu for her support and encouragement while composing this thesis.

II. Assessors

First Assessor: Dr. C.F. van Nostrum

Second Assessor: Prof. dr. ir. W.E. Hennink

III. Table of Contents

I. Acknowledgements	i
II. Assessors	ii
III. Table of Contents	iii
IV. List of Abbreviations	v
V. Abstract.....	vi
1. Introduction	1
1.1. The function of the kidney and the consequences of kidney failure.....	1
1.2. Dialysis	2
1.3. Urea – Chemistry, biological significance and problems	4
1.4. Alternative methods for the removal of urea.....	6
1.4.1. Enzymatic removal using urease	6
1.4.2. Disposal of urea through electrochemical means	7
1.4.3. Non-covalent binding of urea	9
1.4.4. The covalent binding of urea.....	11
1.5. The properties and chemistry of malonaldehyde and triformylmethane.	14
1.5.1. Electrophilicity.....	14
1.5.2. Keto-enol tautomerism.....	15
1.5.3. Self-condensation reactions.....	16
1.5.4. Acidity	16
1.5.5. The reaction of 1,3-dialdehyde structures with urea	17
2. Aims of this study	20
2.1. Motivation	20
2.2. Objective	20
3. Results and Discussion.....	24
3.1. The urea reactivity of a non-enolizable, non-acidic malonaldehyde derivative.	24
3.1.1. Synthesis of 2,2-dimethyl-malonaldehyde (30).	24
3.1.2. Testing the urea reactivity of 2,2-dimethyl-malonaldehyde (30).....	24
3.1.3. Hypothesized reaction mechanism between 2,2-dimethyl-malonaldehyde (30) and urea at pH 7.....	27
3.2. The synthesis of an MDA-functionalised polymer.....	28
3.2.1. The synthesis of poly(vinylamine) (33).....	28
3.2.2. The analysis of poly(TEPA) (37).	30

3.3.	The synthesis of 1,3-dialdehyde precursors.	31
3.3.1.	Potential 1,3-dialdehyde precursors for polymer functionalization.	31
3.3.2.	Potential 1,3-dialdehyde precursors for polymer functionalization.	36
3.3.3.	The synthesis of an electrophilic 1,3-dialdehyde precursor: 2-bromo-tetramethoxypropane (2-Br-TMP) (39).	37
3.4.	Functionalising the chosen polymeric structures.	38
3.4.1.	The functionalisation of poly(glycidyl acrylate) (35) with serinol (69). ...	39
3.4.2.	The functionalization of poly(TEPA) (37) with 2-Br-TMP (39).	40
3.4.3.	The functionalization of poly(vinylamine) (33) with 2-Br-TMP (39).	41
3.5.	Measuring the urea-reactivity of chosen functionalized polymeric structures.	41
3.5.1.	Measuring urea reactivity of 41	42
3.5.2.	Measuring urea reactivity of 45	44
3.5.3.	Measuring urea reactivity of 71	45
3.5.4.	Additional considerations.	45
4.	Conclusions	46
5.	Outlook.....	47
6.	Experimental section.....	49
6.1.	Preface	49
6.1.1.	General information	49
6.1.2.	Solvents	49
6.1.3.	NMR.....	49
6.1.4.	IR	50
6.2.	Experiments	51
6.2.1.	Small-molecule syntheses.	51
6.2.2.	Polymer reactions.	63
6.2.3.	General procedure urea-reactivity measurement small molecules.	67
7.	References.....	68
8.	Table of Figures	77
9.	Table of Tables	81
10.	Appendix.....	82
10.1.	Spectra.....	82
10.2.	Urea reactivity measurements of synthesized polymers.	101

IV. List of Abbreviations

(2,2,6,6-Tetramethylpiperidin-1-yl)oxyl	TEMPO
1,1,3,3-tetramethoxypropane	TMP
2-Bromo-1,1,3,3-tetramethoxypropane	2-Br-TMP
4-Dimethylaminopyridine	DMAP
Activated carbon	AC
Attenuated total reflection infrared	ATR-IR
Azobisisobutyronitrile	AIBN
Chronic kidney disease	CKD
Dihydroxyacetone	DHA
End-stage kidney disease	ESKD
End-stage renal disease	ESRD
Glomerular filtration rate	GFR
Malonaldehyde	MDA
Malonaldehyde sodium salt	NaMDA
N,N'-Dicyclohexylcarbodiimide	DCC
N,N-Diisopropylethylamine	DIPEA
Phenylglyoxaldehyde	PGA
Phosphate buffered saline	PBS
Phosphate-buffered saline	PBS
Poly(N-vinylformamide)	PNVF
Poly(tetraethylenepentamine)	Poly(TEPA)
Poly(vinylamine)	PVAm
Potassium tert-butoxide	KOtBu
p-Toluenesulfonic acid	p-TsOH
Trichloroisocyanuric acid	TCCA
Triethylamine	TEA
Wearable artificial kidney	WAK

V. Abstract

In 2019, it is estimated that the number of people suffering from end-stage kidney disease lies between approximately five to seven million, all of whom are in need of renal replacement therapy. For those of whom a kidney transplant is not an option, a high weekly frequency of dialysis procedures in the hospital is required to replace the function of the kidney.

The development of a wearable kidney device would prove to be a significant improvement on the quality of life of end-stage kidney disease patients, as it would not only provide them with the option to receive treatment independent of the location, but it would allow a more frequent treatment, which would likely reduce the prevalence of uremic symptoms that ultimately contribute to the mortality of the patients. However, the development of such a device is currently hindered due to its inability to effectively remove the smallest uremic toxin – urea.

This thesis builds on the work of *Jong et al.*, which has shown that small-molecule 1,3-dialdehyde structures react rapidly and efficiently with urea, even in highly diluted environments, under acidic conditions. This project focuses on the exploration of the development of 1,3-dialdehyde structures that would react with urea under physiological conditions. Specifically, this is done by varying the substituent in the 2-position of the 1,3-dialdehyde structure to potentially modulate the inherent acidic character of said structures.

Amine-substituted 1,3-dialdehyde structures did not show any significant reactivity towards urea under physiological conditions, facilitating the need for further research in the field. Nevertheless, the novel polymeric structures that were synthesized within the scope of this project could potentially be investigated for other potential uses. Further, the results of this project suggest that the optimization of 1,2-dicarbonyl structures for generating a potent urea sorbent may prove to be more fruitful for the incorporation in a wearable artificial kidney device.

1. Introduction

1.1. The function of the kidney and the consequences of kidney failure

The kidneys function as the filters of the body, continuously removing waste products – more commonly referred to as uremic toxins – as well as excess fluid from the blood while maintaining the acid-base balance in the balance and regulating electrolytes and water.¹

Uremic toxins (“Uremia” coming from the Greek words *ouron* “urine” and *haima* “blood”) can be classified into three different categories. First, there are the small, water-soluble molecules with a molecular weight of less than 0.5 kDa. Some examples include the compounds urea, uric acid and creatinine.² Next, there are small proteins like cytokines and β -2-microglobulin³, and finally, there are protein-bound uremic toxins like p-cresyl sulfate and indoxyl sulfate.⁴ Several structures of the aforementioned molecules are presented in figure 1.

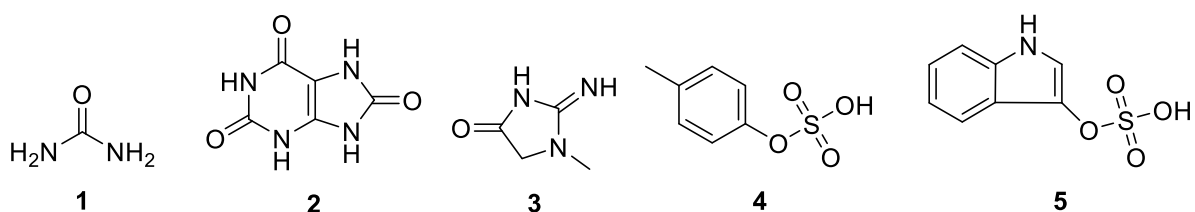


Figure 1. Structures of several uremic toxins. From left to right: Urea, uric acid, creatinine, p-cresyl sulfate, indoxyl sulfate.

There are, however, certain unfortunate scenarios in which the kidney function is severely impaired, while in others, kidney function may be compromised altogether. A wide variety of things can cause this, including diabetes⁵, genetic diseases such as polycystic kidney disease⁶, the use of illicit drugs such as heroin⁷, as well as heart attacks⁸ and urinary tract infections⁹.

The National Kidney Foundation has several criteria to assess whether kidney function is compromised. This includes whether the kidney has been damaged for three months or more, characterized either by pathological abnormalities or other markers of kidney damage such as the composition of blood or urine, or whether the glomerular filtration

rate (GFR) has been lower than 60 ml/min/1.73m². If either is the case, the patient is diagnosed with Chronic Kidney Disease (CKD).¹⁰

Once the GFR falls below a rate of 15 ml/min/1.73m², the condition is referred to as end-stage kidney disease (ESKD) (or end-stage renal disease (ESRD)).¹¹ In this scenario, renal replacement therapy is required to replace the function of the kidney to reduce the severity of so-called “uremic symptoms”. An extensive list of uremic symptoms that most commonly lead to the mortality of the patient is presented in table 1.²

Renal replacement therapy most commonly refers to either dialysis or a kidney transplant. However, dialysis is often the only option due to the severe lack of compatible organ donors available for ESKD patients.¹² While different types of dialysis are available to ESKD patients, this paper shall focus on hemodialysis.

Table 1. A list of uremic symptoms contributing to mortality in ESKD patients.

Anaemia
Cardiac failure
Coagulation disorders
Fluid overload
Hyperparathyroidism
Hypertension
Immune dysfunction
Insulin resistance
Malnutrition
Osteodystrophy
Pericarditis
Vascular disease

1.2. Dialysis

While a kidney transplant is the preferred form of renal placement therapy for ESKD patients, this is often simply not possible due to a severe lack of viable donors – both

diseased and alive.¹² Instead, ESKD patients have no choice but to rely on dialysis instead to aid with the excretion of uremic toxins and excess fluids and electrolytes.

During a hemodialytic procedure, the patient's blood is pumped into a dialyzer. Here, small molecules such as urea can cross a semi-permeable membrane into an aqueous solution called dialysate, after which the blood is pumped back into the body.¹³ This dialysate is a buffered electrolyte solution that is also utilized to regulate the patient's electrolyte balance. Because of this, the dialysate composition needs to be adjusted to the individual patient.¹⁴ Further, excess water in the blood is most commonly removed by a pressure gradient across the membrane. A schematic overview is shown in figure 2.

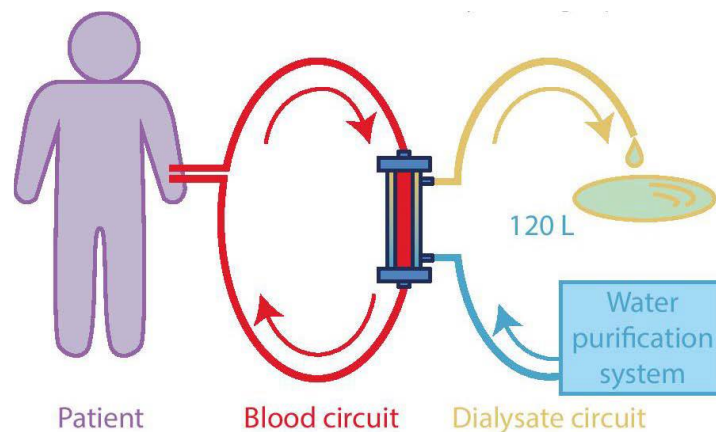


Figure 2. Schematic overview of hemodialysis. Taken from Jong (2019).¹⁵

While dialysis certainly is considered a life-saving treatment, it is not entirely without its drawbacks. Patients have to go to a dialysis clinic 3 to 6 times a week, and a session can take anywhere between 2 and 8 hours. Moreover, while dialysis may provide some relief and slow down the progression of uremic symptoms, it does not get rid of it entirely. It is thus not surprising that many dialysis patients suffer from mental health problems such as depression and anxiety.¹⁶

To improve the quality of life of ESKD patients and the long-term efficacy of the dialysis treatment, a Wearable Artificial Kidney (WAK) device has been proposed as an alternative. This would not only allow for more frequent removal of uremic toxins, thus reducing the built-up of said toxins and their associated side effects, but the compact nature of such a device would provide the patient with far more freedom in regards to the location independence of the treatment, thus improving the quality of life.

Unfortunately, such a device depends on the ability to remove said toxins (as well as fulfil all other purposes of a regular dialysis treatment) while remaining relatively compact. Regular dialysis treatment uses approximately 120 L of dialysate, which cannot be recovered afterwards. Ideally, the volume required by a WAK device would be $< 0.5\text{L}$.¹⁷ While the regeneration of said dialysate would be possible in the form of a closed-loop system¹⁷, one of the main obstacles in realizing a commercial WAK device is the removal of the smallest and most prevalent uremic toxin: urea. A schematic overview of such a regenerative loop is presented in figure 3.

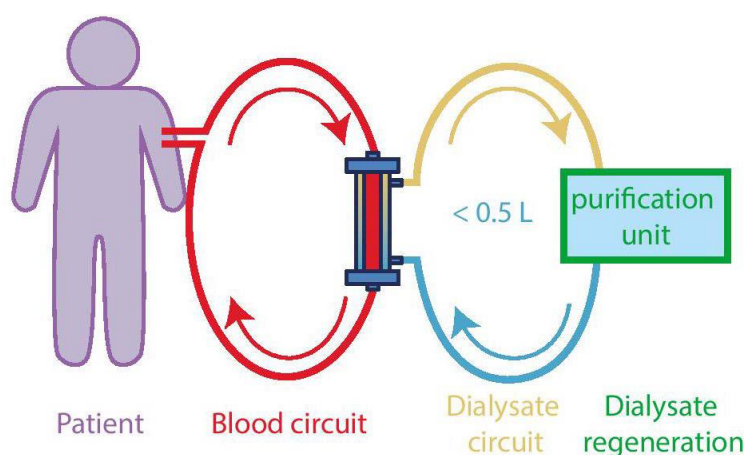


Figure 3. A schematic overview of a Wearable Artificial Kidney (WAK) device with a dialysate regeneration unit.

Taken from Jong (2019).

1.3. Urea – Chemistry, biological significance and problems

Urea¹ is a small, polar molecule that is highly soluble in water. It has one oxygen atom and two nitrogen atoms, all of which can form hydrogen bonds.¹⁸ It is unclear when it was first isolated and characterized, though one of the first recorded instances was in 1727 by Hermann Boerhaave.¹⁹ The compound has three resonance structures, which are presented in figure 4.²⁰

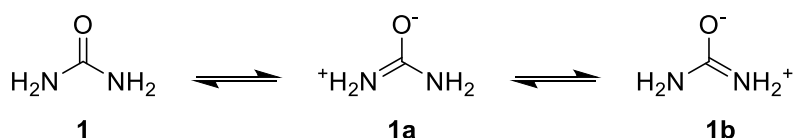


Figure 4. Resonance structures of urea.

¹ Urea may also refer to a class of organic compounds. However, within the scope of this paper, urea will always refer to its simplest form ((H₂N)₂CO).

Similar to peptide bonds, the electron pairs of the individual nitrogen atoms are delocalized over the C-N bond. This gives these bonds a double bond character, while the C-O bond has a single bond character. Ultimately, this leads to an incredibly low chemical reactivity; however, it is still considered a weak nucleophile.²⁰

In nature, urea is found to decompose primarily in two different ways. The first is in an aqueous solution, where it decomposes to a cyanate ion and an ammonium ion through an eliminative mechanism. The formed cyanate ion (7) then further decomposes to carbon dioxide. On the other hand, when urease enzymes decompose urea, it forms a hydrogen carbonate ion and an ammonium ion.²¹ Both decomposition mechanisms are presented in figure 5.

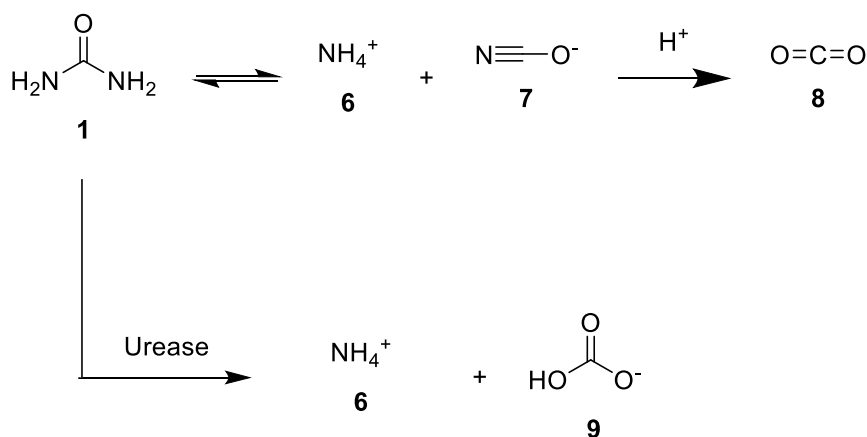


Figure 5. Decomposition of urea in an aqueous medium (top) and with urease (bottom).

The decomposition of urea in an aqueous medium is a very slow reaction; urea has a half-life of 3.6 years. However, when urease is present, this reaction is about 10⁴ times faster.²²

Of course, in the human body, the decomposition of urea is not the goal; instead, it is the end product of the urea cycle. Urea is naturally produced when the liver breaks down proteins and amino acids. Ammonia is a by-product of breaking these nutrients down, which is highly toxic to humans. The body thus converts the ammonia into urea – a safe, non-reactive compound that can be excreted from the body by the kidneys through urine, together with other waste products and electrolytes.^{23,24}

With a daily production of 240 to 470 mmol, urea is the most prevalent uremic toxin that the body needs get excrete, and failure of the body to do so can lead to the rise of the uremic symptoms. Concentrations of above 20 mM urea are generally considered

to be the limit until these symptoms start to appear, ranging from insulin resistance to other symptoms previously mentioned in table 1.²⁵ This is because urea can disrupt the structure, as well as the function, of proteins by breaking intramolecular hydrogen bonds.²⁶ As the kidneys play a central role in the excretion of urea, it is thus evident how the failure of the kidney to do so may appear problematic for the ESKD patient.

In dialysis, urea is removed from the body through diffusion through a semi-permeable membrane, but this requires a large volume of dialysate, making it an unsuitable mechanism for a potential WAK device. Instead, several alternative methods for the disposal of urea have been researched.

1.4. Alternative methods for the removal of urea

1.4.1. Enzymatic removal using urease

Urease (or urea amidohydrolase) is a well-researched enzyme and is the first enzyme to be isolated back in 1926 by James B. Sumner from jack beans, thus proving the protein nature of enzymes.²⁷ Additionally, the research on urease also first proved the biological significance of nickel ions, which research by Zerner et al. (1975) showed to be required for the catalytic effect of the jack bean urease isolated nearly 50 years prior by Sumner.²⁸ It is estimated that the hydrolysis of urea whilst being catalysed by urease is at least 10^{14} times faster than the uncatalyzed reaction, and urease is widely seen as the most efficient enzyme known to date.

While different urease enzymes exist, research suggests that the active sites are all incredibly similar and function practically the same. These active sites contain two nickel atoms and a carbamylated lysine moiety, four histidine moieties, and one aspartate moiety. Furthermore, a hydroxide ion connects the two nickel atoms, which form a cluster together with three water molecules.²⁹

When urea enters the active site of a urease enzyme, it undergoes a complex mechanism that ultimately hydrolyzes the molecule, forming a carbamate ion and an ammonium ion. The catalytic mechanism is presented in figure 6.³⁰

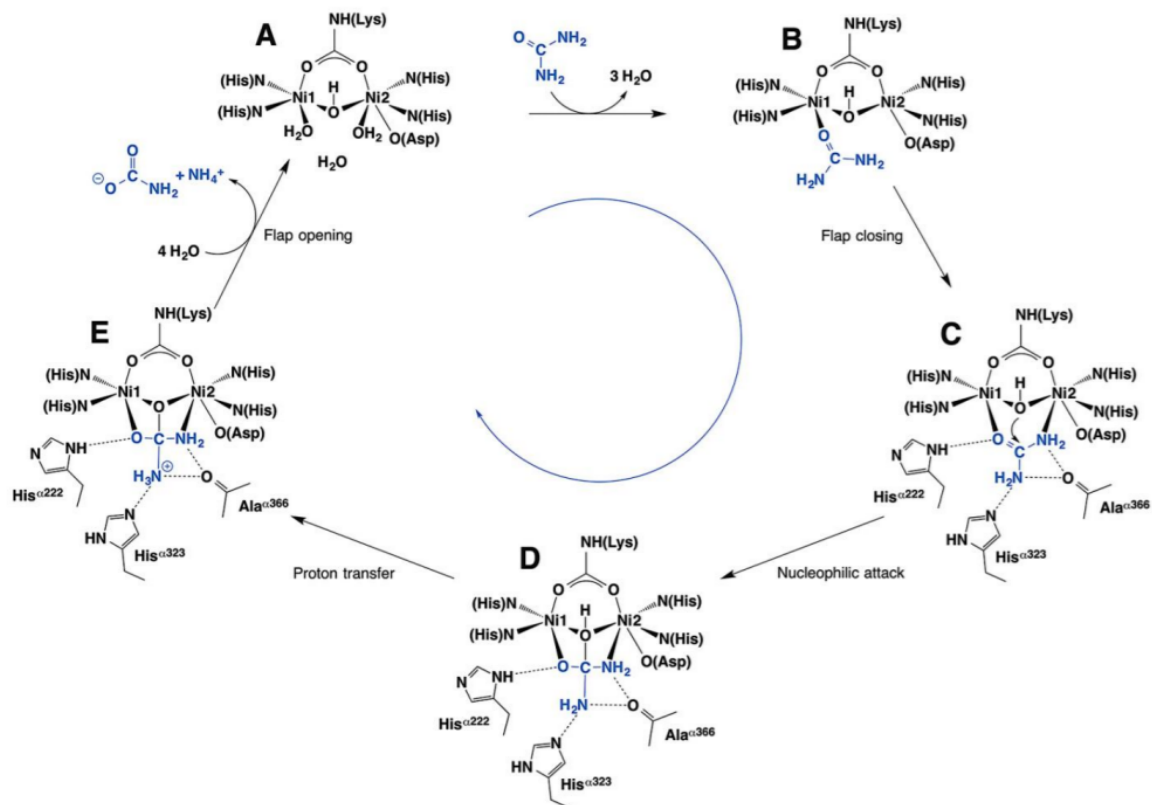


Figure 6. Hydrolysis mechanism of urea by urease. Taken from Kappaun et al. (2018).³⁰

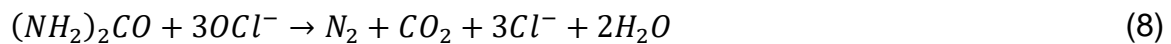
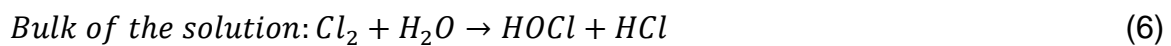
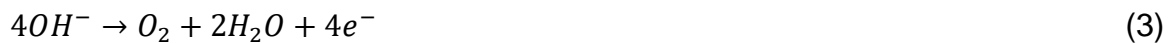
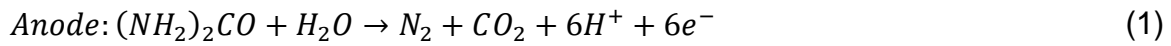
Whilst the efficiency of the urease enzyme might make it seem as though it would be a suitable candidate for the decomposition of urea, the formed ammonia (ammonium under physiological conditions) is, in fact, more toxic to the human body than urea, especially in the short-term. A review by Walker (2009) suggests that patients that suffer from hyperammonemia due to a defect in the urea cycle suffer from severe brain damage.³¹

1.4.2. Disposal of urea through electrochemical means

Urea is produced in an industrial setting in tremendous amounts, but this leads to a large amount of wastewater that contains urea in varying concentrations. In order to remove the urea from these wastewaters, several methods are being employed, the one currently being most favourable being the electrochemical decomposition due to the non-toxic byproducts, consisting of nitrogen N₂, carbon dioxide CO₂ and water.³²

This method has also been investigated for dialysate regeneration in artificial kidneys.³³⁻³⁵ For this process, platinum or titanium electrodes covered with ruthenium

and titanium oxide are used, and it was found that urea could, indeed, be decomposed into the non-toxic products mentioned above. However, when chloride ions are present, a problem arises. The electrolysis is presented in equations 1 - 8.



Evidently, the electrochemical decomposition of urea in the presence of chloride ions proceeds over a secondary route, namely via a highly reactive hypochlorite species. This happens in a multi-step process, including the formation of monochlorourea, then dichlorourea, which is ultimately decomposed by further hypochlorite ions to form the non-toxic gaseous products mentioned before.³⁶ However, several other toxic side products may also be formed, albeit in small amounts. These include nitrate (NO_3^-), ammonia (NH_3), nitrite (NO_2^-), chloramines (NH_xCl_y), as well as other active chlorine species other than hypochlorite. These byproducts can cause serious damage to the human body, ranging from the aforementioned brain damage caused by ammonia³¹ to gastric cancer caused by nitrate.³⁷ Control over the formation of these toxic byproducts is thus crucial if the electrochemical decomposition were ever to be considered a means to dispose of urea within the scope of a WAK device.

1.4.3. Non-covalent binding of urea

An alternative to the decomposition of urea through enzymatic or electrochemical means would be to bind urea with a sorbent material, either by forming covalent or coordination bonds or through non-covalent interactions such as hydrogen bonds or van der Waals forces. One of the main benefits would be that there is no risk of toxic byproducts being formed. On the other hand, the sorbent material would have to be highly efficient at binding urea specifically due to urea's similarity in reactivity to water³⁸ and the large excess of water present compared to urea (55 M vs approximately 60 mM).

Several sorbent materials have been studied in the past, and when it comes to sorbent materials, one of the first that would naturally come to mind would be activated carbon (AC), and indeed, extensive research has been done on its viability as a urea sorbent. Kameda et al. (2020) investigated the viability of using spherical AC due to its well-researched high absorptive character.³⁹ A previous study done by the same group already published a kinetics study of the physical absorption of urea in aqueous solutions using spherical AC, showing a sort of multi-layered absorption through dipole-dipole interactions.⁴⁰ A schematic overview is presented in figure 7.

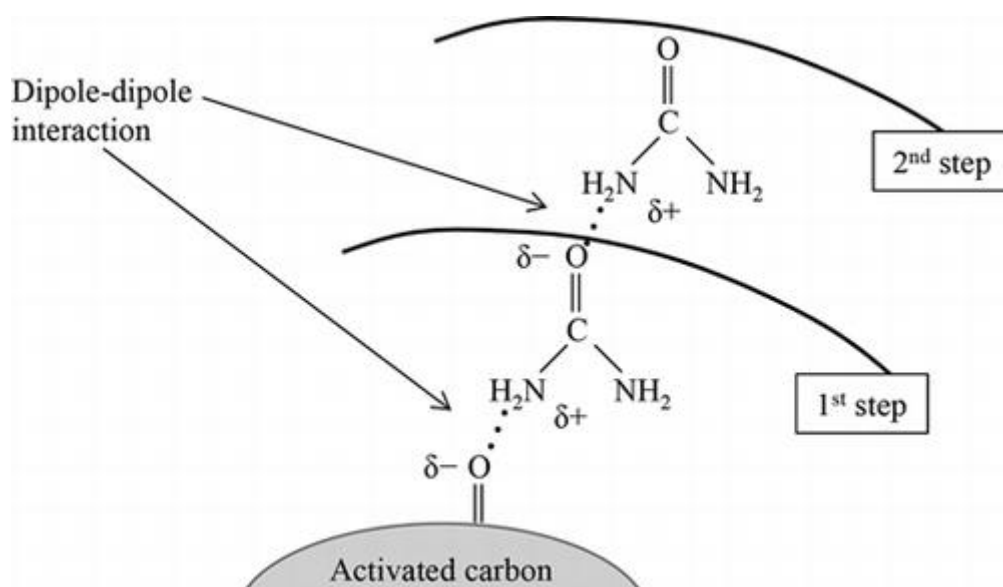


Figure 7. Schematic overview of the interaction between urea and spherical AC, as found by Kameda et al. (2016).⁴⁰

The group found that the binding of urea is an exothermic reaction, the rate of which increases at lower temperatures. They investigated the urea binding capacity of

spherical AC at 10, 30 and 60 degrees Celsius, finding that the amount of urea removed is 1.1 mg/g (0.018 mmol/g), 0.9 mg/g (0.0015 mmol/g) and 0.9 mg/g respectively. Evidently, as the daily amount of urea produced by the human body is about 400 mmol²⁴, the binding capacity of spherical AC simply is not sufficient to act as a urea sorbent, though it could still prove useful in a WAK device due to its capability to bind other, larger uremic toxins.⁴¹ For example, the daily production of uric acid is approximately 750 – 800 mg per day, and AC was found to bind 20.2 – 24.3 mg/g, depending on the temperature.³⁹

Another class of materials that several groups have investigated for its urea-binding capabilities are MXenes. These are two-dimensional structures, which were first discovered in 2011.⁴² They have a general formula of $M_{n+1}X_nT_x$, of which M are transition metals such as titanium, X represents carbon or nitrogen and T represents terminal groups such as hydroxy- or fluoride groups. Several studies have shown the possibilities when it comes to fine-tuning these structures to allow them to absorb certain structures within their crystal lattice, so it is postulated that it would be possible to create such a structure that is capable of absorbing urea.^{43,44} *Meng et al. (2018)* suggest that the urea affinity could further be increased by selecting terminal groups that can interact with urea, such as hydroxy-groups, and so they investigated the urea binding capacity of several MXenes.⁴⁵ They found that the MXene with the highest urea binding capacity was $Ti_3C_2T_x$ with oxygen-containing surface groups, with a binding capacity of 9.7 mg/g (0.16 mmol/g). While this certainly is significantly better than the aforementioned binding capacity of AC, it would still require up to 2.5 kg of the aforementioned MXene to remove the amount of urea produced in the human body daily. It should also be noted that this study relies on the increase of urea affinity using oxygen-containing terminal groups that can interact with the amines of urea. However, within the scope of a WAK device, a tremendous excess of water would also be present, thus competing for these interactions, and as MXene nano materials generally hugely rely on electrostatic interactions, it remains the question as to whether these materials will ever be able to bind a tremendously diluted urea solution with sufficient efficiency.

This appears to be the main obstacle regarding urea binding within the scope of a WAK device: the competition between the urea molecules and the large excess of water molecules with the sorbent materials mentioned above. Other well-researched

materials such as amino-functionalized silica⁴⁶ and zeolites (aluminosilicate networks that are widely used as ion-exchangers)⁴⁷ also depend on these same interactions.

The similarity of urea to water makes the development of a sorbent material based purely on non-covalent bonds such as hydrogen bonds unlikely due to the large excess of water present. Additionally, non-covalently bound urea would be in equilibrium with dissolved urea, and as the concentration of urea in the dialysate would decrease over time, so would the amount of urea being bound. Thus, binding urea through the formation of covalent bonds (chemisorption) would be more suitable, using a sorbent material that is functionalized with groups that can irreversibly react with urea under physiological conditions. To this end, polymeric structures could be used that are functionalized with groups that show a high reactivity towards urea. However, it is also important that they are, on the one hand, compatible with the human body (i.e. no strong acid group) while also not being able to react with water irreversibly.

1.4.4. The covalent binding of urea

1.4.4.1. The chemistry of urea

As mentioned in a previous chapter, urea is generally a relatively unreactive compound, so finding conditions under which it will react under physiological conditions may appear challenging at first. The Biginelli Pyrimidone Synthesis (see figure 8) is a classic reaction that involves urea, and though it is a multicomponent reaction and thus not suitable for the application in a WAK device, it does give certain hints about urea-reactive groups due to its relatively mild conditions.⁴⁸

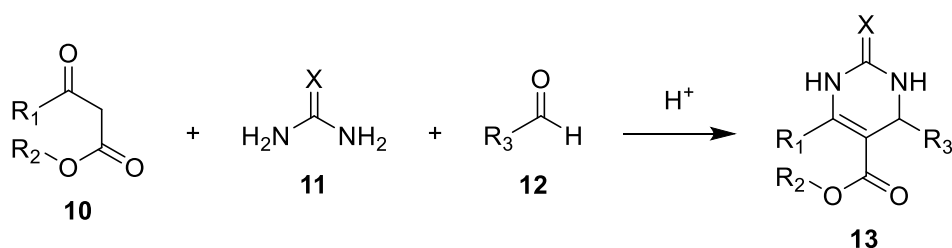


Figure 8. The Biginelli Pyrimidone Synthesis: A multicomponent pyrimidone synthesis from (thio)urea (11), an aldehyde (12) and a β -keto ester (10).

The acid functions as a catalyst, and while the reaction rate difference between the catalysed and uncatalysed reaction is not known, it does show that urea has the capability of reacting with both 1,3-dicarbonyl structures, as well as aldehydes.

The literature has described several other acid-catalysed reactions with urea under otherwise mild conditions. *Lin et al. (2008)* have described the synthesis of methylglycolurils from methylglyoxal and urea under acidic conditions⁴⁹, while *Baccolini et al. (2011)* described a similar reaction catalysed by a cyclic phosphorous compound using several different 1,2-dicarbonyl structures.⁵⁰ A study by *Menor-Salvan et al. (2020)* took a look at the role of urea in prebiotic synthesis pathways, suggesting that mere environmental factors such as thawing, drying and wetting may be sufficient that initiate reactions between urea and other prebiotic compounds. They indeed found this to be the case, particularly with malonic acid to form barbituric acid, as well as malondiamide to form aromatic compound **21**.⁵¹ The aforementioned reactions are presented in figure 9.

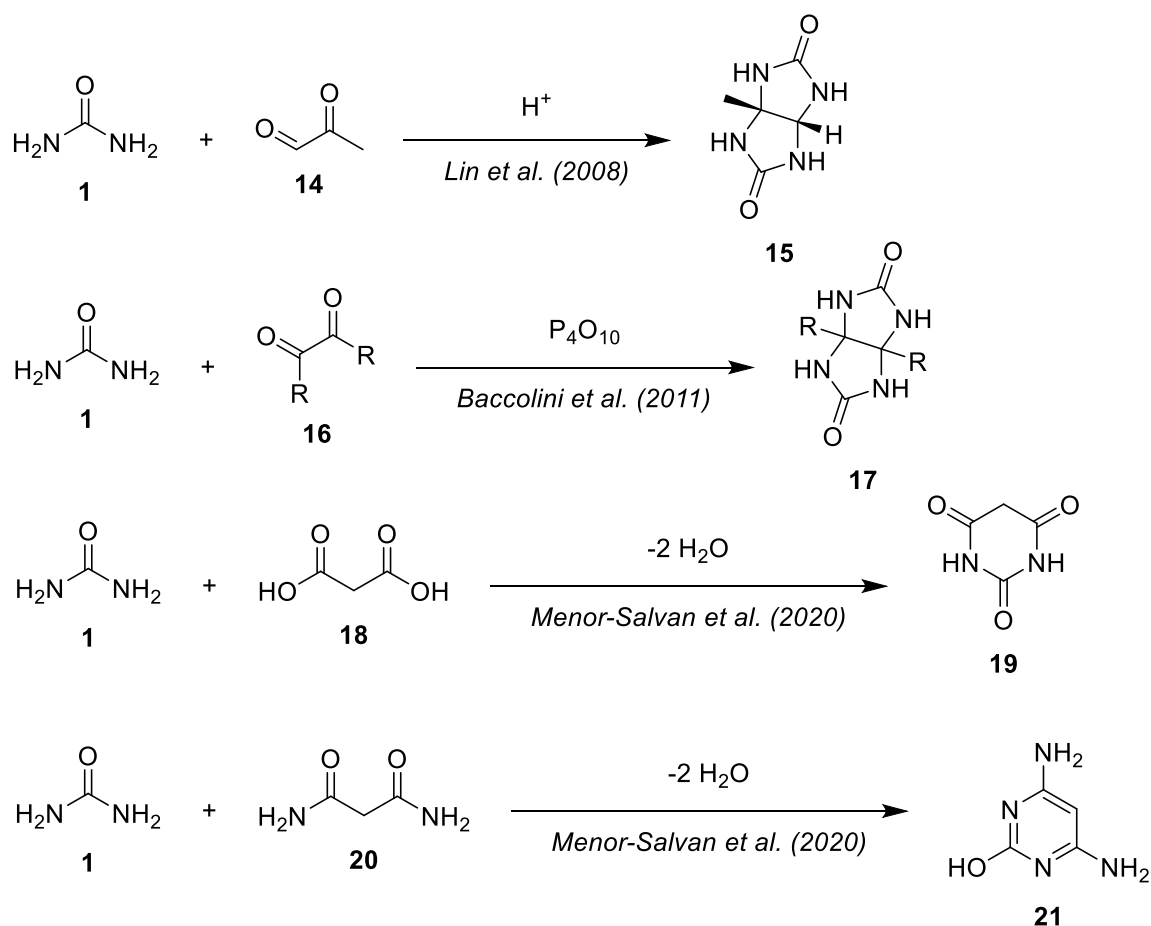


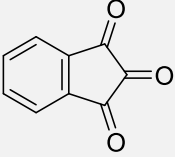
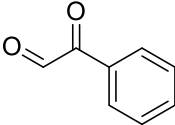
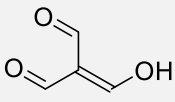
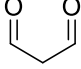
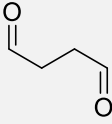
Figure 9. A brief overview of several representative reactions of urea under mild conditions.

1.4.4.2. The reaction of urea with vicinal carbonyl structures.

A recent study by *Jong et al. (2019)* investigated the reactivity of urea with vicinal carbonyl structures more closely, specifically also determining the reaction rate under the conditions under which a WAK device would operate (approximately pH 7.4, 50°C), as well as under acidic conditions (pH 2).⁵² This study leans on previous research papers showing uncatalyzed reactions between urea and various vicinal carbonyl compounds such as ninhydrin and phenylglyoxal, among several aldehydes, and determined the second-order rate constant k_2 of the reaction between urea and a large variety of carbonyl compounds in PBS solution.^{53–57} Some of the most noteworthy results are presented in table 2.

As shown in the table below, ninhydrin and phenylglyoxal, representative of 1,2-dicarbonyl structures, react with urea at a decent rate under physiological conditions, while 1,3-dialdehyde structures appear to show no significant reactivity towards urea at a neutral pH. However, the fact that the reaction rate of triformylmethane and malonaldehyde is nearly three times higher than that of ninhydrin certainly makes them worth investigating nevertheless, especially considering that attempts at increasing the reaction rate of ninhydrin through adding a large variety of different substituents to the aromatic ring appeared to be fruitless.⁵⁵ A deeper dive into the nature of 1,3-dialdehyde structures under physiological conditions and their reaction pathway with urea may provide further information on how to fine-tune these molecules to make their usage in a WAK device plausible.

Table 2. Investigated vicinal carbonyl structures with the highest rate constant when reacting with urea at pH 2/7.4 at 50 °C, as found by *Jong et al. (2019)*.

Name	Structure	k_2 [$M^{-1}h^{-1}$] at pH 7.4	k_2 [$M^{-1}h^{-1}$] at pH 2
Ninhydrin	 22	6.8±0.6	n/a
Phenylglyoxal	 23	3.7±0.1	n/a
Triformylmethane ²	 24	<0.1	18.4±5.2
Malonaldehyde	 25	<0.1	18.1±2.3
Succinaldehyde	 26	<0.1	10.8±0.8

1.5. The properties and chemistry of malonaldehyde and triformylmethane.

1.5.1. Electrophilicity

An aldehyde by itself is already a highly reactive group. This is generally explained due to the partial positive charge of the carbonyl carbon, which is stronger than that of most other carbonyl functional groups due to the lack of an electron-donating group where the hydrogen atom resides. This makes aldehydes excellent electrophiles, which goes

² The reaction between triformylmethane and urea was measured at 20 °C due to its high reactivity.

even more so for 1,3 dialdehyde structures such as malonaldehyde and triformylmethane.

In the case of malonaldehyde, both aldehyde groups contain a highly reactive, electrophilic carbon atom, which will readily react with a wide variety of nucleophiles under mild conditions. This includes basic amino acid residues, which generate Schiff bases.⁵⁸ However, this high reactivity also leads it to react readily with itself. This will further be elaborated on in another chapter.

As one might expect, triformylmethane, with its three aldehydes, is even more reactive than malonaldehyde, though because it is not a naturally-occurring compound like malonaldehyde, as well as its somewhat harsh synthesis conditions⁵⁹, not as many reactions are described in literature. However, the reactions that were indeed described all occurred under mild conditions, often at room temperature or well below zero. Similar to malonaldehyde, reactions with nitrogen-containing compounds are the most commonly described reactions, thus further confirming the suspicion that aldehyde-containing structures may be suitable for the implementation in a WAK device.

1.5.2. Keto-enol tautomerism

Like most carbonyl-containing compounds, malonaldehyde and triformylmethane are in equilibrium with their enol-form. Indeed, researchers have found the Z-isomer of the malonaldehyde enol to be the most stable form due to the formation of intramolecular hydrogen bonds⁶⁰, and the same was found for triformylmethane.⁶¹ The equilibria are presented in figure 10.

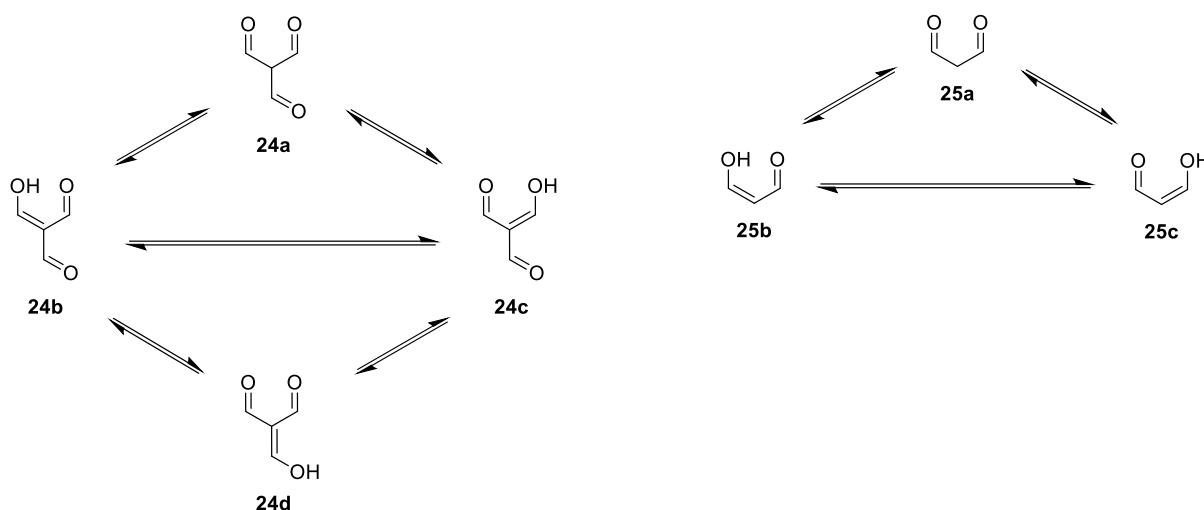


Figure 10. Keto-enol tautomerism of triformylmethane (left) and malonaldehyde (right).

1.5.3. Self-condensation reactions

As shown in figure 10, both malonaldehyde and triformylmethane contain an enol group in their most stable form. However, the nucleophilicity of said group would enable both compounds to react with themselves with the free, electrophilic aldehyde groups. It was found that this reaction does indeed occur at room temperature at a rather rapid rate, thus creating an obstacle regarding the implementation of such compounds in a WAK device.

An overview of the self-condensation of malonaldehyde is presented in figure 11, taken from the work of *Riggins et al. (2001)*.⁶²

1.5.4. Acidity

The acidity of 1,3-dicarbonyl structures widely varies based on the nature of the carbonyl groups and further substituents. Certain malonates may have pK_a values of 13, while structures like Meldrum's acid have a pK_a of only 4.97.

Malonaldehyde has a pK_a of 4.46³, meaning that it is present in its deprotonated form under physiological conditions.⁶³ The same goes for triformylmethane, which was found to be a strong organic acid with a pK_a of 2.0 – 2.3.⁶⁴ It thus comes as no surprise that reactions with both compounds are generally performed under acidic conditions to

³ Values found in literature may vary slightly, but are generally between 4.0 and 4.5.

ensure that they are present in their protonated form, as the negative charge caused by the deprotonation may impact the reactivity of said compounds.

As previously described and shown in table 2, *Jong et al. (2019)* found that malonaldehyde and triformylmethane would only react with urea at a pH of 2, while not showing any reactivity towards urea under physiological conditions.⁵² It can thus be assumed that the deprotonation severely impacts the ability of the structures to react with urea, though other factors may also play a role.

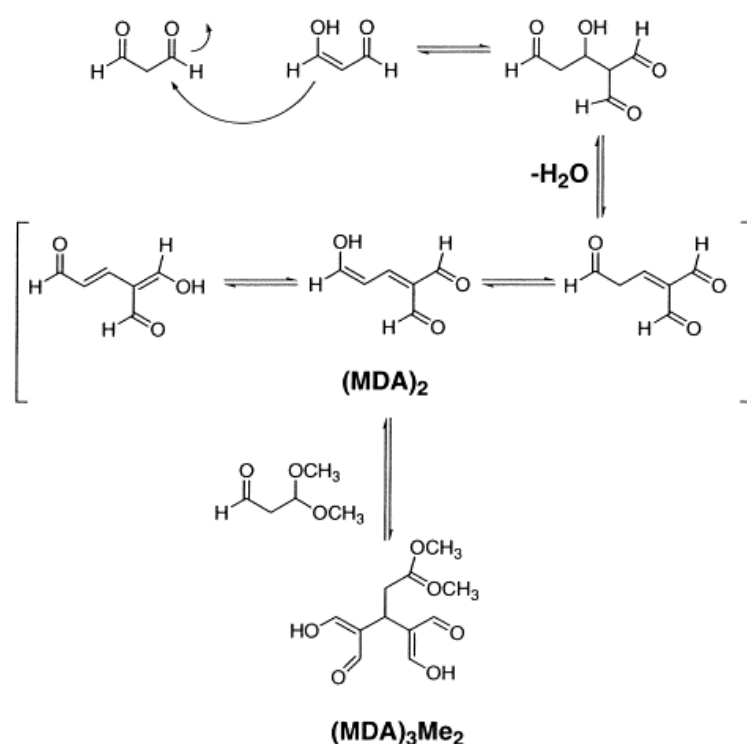


Figure 11. Self-condensation reaction of malonaldehyde (MDA). Taken from *Riggins et al. (2001)*.

1.5.5. The reaction of 1,3-dialdehyde structures with urea

In addition to the work of *Jong et al. (2019)*, the reaction between urea and triformylmethane has already previously been described by *Arnold et al. (1991)*, showing the reaction will readily occur in water without further additives within just three hours with excellent yields to form **27**.⁵⁷ The reaction is shown in figure 12. Other than in the works of the two aforementioned groups, this reaction is not mentioned in

literature, and so the potential formation of other products, as well as the mechanism of the reaction, is not well-studied.

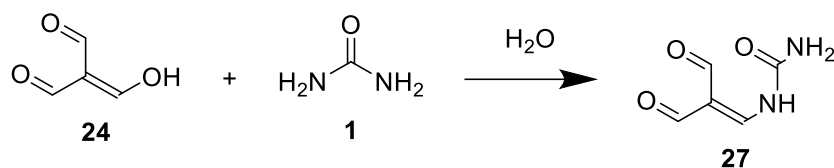


Figure 12. The reaction of triformylmethane and urea in water according to the research of *Arnold et al. (1991)*.

On the other hand, Malonaldehyde appears to react through a different mechanism. According to the work of *Jong et al. (2019)* and *Tsreng & Kalhan (1982)*, malonaldehyde reacts with urea to form an aromatic end-product.^{52,65} This reaction is shown in figure 13. This is rather interesting, as it can be assumed that forming an aromatic ring would make the reaction between urea and malonaldehyde rather favourable. However, to gain further insights into the specific factors that may influence the reaction between urea and a 1,3-dialdehyde structure, it is important to regard the reaction mechanism.

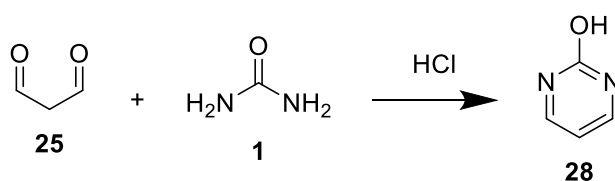


Figure 13. The reaction of malonaldehyde and urea in water according to the research of *Tsreng & Kalhan (1982)*.

A reaction mechanism between malonaldehyde and urea was proposed by *Jong et al. (2019)*.⁵² In the hypothesized mechanism, one of the NH₂ groups of urea attacks the aldehyde carbon, leading to the formation of the hemiaminal. Then, in a subsequent step, the second NH₂ group does the same with the other aldehyde carbon, leading to an intramolecular cyclization reaction. However, this aminal structure was found to be unstable under neutral conditions due to its equilibrium with the previous stage. However, water can be eliminated under acidic conditions to form an aromatic compound **28**. An overview of this reaction mechanism is shown in figure 14.

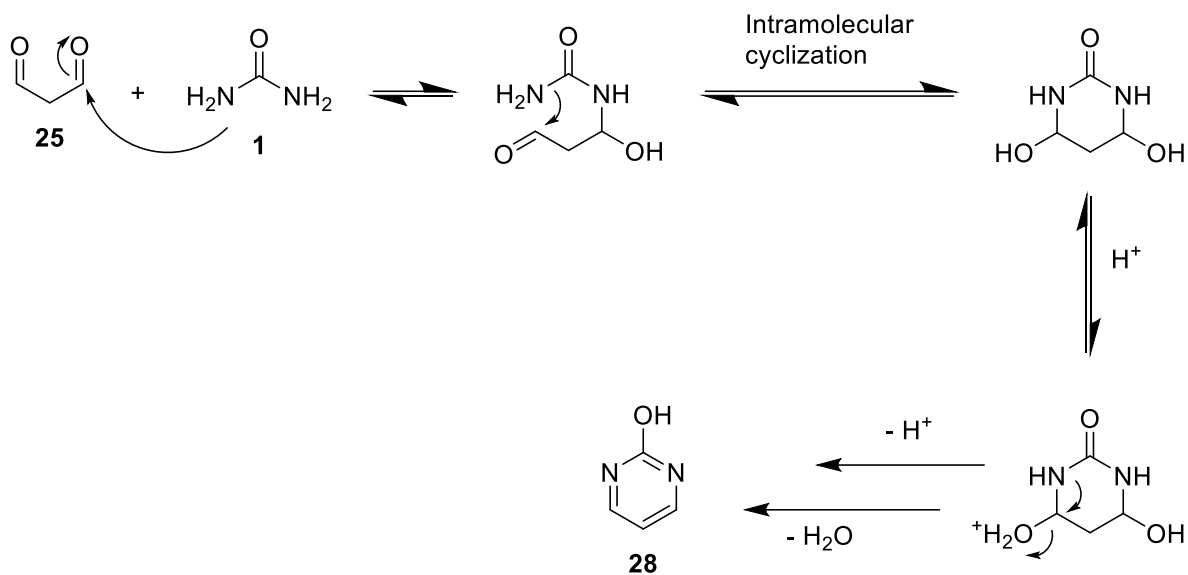


Figure 14. Hypothesized reaction mechanism between urea and malonaldehyde as proposed by *Jong et al.* (2019).

It is important to note that, due to malonaldehyde's inherited acidity, no external acid needs to be added for the elimination step.

2. Aims of this study

2.1. Motivation

As discussed in the previous chapters, a sorbent material that selectively binds urea covalently would be ideal for removing urea within the scope of a WAK device. While such materials, functionalized with 1,2-dicarbonyl structures such as phenylglyoxal (PGA) and ninhydrin have already been developed, they have their limitations. These limitations include relatively low reaction rates, low degrees of functionalization, expensive starting materials, and complex synthesis pathways.

While the reactivity of urea-reactive compounds is expected to decrease slightly when attached to a polymeric backbone, the high reaction rates measured for 1,3-dialdehyde structures like malonaldehyde and triformylmethane would more than compensate for this slight loss in reactivity. However, it is yet to be seen whether these compounds can react with urea under physiological conditions.

2.2. Objective

This study aims to explore whether a 1,3-dialdehyde structure can be developed that is capable of reacting with urea under physiological conditions. Malonaldehyde (MDA) is the structure of choice for this study because it is more easily accessible than triformylmethane.

Within the scope of this study, factors that may affect the reactivity of malonaldehyde-like structures shall be investigated, and the synthesis of a urea-reactive material shall be attempted based on the found results.

The focus of this project shall lie on the variation of the substituents of the central carbon. In order for 1,3-dialdehyde structures based on MDA to be used under physiological conditions, the high acidity of the structure needs to be addressed.

Initially, the role of the central acidic protons shall be assessed by synthesizing an MDA derivative without central protons. This structure shall then be assessed based on its reactivity towards urea. For this purpose, 2,2-dimethyl-malonaldehyde (**30**) shall be synthesized. The reason for choosing this structure is due to its impeccable similarity to MDA and the fact that it is expected that it can easily be synthesized from

the readily available diol **29**. The reaction scheme is shown in figure 15. Additionally, self-condensation reactions are not expected to obstruct the experiment with a model compound such as **30**, as the di-substituted MDA-derivative cannot form its enol form.

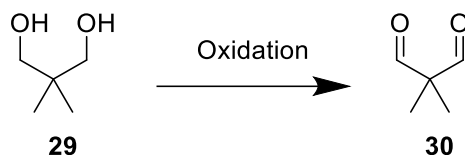


Figure 15. Synthesis pathway of **30**.

Should the acidic proton be essential for the reactivity of such structures with urea, the next step would be the generation of an MDA-like structure with merely one substituent on the central carbon atom. By doing so, it is expected that the pK_a of the acidic proton can be modulated, ideally to a value that is compatible with physiological systems while still participating in the reaction mechanism presented in figure 14.

To estimate how certain moieties will affect the pK_a of the MDA-derivative, a hypothesis is proposed based on the electron-withdrawing and -donating properties of certain substituents in 2-position. As similar trends could be observed in structures such as phenol and aniline, it is expected that the acidity of an MDA-derivative will follow a similar trend.^{66,67} The expected pK_a trend is depicted in figure 16, with known values already having been added.

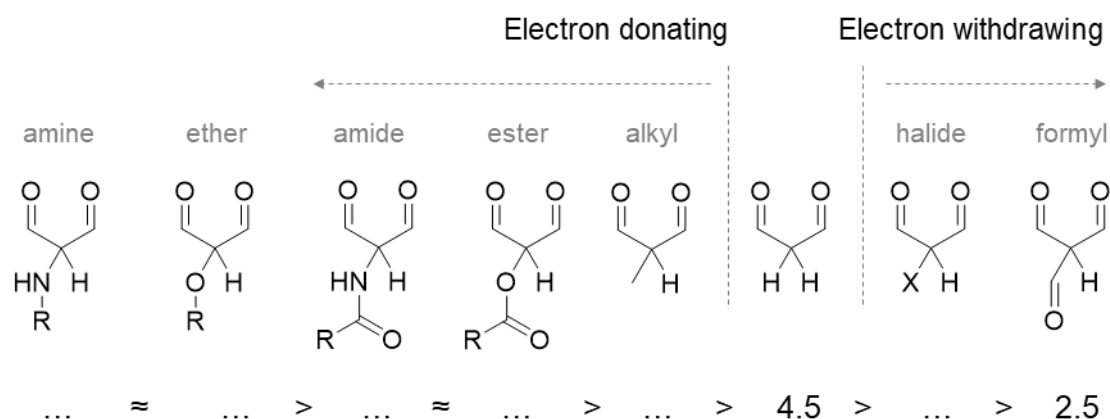


Figure 16. Expected decreasing order of pK_a -values of enolizable MDA-derivatives based on the electron-donating / -withdrawing effect of substituents in the 2-position.

In order to prevent self-polymerization during the experiments, it is important to identify a structure that can easily be modified and, at a final stage, be converted into a 1,3-

dialdehyde structure. Further, to prevent self-polymerization from being a competing reaction when testing the reactivity of synthesized structures with urea, it was chosen to attach protected MDA analogues to polymers, after which they would be deprotected once immobilized on the polymer backbone. It is expected that this ought to suppress self-condensation, as shown in figure 11.

This project predominantly focuses on the utilization of amine-functionalised polymers. This decision was made based on the fact that these polymers are well-described in literature, the fact that the expected effect on the pK_a is highest as per the hypothesis depicted in figure 16, as well as the fact that it is expected that the nucleophilicity of these nitrogen-based functional groups would be beneficial for the attachment of 1,3-dialdehyde structures. It is important that the synthesized polymers are porous to allow for a higher degree of functionalization degree by weight.

The chosen amine-based polymer shall be poly(vinylamine) (**33**). This shall be synthesized by first generating poly(N-vinyl formamide) (**32**), followed by a hydrolysis step, either acidic or basic. PNVF shall be synthesized using N-vinylformamide (**31**) and 10% divinylbenzene as a crosslinker. An overview of the reaction scheme is presented in figure 17.

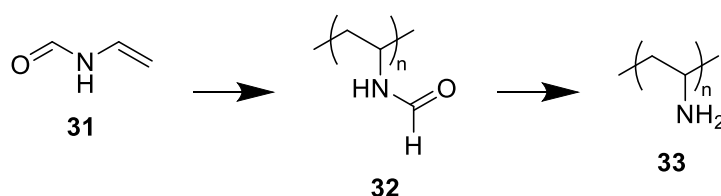


Figure 17. Synthesis pathway of **33**.

Additionally, to rule out potential issues regarding a low functionalization degree, a tetraethylene pentaamine-based polymer was also synthesized. With five amine groups per monomeric unit, it is expected that a low functionalization ought not to be a problem. This polymer (**37**) is synthesized by using Poly(glycidyl acrylate) (**35**) as a precursor, as shown in figure 18. **35** was chosen as a suitable precursor because it has a reactive epoxy group, which is highly suitable for post-polymerization modifications.

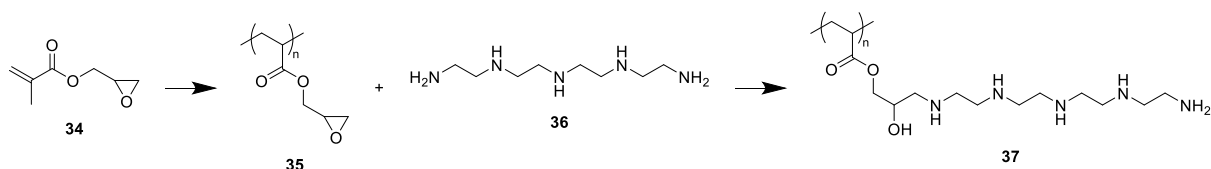


Figure 18. Synthesis pathway of **37**.

As both amine-based polymers contain nucleophilic functional groups, an MDA-intermediate with both aldehyde groups protected and an electrophilic central moiety needs to be developed. To this end, 1,1,3,3-tetramethoxypropane (TMP) (**38**), which is readily available as an MDA precursor, shall be brominated at the central carbon to form **39**. As it is important that **39** does not get hydrolysed before it is attached to the respective polymers, the synthesis and isolation shall be optimized based on the needs of this project. Once the TMP-moiety is attached to the respective polymer, it shall be deprotected through acidic hydrolysis.

A complete overview of the planned reactions is depicted in figure 19.

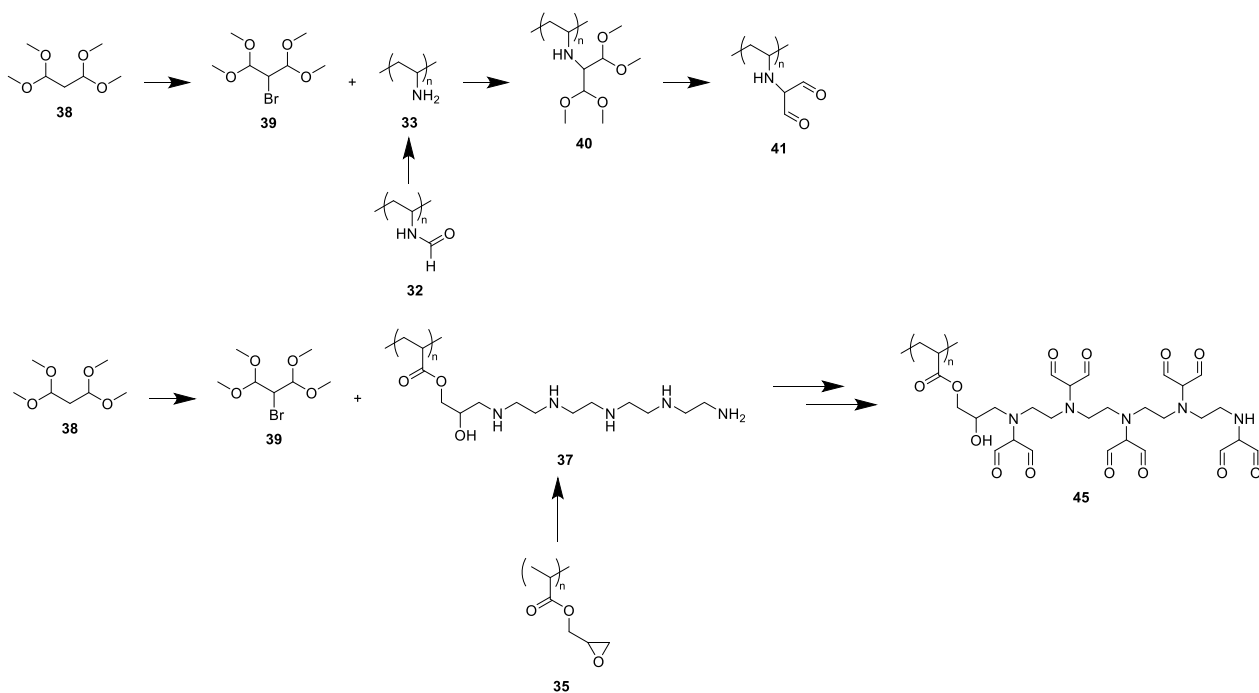


Figure 19. Synthesis pathway of target structures **41** and **45**.

3. Results and Discussion

In the following chapter, the conducted reactions and the urea reactivity tests shall be described in a logical order while discussing the future potential and/or problems when relevant. Unless specifically relevant for the discussion, spectra will be included in the appendix and referred to.

3.1. The urea reactivity of a non-enolizable, non-acidic malonaldehyde derivative.

3.1.1. Synthesis of 2,2-dimethyl-malonaldehyde (30).

For the synthesis of **30**, 2,2-dimethyl-propane-1,3-diol (**29**) was oxidized based on a protocol by *De Luca et al. (2001)*, in which the oxidation of primary alcohols is described using trichloroisocyanuric acid (TCCA) and (2,2,6,6-Tetramethylpiperidin-1-yl)oxyl (TEMPO).⁶⁸ This method was chosen based on its high reported conversion rates and mild reaction conditions; while more classic oxidation procedures such as Swern Oxidation require cooling of the reaction to -40 °C, the procedure proposed by the aforementioned authors mostly proceeds at room temperature. The reaction proceeded in dry DCM using 2.10 equivalents of TCCA to oxidize both hydroxy groups and 0.02 equivalents of TEMPO, which was added while cooling the reaction mixture with an ice bath. After 30 minutes, the reaction mixture was filtered through a celite pad and washed with both Na₂CO₃ and 1 M HCl to yield **30** with a conversion rate of 72% (figure 20).

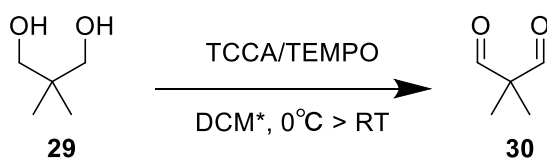


Figure 20. The synthesis of **30**.

It was found that **30** is not shelf-stable, and so a fresh batch was made and tested immediately for its urea reactivity.

3.1.2. Testing the urea reactivity of 2,2-dimethyl-malonaldehyde (30).

The reactivity of **30** with urea was tested using a protocol published by *Jong et al. (2019)*. A solution of 0.5 mmol ¹³C-labelled urea in 16.7 ml PBS was

prepared and heated to 323.15 K. The pH is measured regularly to ensure that it remains neutral. Then, 0.5 mmol of **30** was added, and samples of the reactions mixture were taken at regular intervals, of which ^{13}C -NMR spectra were recorded. A schematic overview is presented in figure 21.

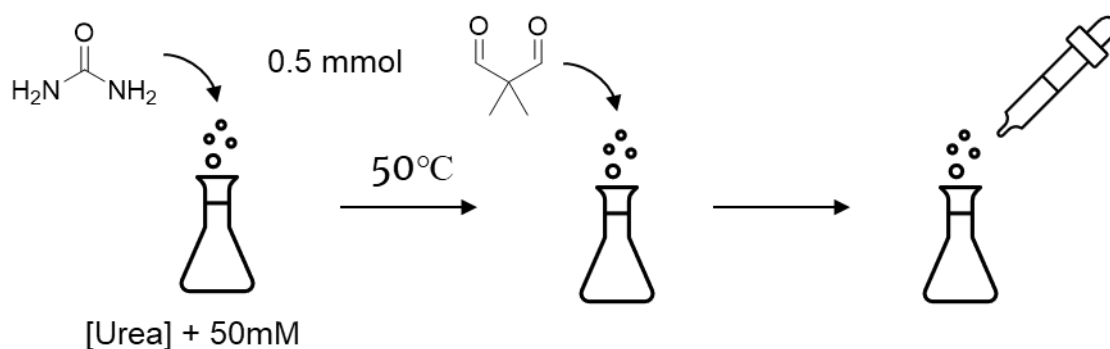


Figure 21. Schematic overview of measuring the urea reactivity of compound **30**.

^{13}C -labelled urea has a peak at approximately 162 ppm, while *Jong et al. (2019)* have previously shown that bound urea has a peak with a high field shift towards approximately 158 ppm.

After two hours, only the original ^{13}C -labelled urea peak at 161.93 ppm was visible, suggesting that compound **30** does not react with urea under physiological conditions (figure 22).

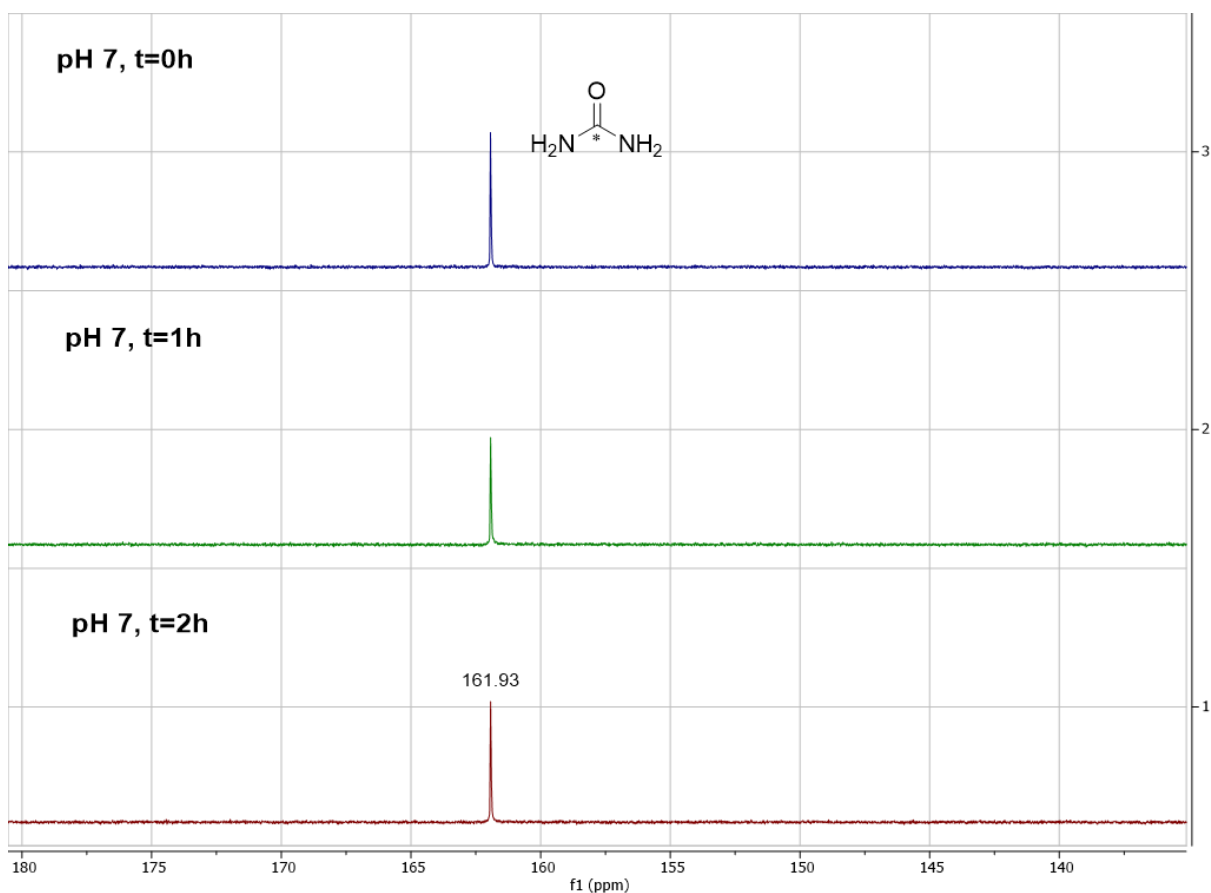


Figure 22. Qualitative ^{13}C -NMR spectrum over time at pH 7 of **30**. ^{13}C -labelled urea gives a signal at 161.93 ppm, and no product formation can be observed.

To investigate the role of acid in the reaction between urea and **30**, the same experiment was repeated at pH 1, though otherwise under the same conditions. A sample was taken after the reaction was stirred overnight, and indeed, the ^{13}C -labelled urea peak had completely vanished while a product peak had formed at 155.98 ppm (figure 23). The product structure was not determined within the scope of this project.

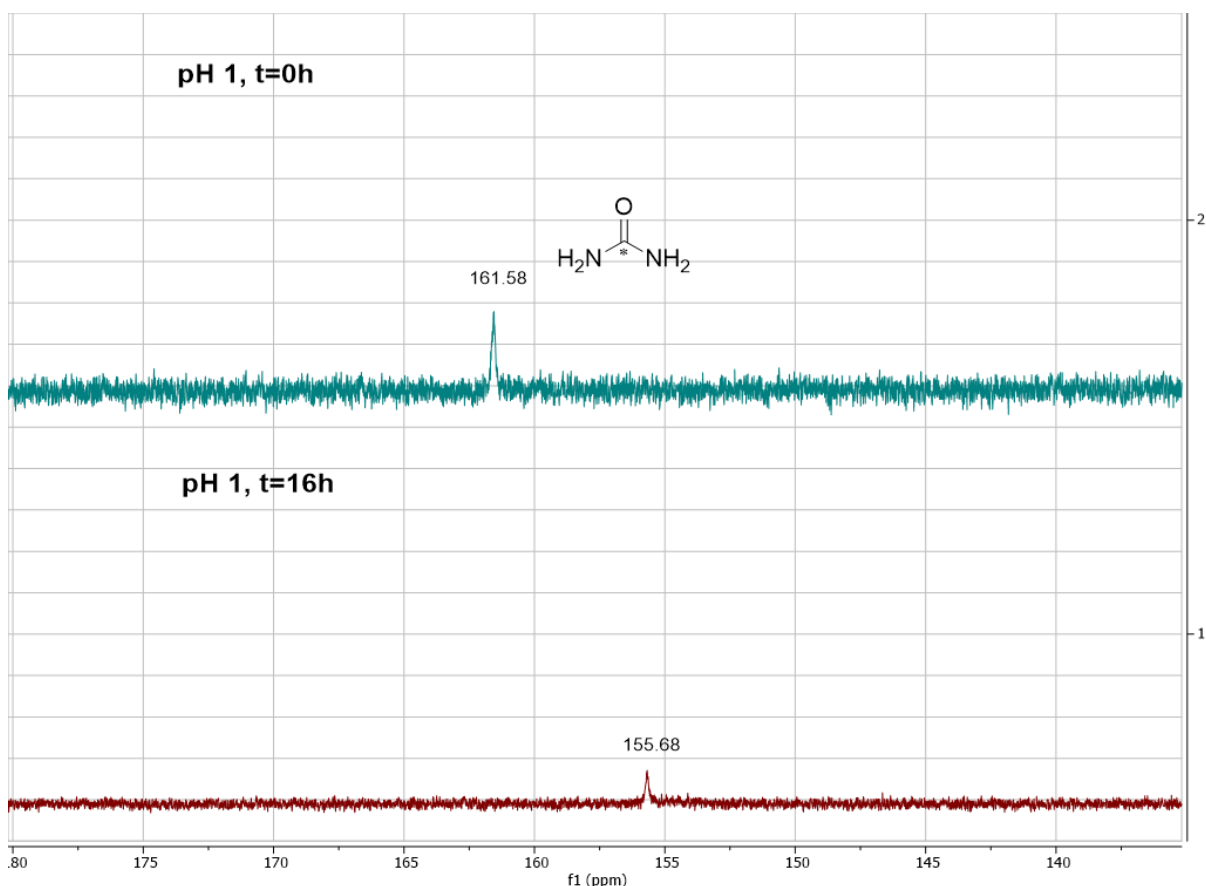


Figure 23. Qualitative ^{13}C - NMR spectrum over time at pH 1 of **30**. ^{13}C -labelled urea gives a signal at 161.93 ppm; a product peak is formed at 155.68 ppm.

3.1.3. Hypothesized reaction mechanism between 2,2-dimethyl-malonaldehyde (**30**) and urea at pH 7.

As previously described in figure 14, malonaldehyde is expected to form an aromatic end-product when reacting with urea. Indeed, several literature bodies have found this to be the case, albeit under acidic conditions.^{69,70} However, when the central carbon has two substituents, the formation of an aromatic compound would violate the octet rule, and so the only possibility would be the formation of the di-imine. Unfortunately, without the ability to form a more stable imine-enamine structure and the fact that imines generally only form under acidic conditions, it appears as though di-substituted MDA-derivatives are not suitable for the binding of urea under physiological conditions.

An overview of the aforementioned equilibria and intermediates is presented in figure 24.

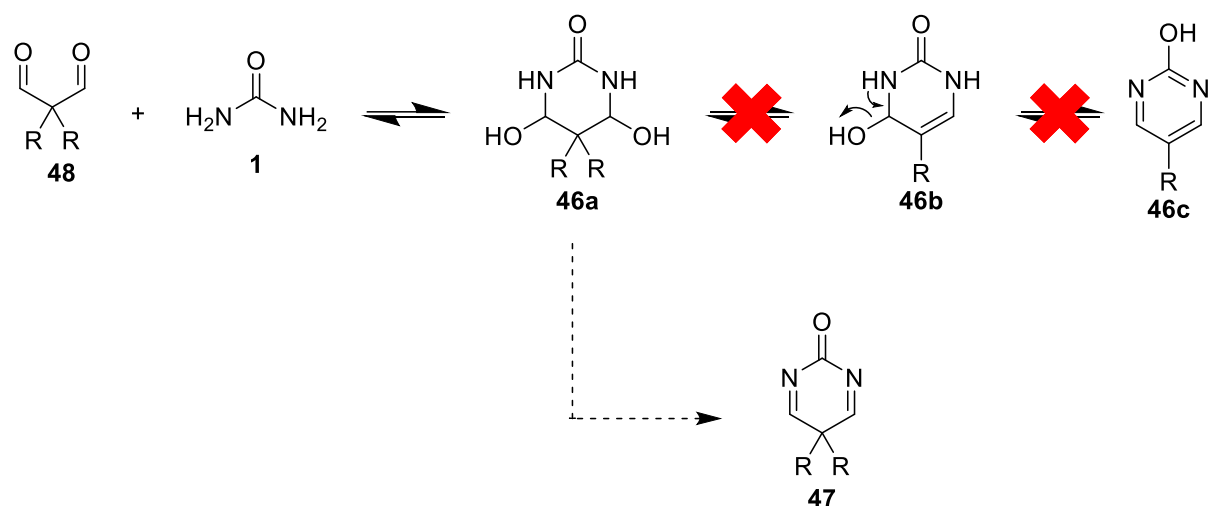


Figure 24. Schematic representation of the reaction between a disubstituted MDA-derivative and urea. The lack of a central proton prevents the formation of a stable end-product; instead, it is hypothesized that an unstable di-imine (**47**) is formed.

The experiment with compound **30** and the hypothesis presented in figure 24 indicate that an MDA-derivative simply cannot react with urea under physiological conditions, i.e. without an acid present. As previously described in chapter 2.2., the next step ought to be the synthesis of a mono-substituted MDA-derivative.

3.2. The synthesis of an MDA-functionalised polymer.

As previously described, this project focuses on the synthesis of an MDA-functionalised polymer to rule out potential competing self-condensation reactions. The chosen structures were synthesized in the lab.

3.2.1. The synthesis of poly(vinylamine) (**33**).

The synthesis of **33** is done through the hydrolysis of **32**. This is because the theoretical monomer, vinyl amine, is not stable.

Initially, **32** is generated by creating a solvent/non-solvent system consisting of toluene and 1-dodecanol in a ratio of 1:2. The solvent system was purged through bubbling nitrogen for about half an hour, after which N-vinyl formamide was added, as well as divinylbenzene as a crosslinker. Finally, Azobisisobutyronitrile (AIBN) was added as a

thermal initiator, and the reaction mixture was heated to 55 °C in a closed snap vial for several hours to form PNVF as a macro-porous polymer monolith.

Subsequently, the synthesized PNVF monolith is hydrolysed to form the desired PVAm. In literature, this reaction is described to be done in two different ways: acidic- and basic hydrolysis.⁷¹ Basic hydrolysis appears to be preferred, as reported data by *Gu et al. (2002)* suggest that basic hydrolysis leads to a more complete conversion. The authors hypothesize that this is due to the formation of charged NH₃⁺-groups, which prevent full conversion due to cationic repulsion. This is also in line with the findings of *Pinschmidt et al. (1996)*, who found that the conversion to **33** under acidic conditions cannot surpass 80%.⁷² On the other hand, *Witek et al. (2007)* report that a full conversion could not be achieved regardless of acidic or basic hydrolysis. They report that, during basic hydrolysis, the distinct smell of ammonia could be perceived, suggesting the deterioration of the polymer to some extent. This is in line with their findings regarding the formation of amidine rings, which then decompose into amine groups attached to the polymer backbone and hydroxy groups. These structural changes appear to depend on the reaction time. A schematic depiction of this is presented in figure 26. Despite this, it is the preferred method over acidic hydrolysis regarding conversion rates.⁷³ For this reason, as well as the lack of a more efficient alternative procedure, basic hydrolysis was chosen within the scope of this project.

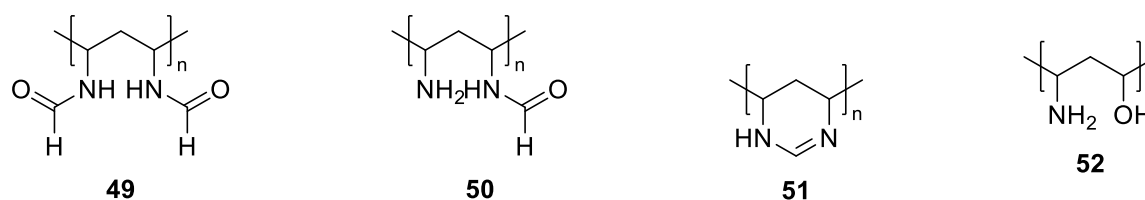


Figure 25. Perceived changes during basic hydrolysis by *Witek et al. (2007)*. Within 5 minutes, both the formation of the first amine groups, as well as the amidine rings (as seen in **51**), can be observed. After 90 minutes, the amidine ring signals disappear, while both formaldehyde signals disappear after 240 minutes. The formation of hydroxy signals (as seen in **52**) can be observed after 20 minutes.

Based on a protocol by *Witek et al. (2007)*, PNVF was stirred in 2 M NaOH for 4 hours at 60 °C. The polymer was analysed using attenuated total reflection infrared (ATR-IR) spectroscopy, as solid-state NMR was not readily available during this project.

The attained structure was compared to data published by *Zhao et al. (2010)*. Most significant are the signals at 1660 cm⁻¹, which is interpreted at the C=O stretch of the

formaldehyde structure, as well as the band at approximately 3300 cm^{-1} , interpreted as the N-H stretch of a primary amine, which would come from the desired PVAm structure. The peak at 3260 cm^{-1} may suggest the presence of hydroxy groups, as would be in line with what was previously described in figure 25. The peak at 2922 cm^{-1} may show the stretching vibration of C-H of the polymeric backbone, but may overlap with the stretching N-H vibration, as described in the aforementioned paper. Finally, the peak at 795 cm^{-1} may show the out-of-plane wagging vibration of N-H.

In conclusion, the presence of the C=O stretch peak suggests that a conversion rate of 100% could not be obtained, though this was within the expectations of the results. Additionally, the presence of hydroxy groups is not surprising, though this, in addition to the incomplete conversion, may lead to poor functionalization yields in other experiments. However, as further attempts at improving the yield (i.e. adjusting reaction time, temperature and basicity) did not seem to have any additional positive effect on the conversion, the sample of which the spectrum was described above was used for further experiments.

3.2.2. The analysis of poly(TEPA) (37).

For this project, **37** was synthesized by Dr Piet Driest. Poly(glycidyl acrylate) was synthesized similarly to PNVF through free radical polymerization, which is a well-described procedure in literature.^{74,75} ATR-IR data shows peaks at 1724 cm^{-1} , corresponding to the C=O ester stretching vibration, and 1145 cm^{-1} , corresponding to the C-O stretching vibration. A comparison with the data published by *Benaglia et al. (2013)* suggests that the reaction was, indeed, successful.⁷⁶

As previously described, poly(glycidyl acrylate) is often used for its convenient post-polymerization functionalization properties thanks to the presence of the epoxide ring. As described by *Muzammil et al. (2017)*, it can conveniently be functionalized through the reaction with an amine at elevated temperatures without the need for further reagents. However, it should be noted that they also describe the fact that larger amines lead to lower functionality, though this still appears to be well over 70%, and even the use of structurally similar triethylenetetramine appears to have been possible with a decent yield.⁷⁵

The functionalization of poly(glycidyl acrylate) with tetraethylenepentamine (**36**) appears to have been successful, as indicated by the recorded ATR-IR spectrum. It should be noted that it is unlikely that the epoxide ring only reacted with the primary amine, as it could have also reacted with the secondary amines, though this will not matter for the ultimate application. Most notable is the rise of the peak at 3297 cm^{-1} , which is interpreted as the N-H stretch vibration. As this molecule has yet to be described in literature at the date of writing this report, it was not possible to compare the IR data to values reported by other groups. However, the clear rise of the N-H stretch vibrational peak is sufficient to conclude that the functionalization has succeeded to an extent suitable for the application within the scope of this project.

3.3. The synthesis of 1,3-dialdehyde precursors.

In addition to the structures that were synthesized to be attached to the polymeric structures described in previous chapters, several structures have been examined for their use as a 1,3-dialdehyde precursor. Several of these structures are described in the following chapters, including considerations when it came to why these structures were chosen.

3.3.1. Potential 1,3-dialdehyde precursors for polymer functionalization.

3.3.1.1. Malonaldehyde sodium salt NaMDA (**53**).

As previously described, malonaldehyde was found to react with urea at an impressive rate under acidic conditions. Under regular conditions, however, it is not stable in the slightest and will immediately self-polymerize. This is why chemical suppliers offer 1,1,3,3-tetramethoxypropane (**38**) as a convenient precursor instead. This di-acetal structure can conveniently be hydrolysed under mildly acidic conditions to form malonaldehyde in highly diluted solutions. However, the solution requires cooling at all times to prevent a significant degree of self-polymerization, and even then, the reactivity of malonaldehyde towards itself cannot be prevented fully.

However, its sodium salt is described as a stabilized form of malonaldehyde.⁷⁷ It can conveniently be synthesized by dissolving **38** in 0.1 M HCl for 24 hours at 5 °C. The solution is then brought to pH 10 with 10 M NaOH to swiftly form **53** while minimizing

self-polymerization. Then, activated carbon is added to the solution to filter out any self-polymerisation products that may have formed. After another 24 hours, the activated carbon is filtered off, and the water is removed *in vacuo*. ¹H-NMR data and the recorded ATR-IR spectrum show that the synthesis was successful.

It was expected that it would potentially be possible to functionalize **53** at the central carbon position through a C-acylation, as is a well-described reaction in literature for 1,3-dicarbonyl structures.⁷⁸ It is expected that **53** is “locked” into its enolate form with the negative charge localized at one of the oxygen atoms. The nucleophilicity of the enolate was thought to be useful for the functionalization of **53** at the central carbon, though after several attempts, this appeared to be more complicated than initially expected.

Several reaction conditions to have **53** react with propionyl chloride (**54**), a highly-reactive electrophile, were attempted, as shown in figure 26.

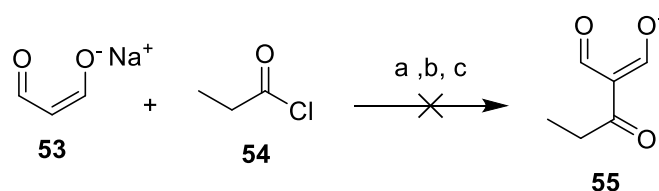


Figure 26. Attempted C-acylation of **53**. a: DCC, DMAP, MeCN; b: MgCl₂, TEA, MeCN; c: TEA, MeCN

DMAP and MgCl₂ were added in their individual attempts to prevent competing O-acylation reactions, and both conditions are well-described as suitable reaction conditions for C-acylations of 1,3-dicarbonyl structures. However, neither of these conditions was ultimately successful at synthesizing **55**. To confirm the efficacy of these conditions, a test reaction was conducted with diethyl malonate **56** using MgCl₂, TEA and MeCN, as shown in figure 27. This reaction was successful and led to the formation of **57**, as indicated by the recorded NMR data.

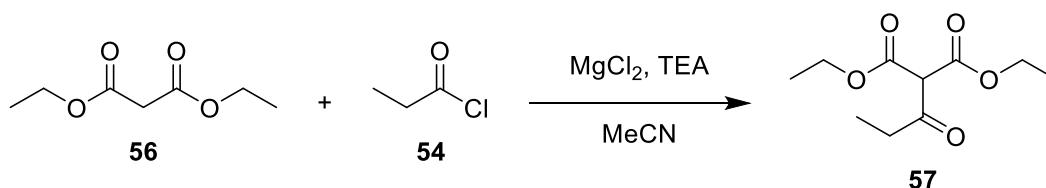


Figure 27. The synthesis of **57**.

To exclude from potential interference of Mg^{2+} ions due to the negative charge of **53**, the reaction was attempted without $MgCl_2$, even though this would, in theory, lead to competing O-acylations. However, the same result could be observed.

One potential explanation could be the use of MeCN as a solvent, which was chosen due to the poor solubility of salts in other organic solvents. However, literature suggests that a side reaction between the solvent and the aldehyde may be possible to form **60** under basic conditions, as shown in figure 28.⁷⁹

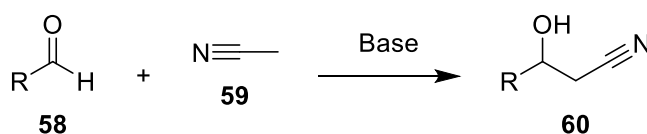


Figure 28. The hypothesized reaction between the aldehyde group of **53** and the solvent acetonitrile.

Whilst **53** appeared to be an unsuitable compound for urea binding, it provided some essential information for this project. The recording of its ATR-IR spectrum provided the signals that are to be expected if the functionalization of a polymer with a 1,3-dialdehyde moiety, namely the C=O stretch of this moiety at approximately 1601 cm^{-1} , as well as the CHO stretch at approximately 2775 cm^{-1} , providing valuable information for the analysis of polymers using the same method.

3.3.1.2. Dihydroxyacetone (**61**).

Dihydroxyacetone (**61**) is a well-researched compound due to its usage in the cosmetics industry, particularly in the sun-tanning industry.⁸⁰ Structurally, it is a 1,3-diol with a carbonyl group in the centre, which could potentially be utilized to couple **61** to an amine-functionalised polymer through reductive amination. The 1,3-diol moiety could then be oxidized using the previously used TCCA/TEMPO oxidation method.

In literature, reductive aminations with **61** are done in a multitude of ways, the most prominent method being the usage of sodium cyanoborohydride. However, its unavailability in the laboratory and its high price led to the exploration of alternative methods that could potentially be utilized in larger scales.

Several test reactions were conducted to see whether **61** could indeed be coupled via nitrogen-containing. The first reaction utilized allyl amine, as, should this reaction be

successful, the double bond that would be introduced could potentially be utilized to generate a polymer. Based on a procedure published by *Liu et al. (2013)*⁸¹, both allyl amine and **61** were dissolved in MeOH, after which NaBH₄ was added, and the mixture was stirred at 50 °C overnight. Alas, the reaction mixture turned into a brown, viscose liquid, and the desired product could not be detected with NMR. An alternative, yet similar method based on the work of *Shao et al. (2004)*⁸², using benzene as a solvent and adding a catalytic amount of p-toluenesulfonic acid (p-TsOH), yielded the same result, turning the reaction mixture into a brown, viscose liquid.

Next, a Leuckart amide synthesis was attempted based on the work of *Kobayashi et al. (2013)*.⁸³ In this procedure, **61** is dissolved in formic acid with formamide (**64**) and heated to 180 °C for two days. This reaction led to the same result as the previously conducted reactions: a brown, viscose liquid, in which the product could not be detected through NMR.

An overview of the conducted reactions is presented in figure 29.

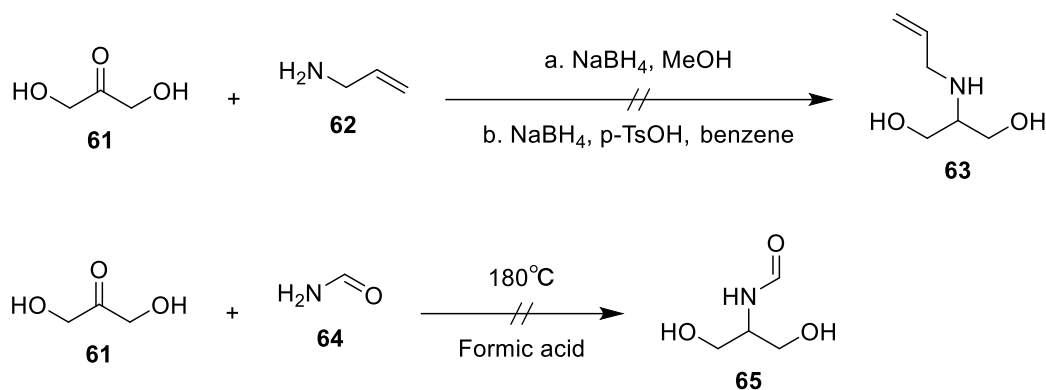


Figure 29. Top: Reductive amination of **61** with allyl amine (**62**). Bottom: Leuckart Amide Synthesis with **61** and formamide (**64**).

It was concluded that the main problem in using **61** would be its thermal instability. Even at room temperature, **61** will degrade into numerous degradation products over time, and even merely increasing the temperature to 40 °C significantly increases the degradation rate.⁸⁴ It was thus determined that **61** would not be a suitable 1,3-dialdehyde precursor for the scope of this project. However, it should be noted that several other methods have been published for the reductive amination of **61**, which could potentially be explored in future projects. For a proof-of-concept, a procedure utilizing sodium cyanoborohydride^{85,86} or sodium tris(acetoxy)borohydride⁸⁷ could be

attempted. Alternatively, the usage of hydrogen at increased pressure is also described, both using PtO₂⁸⁸ and Raney nickel⁸⁹.

3.3.1.3. Malonaldehyde bis(Phenylimine) (**66**).

Malonaldehyde bis(phenylimine) (**66**) is a fluorescent cyanine dye and, at its core, is a protected form of malonaldehyde. The possibility of functionalizing this compound at its central carbon was explored. Similar to the keto-enol tautomerism observed in 1,3-dicarbonyl compounds, **66** shows imine-enamine tautomerism, and so it is expected that the central carbon has a similar nucleophilic nature. To this end, its hydrochloride salt was first neutralized with an aqueous 5 M NaOH solution, yielding **66**. Then, the product was dissolved in acetonitrile, to which **54** was added dropwise. No base was added due to the expected basic nature of **66**, as it could be classified as a Schiff's base. The reaction mixture was then stirred for two days, though no conversion could be observed. Several other conditions were tested, including the usage of a Lewis acid to potentially increase the selectivity of the reaction in the same way it does for 1,3-dicarbonyls⁷⁸, the addition of KOtBu as a strong base, as **66** is assumed to be rather basic itself, as well as the addition of LiCl, as literature suggests that the lithium-ion may coordinate **66** in order to allow for a reaction at the central carbon⁹⁰, though none led to the generation of the desired product, suggesting that the central carbon in this compound may be too unreactive, potentially due to the stability of the conjugated system that is formed by the keto-enol tautomerism in adding to the two aromatic rings. The general reaction scheme is shown in figure 30, and the conditions are summarized in table 3.

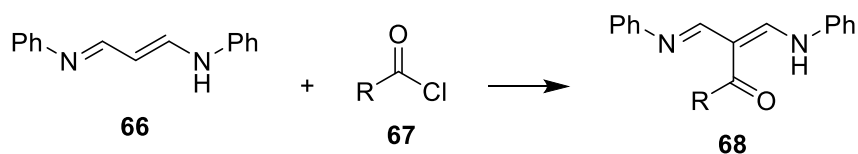


Figure 30. Reaction scheme of the functionalisation of the central carbon of **66**.

Table 3. Reaction conditions for the functionalisation of **66**.

	R =	Base	Additional reagents	Solvent	Result
1	Propyl	-	-	Toluene	x

2	t-Butyl	-	-	Toluene	x
3	t-Butyl	KOtBu	-	Toluene	x
4	t-Butyl	KOtBu	MgCl ₂	Toluene	x
5	t-Butyl	KOtBu	LiCl	Toluene	x

3.3.1.4. Serinol (**69**).

Similar to **61**, serinol (**69**) is a 1,3-diol with a reactive group at its central carbon, though while **61** has an electrophilic carbonyl group, **69** has a nucleophilic amine. The high cost of **69** at the time of writing this report may make it unsuitable for large-scale usage, but it could prove useful for generating a 1,3-dialdehyde-functionalised polymer for a proof-of-concept, which is, ultimately, the goal of this project.

The alkylation of the central amine group is well-described in literature with good yields, so adding **69** to a reactive polymer is expected not to be problematic.^{91–93} In particular, the work of *Fagerström et al. (2006)* proves interesting, as it describes the reaction between the **69** amine and an epoxide.⁹⁴ This suggests that **69** could likely be connected to the poly(glycidyl acrylate) available in this project.

Additionally, attempts have been made to oxidize **69** to form 2-amino-malonaldehyde to test its reactivity with urea. However, after several attempts, it became evident that the solubility of **69** in organic solvents would become a problem. Unfortunately, **69** only dissolves adequately in polar, organic solvents such as ethanol and water. However, these solvents are not compatible with oxidation conditions such as the aforementioned TCCA/TEMPO method, and a Swern- or Dess-Martin-oxidation would not be possible due to these limitations. For this reason, the focus was put on connecting **69** to poly(glycidyl acrylate), which will be described in a later chapter.

3.3.2. Potential 1,3-dialdehyde precursors for polymer functionalization.

When selecting suitable 1,3-dialdehyde precursors to be attached to polymeric structures, several factors need to be considered. As mentioned previously, **69** can be attached to poly(glycidyl acrylate) using the nucleophilic amine at the central position to induce a ring-opening reaction with the epoxide. When it comes to functionalizing

the amine-based polymers, however, an electrophilic structure is required to use the nucleophilic nature of the amines.

As **69** has been described in a previous chapter, the synthesis and optimization of the electrophilic precursor are described in the following.

3.3.3. The synthesis of an electrophilic 1,3-dialdehyde precursor: 2-Bromo-tetramethoxypropane (2-Br-TMP) (**39**).

As previously described, **38** is a protected derivative of malonaldehyde that can conveniently be deprotected under mildly acidic conditions. However, although one could assume that the central carbon has a rather low electron density due to the four ethers in its close proximity, in reality, it is rather unreactive.

Bredereck et al. (1962) previously described the bromination of the central carbon using N-bromosuccinimide and dibenzoyl peroxide, albeit with low reported yields (figure 31).⁹⁵ Unfortunately, the results reported in the paper could not be reproduced reliably. In particular, the purification through vacuum distillation at approximately 105 °C appeared rather odd, as the compound itself was observed to be thermally unstable.

Another work by *Eisert et al. (1960)* reported the synthesis of the same compound using bromine (figure 31).⁹⁶ Nevertheless, the same problem persisted regarding the purification of the compound. Ultimately, however, it was deemed to be acceptable to continue the experiments with an impure sample, as potentially unreacted compounds were not expected to interfere with the functionalization of the polymers.

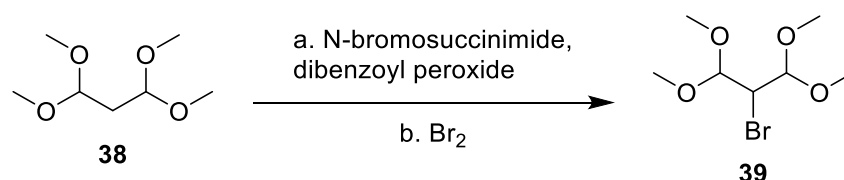


Figure 31. Bromination of the central carbon atom of **38** via the procedure of a) *Bredereck et al. (1962)* and b) *Eisert et al. (1960)*.

39 was observed to be a yellow oil that appeared shelf-stable for a limited amount of time at 4 °C, but, contrary to **38**, was found to hydrolyze to 2-bromomalonaldehyde by merely being exposed to air, leading to the formation of yellow crystals. The crystal

structure was determined to confirm the formation of the correct product and has been attached in the appendix of this thesis.

As **39** appeared to hydrolyze more readily than **38**, and as purification steps to obtain the pure compound were deemed unnecessary for the purpose of this work, it was deemed beneficial to immediately use the generated batch of **39** to functionalize the chosen polymers. However, to remove residual bromine and hydrobromic acid formed during the reaction, a neutralization step was deemed beneficial, especially as the functionalization is done under basic conditions.

For the neutralization, two different methods have been explored. The first method utilizes the introduction of an aqueous Na_2CO_3 solution, which proved to be effective. However, due to the hydrolysis sensitivity of **39**, a neutralization method that does not introduce water to the system would be preferred. Using a K_2CO_3 slurry in dry DCM would allow the HBr to be neutralized without introducing water to the system, which led to a similar degree of purity. While both methods led to a yield of approximately 58 – 65%, the use of a K_2CO_3 slurry was preferred for the reasons specified above.

3.4. Functionalising the chosen polymeric structures.

Substitution reactions between both primary and secondary amines and bromides are well-described in literature using many different reagents, though generally, the reaction is facilitated through the use of a base such as triethylamine (TEA) or N,N-diisopropylethylamine (DIPEA).^{97–100} The ring-opening reaction between **69** and an epoxide has also been described in several works.^{94,101} Using the foundations laid by these works, the functionalization of the polymeric structures is described in the next chapters.

It is important to note that a high degree of functionalisation is not required, as the goal of this study is to determine qualitatively whether the synthesized materials are capable of binding urea. Even a lower functionalisation degree of approximately 40 – 50% or lower ought to be sufficient, as shown by *Jong et al. (2019)*.¹⁵

The samples will be analysed with ATR-IR spectrometry, and the most notable peaks shall be mentioned in the text. The IR spectra shall be included in the appendix of this work.

3.4.1. The functionalisation of poly(glycidyl acrylate) (**35**) with serinol (**69**).

As previously mentioned, the synthesis of porous **35** was done by Dr Piet Driest. The functionalization of the polymer with **69** could conveniently be done by adding the polymer to a solution of **69** in DMF, which was then heated to about 80 °C overnight. The resulting structure was then oxidized using the aforementioned TCCA/TEMPO conditions. An overview of the reactions is presented in figure 32.

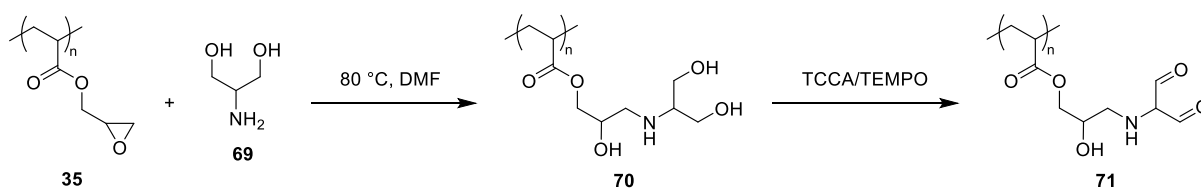


Figure 32. The functionalisation of **35** with **69**.

To determine whether the reaction was successful, **70** and **71** were examined with ATR-IR spectrometry. Comparing the IR spectra of **35** and **70**, the addition of **69** to the polymer can clearly be observed through the rise of NH vibration peaks at around 2937 cm^{-1} , as well as the clear formation of the alcohol stretch peak at 3305 cm^{-1} , showing that the ring-opening reaction did, indeed, occur. Further, the alcohol peak vanished after the oxidation reaction, suggesting that the hydroxy group formed through the ring-opening reaction was also oxidized. A small peak at 2789 cm^{-1} is interpreted as the rise of the aldehyde C-H peak. However, the C=O carbonyl peak of the aldehyde groups cannot be clearly observed, perhaps due to overlapping with the carbonyl peaks of the formed ketone, as well as the ester C=O. However, a peak at 1710 cm^{-1} , contrary to the previously present ester carbonyl peak at 1720 cm^{-1} , also suggests that the secondary amine may have been oxidized to form an imine, as shown in figure 33. This would lead to a structure without a central proton, which, as mentioned previously, would obstruct the structure from reacting with urea. Ultimately, whether or not the polymer will be able to react with urea shall be assessed in a later chapter.

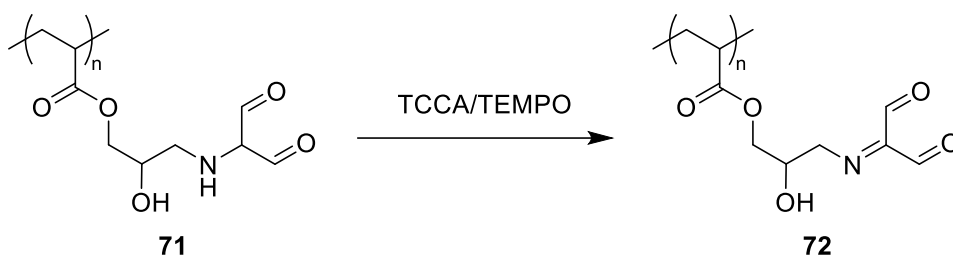


Figure 33. Potential oxidation of the secondary amine, leading to a 1,3-dialdehyde structure with a quaternary central carbon atom (**72**).

3.4.2. The functionalization of poly(TEPA) (**37**) with 2-Br-TMP (**39**).

As previously described, **39** is immediately used to functionalise **37** after the neutralization step. After the K_2CO_3 slurry was added, the reaction mixture was stirred for 15 minutes to neutralize the sample. The solids were then filtered off, and **37** was added to the solution. Then, 10 equivalents of DIPEA were added, and the reaction mixture was stirred overnight. After washing the polymer thoroughly with MeCN and water and subsequent drying, it was hydrolysed in 1 M HCl overnight. Finally, it was analysed with ATR-IR spectrometry.

With the emergence of a strong peak at 1602 cm^{-1} after the reaction, it can be assumed that the coupling reaction was successful with a satisfactory yield. The reaction scheme is presented in figure 34.

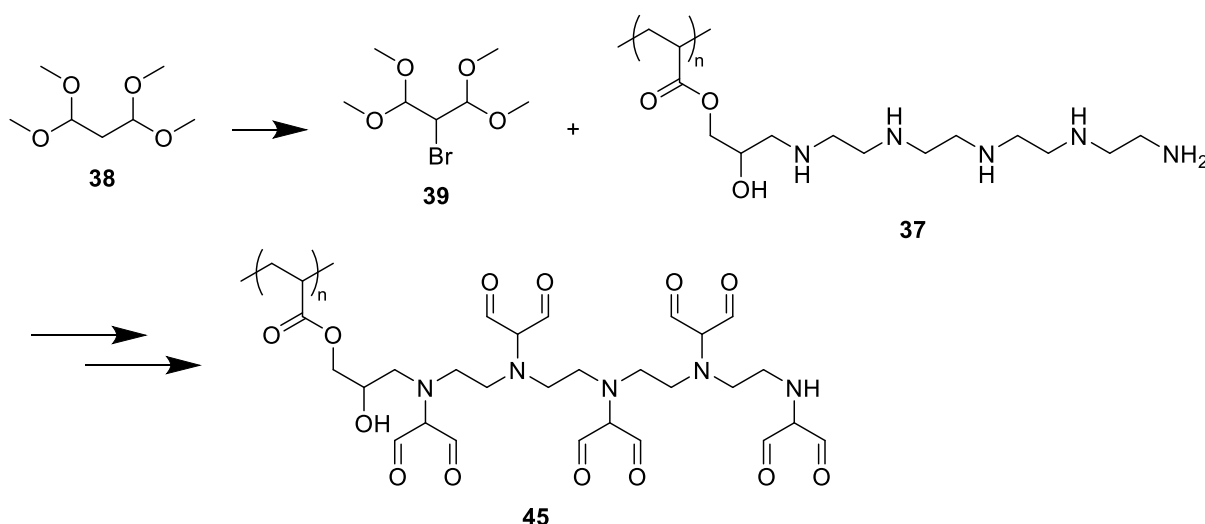


Figure 34. Reaction overview of the functionalisation of **37**.

3.4.3. The functionalization of poly(vinylamine) (**33**) with 2-Br-TMP (**39**).

The functionalization of **33** was done via the same procedure as described in 3.4.2. The polymer was subsequently also analysed using ATR-IR spectrometry.

Similar to the functionalised **37**, this sample shows the formation of a peak at 1601 cm^{-1} , suggesting that the functionalisation was successful to a certain extent. However, as mentioned in the previous chapters, the degree to which poly(N-vinyl formamide) was converted to **33** is unclear, which ought to be kept in mind.

The reaction scheme is shown in figure 35.

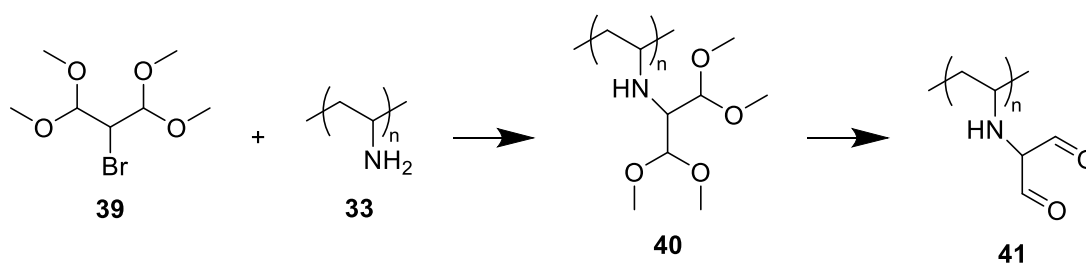


Figure 35. Reaction overview of the functionalisation of **33**.

3.5. **Measuring the urea-reactivity of chosen functionalized polymeric structures.**

The ability of the prepared materials to bind urea is determined for **41**, **45** and **71**. All three samples were measured through addition to a 50 mM urea solution in PBS at 323.15 K to ensure sufficient swelling of the material to allow urea to penetrate the pores of the materials and replicate the conditions of a dialysis procedure.

To determine whether the materials can bind urea, samples are taken from the solution at regular intervals to determine the decrease in urea concentration. For this, the supernatant was filtered and analysed using a colourimetric urea assay kit. A schematic overview is depicted in figure 36.

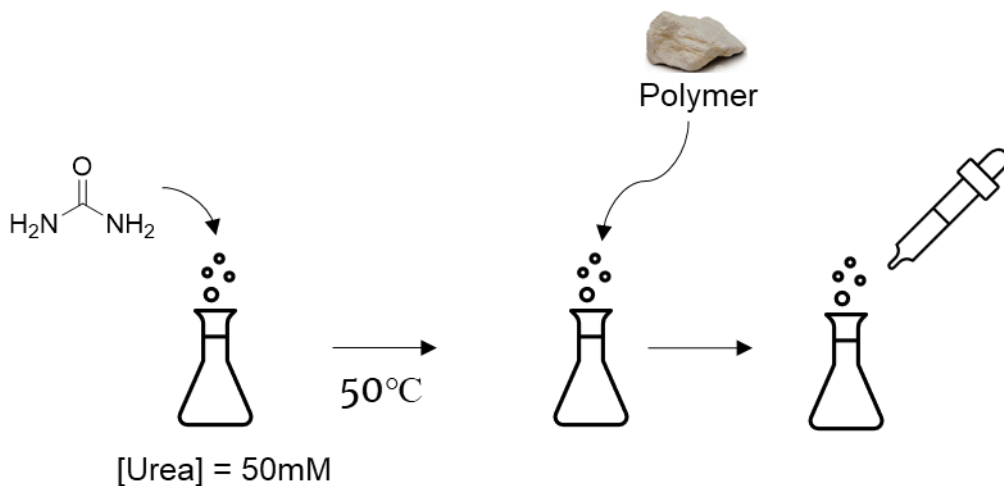


Figure 36. Schematic overview of the urea-reactivity measurement of the synthesized polymeric structures.

The samples were taken after 0.5, 1, 2, 4, 8 and 24 hours. The measured urea concentrations are plotted, showing the urea concentration on the y-axis and the time progression on the x-axis.

3.5.1. Measuring urea reactivity of 41.

The urea-reactivity measurement of **41** is shown in figure 37.

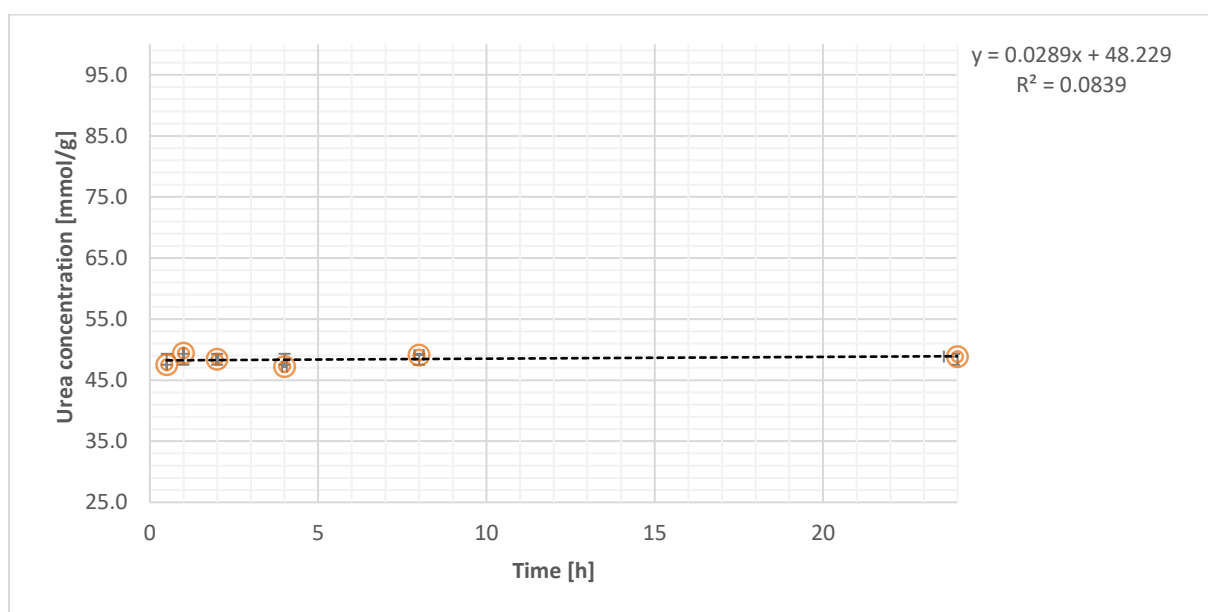


Figure 37. Graphical depiction of the change in urea concentration of the supernatant of **41** in PBS at 323.15 K.

Through regression analysis, the data would suggest that the urea concentration increases, though this can be attributed to the error margin of the measurement. Evidently, **41** does not show the ability to bind urea at a neutral pH.

The precise reason for this is unknown, though several factors that may have impacted the results are the fact that the functionalisation degree of the material is difficult to determine accurately through merely using ATR-IR spectrometry. Additionally, it is entirely possible that the 1,3-dialdehyde structure with a secondary amine attached to its central carbon simply does not react with urea at a neutral pH, similar to malonaldehyde.

3.5.2. Measuring urea reactivity of 45.

The urea-reactivity measurement of **45** is shown in figure 38.

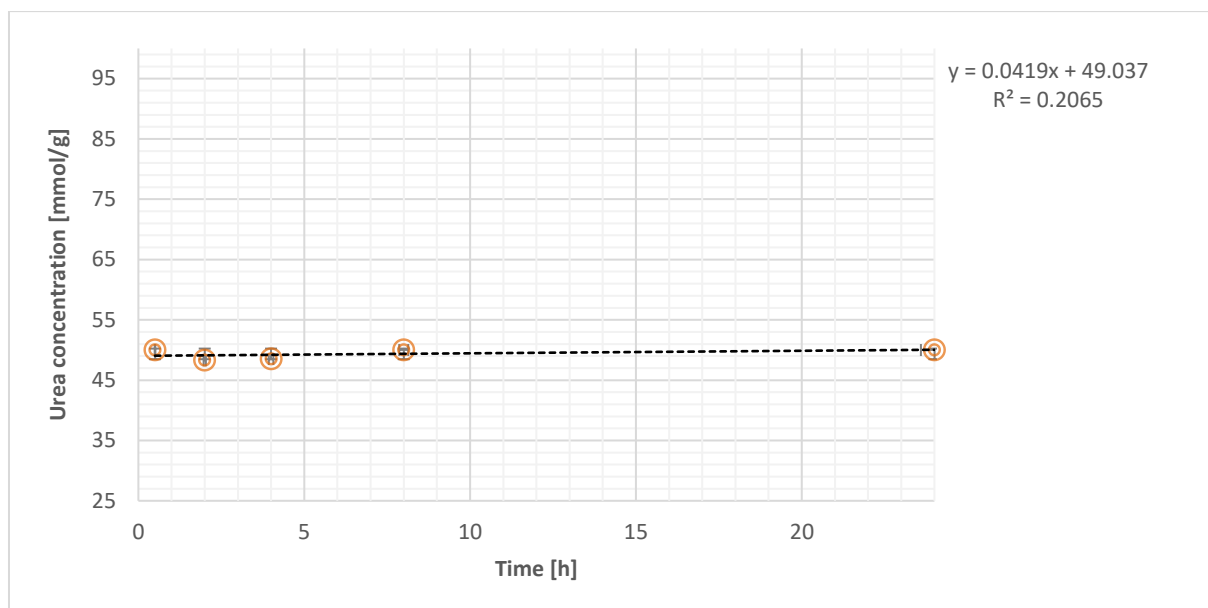


Figure 38. Graphical depiction of the change in urea concentration of the supernatant of **45** in PBS at 323.15 K.

Similar to the measurement of **41**, the supernatant of **45** does not show a decrease in urea concentration. As the IR-data of **45** shows a clear formation of a peak that can be attributed to the 1,3-dialdehyde structure, this data would suggest that a 2-amino-1,3-dialdehyde structure is indeed not capable of reacting with urea under physiological conditions.

3.5.3. Measuring urea reactivity of 71.

The urea-reactivity measurement of **71** is shown in figure 39.

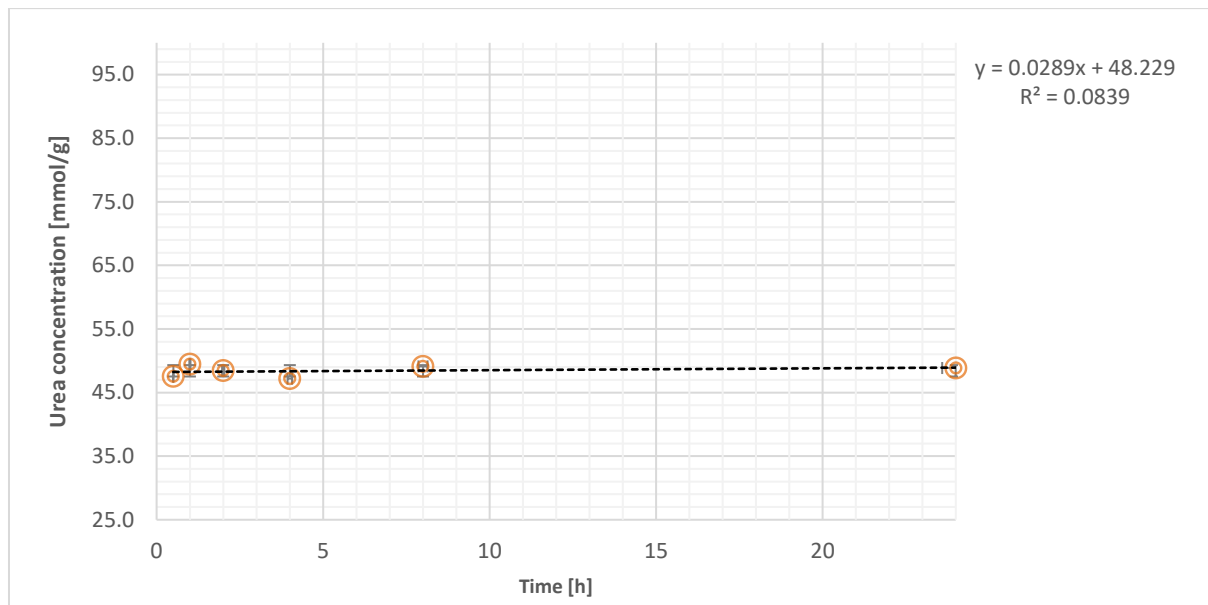


Figure 39. Graphical depiction of the change in urea concentration of the supernatant of **71** in PBS at 323.15 K.

As expected, based on the results of **41** and **45**, **71** does not show the ability to bind urea, either.

3.5.4. Additional considerations.

It should be noted that, while the precursor materials PNVF and **35** have relatively well-described properties, the same cannot be said of the functionalised structures. It is unknown whether the functionalisation may have negatively impacted the ability of the polymeric structures to swell sufficiently for urea to penetrate the pores, or whether the porosity was negatively affected. However, the further analysis of these materials falls outside the scope of this project, and, as none of the materials shows any urea binding capacity, this is unlikely to be beneficial.

4. Conclusions

Within the scope of this thesis, various valuable pieces of information could be collected on the utility of 1,3-dialdehyde-functionalised structures for the binding of urea in a WAK device. While **41**, **45** and **71** may not have shown the ability to bind urea under physiological conditions, they are nevertheless interesting structures that could potentially be investigated for other applications. If the synthesized materials show similar reactivity to malonaldehyde under more acidic conditions, they could potentially be utilized as recyclable, green alternatives to remove urea from wastewater, assuming that the binding is reversible under certain conditions. Due to time constraints, however, this was not investigated within the scope of this project.

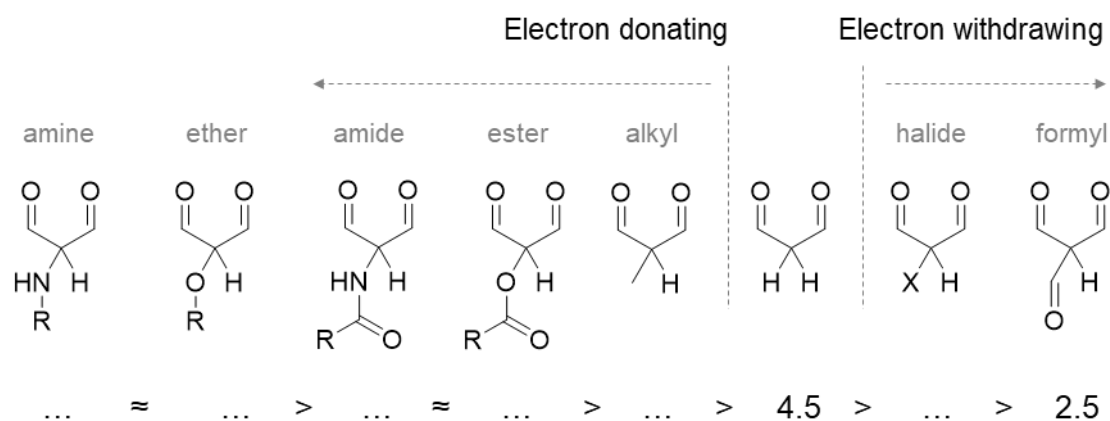


Figure 40. Expected decreasing order of pK_A-values of enolizable MDA-derivatives based on the electron-donating / -withdrawing effect of substituents in the 2-position.

As previously mentioned (and shown in figure 40), it is expected that an amine connected to the central carbon of a 1,3-dialdehyde structure would have the largest effect on the pH of the central proton. As the results of this study show that these structures cannot bind urea under physiological conditions, it seems unlikely that ethers, amides and esters would. In the case of alkyl-substituted structures, several papers report that alkylated malonaldehyde derivatives react with urea under acidic conditions with heating, making it unlikely that the synthesis of a polymer with alkylated 1,3-dialdehyde structures would be fruitful for the application in a WAK device.^{69,70}

5. Outlook

Whilst, based on the results of this project, the utilization of 1,3-dialdehyde structures for the binding of urea under physiological conditions may not be suited, there is still plenty of room for optimization of the 1,2-dicarbonyl structures mentioned in the literature review of this thesis. While ninhydrin-functionalised polymeric structures appear to have the highest urea binding capacity at the time of writing this work, it does come with its own set of challenges, including the relative difficulty in its synthesis pathway and the expensive starting materials required. On the other hand, Phenylglyoxal-type sorbents utilize relatively cheap starting materials and can easily be synthesized, though they have a lower binding capacity. Of course, a major drawback for both structures is the high molecular weight per monomeric unit due to the presence of the aromatic ring.

The work of *Baccollini et al. (2011)* shows that the reactivity between glyoxal, as well as several simple derivatives, and urea (as well as thiourea) could be boosted through catalysis with cyclic phosphorous compounds, using P_2O_5 to gain quantitative yields in merely 10 minutes at room temperature in water.⁵⁰ Within the scope of this project, an experiment was conducted to investigate whether this catalytic mechanism could potentially be utilized for phenylglyoxal-type sorbents. To this end, phenylglyoxal was dissolved in PBS with 50 mM urea with an equivalent P_2O_5 . Indeed, after two hours, the reaction product formation could be detected in ^{13}C -NMR (the data can be found in the appendix of this work). Though the kinetics of this conversion were not determined, it could certainly be an interesting pathway to explore in a future project. However, as the paper suggests that the catalytic effect depends on the cyclic nature of the phosphorous compound, perhaps a more bio-compatible alternative to P_2O_5 (as well as a less acidic one) would be recommended. The works of *Lim & Seib (2003)* and *Illy et al. (2015)* provide valuable information in this regard, and sodium trimetaphosphate, used in the food industry as an efficient starch cross-linking agent with very low toxicity, may prove to be an interesting candidate.^{102,103}

Further, the reduction of molecular weight per monomeric unit may allow for more urea binding per gram of sorbent material. The experiments of this work

binding serinol to poly(glycidyl acrylate) may provide valuable information in this regard. In particular, 3-amino-propane-1,3-diol, as shown in figure 41, may prove to be useful in this regard.

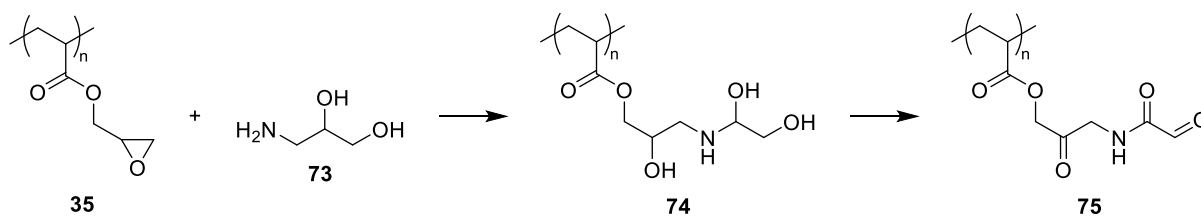


Figure 41. Hypothesized functionalisation of poly(glycidyl acrylate) (**35**) with 3-amino-propane-1,3-diol (**73**), followed by an oxidation step to form polymeric structure **75**.

6. Experimental section

6.1. Preface

6.1.1. General information

Air- and moisture-sensitive reactions were carried out under a nitrogen atmosphere. Moisture- and air-sensitive reagents were transferred into disposable syringes and cannulas previously rinsed with nitrogen. The chemicals used were purchased from the companies ACROS, ALFA AESAR, APPLICHEM, CARBOLUTION CHEMICALS, FLUKA, MERCK, ROTH, SIGMA-ALDRICH and VWR CHEMICALS and used directly.

6.1.2. Solvents

The solvents used for the reactions were of "for synthesis" or "for analysis" quality and were used without further purification. All dry solvents were stored under a nitrogen atmosphere and on molecular sieve.

6.1.3. NMR

All NMR spectra were measured on an AGILENT 400-MR DD2 equipped with a OneNMR probe or a BRUKER 600 MHz with a BBI probe. In the ^1H and ^{13}C experiments, the shifts were related to the residual proton content of the solvent and to the carbon atoms of the solvent:

	^1H -NMR	^{13}C -NMR
d_1 -Chloroform	7.26 ppm	77.0 ppm
d_6 -DMSO	2.50 ppm	39.5 ppm
d_4 -Methanol	3.31 ppm	49.0 ppm
D_2O	4.79 ppm	-

All chemical shifts δ are in ppm and all coupling constants J in Hz. The following abbreviations were used to describe the spectra: s (singlet), d (doublet), t (triplet), and m (multiplet). It should be noted that the integrations reported may be higher than expected for the target compounds due to impurities that were not removed from the sample, as they were deemed unproblematic for further reactions.

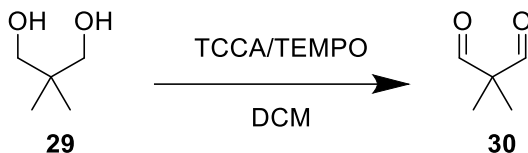
6.1.4. IR

For recording the infrared spectra, a PERKINELMER ATR-IR probe was utilized. The recorded data were visualized and edited using PerkinElmer Spectrum Version 10.4.3.

6.2. Experiments

6.2.1. Small-molecule syntheses.

6.2.1.1. The synthesis of 2,2-dimethyl-malonaldehyde (**30**).



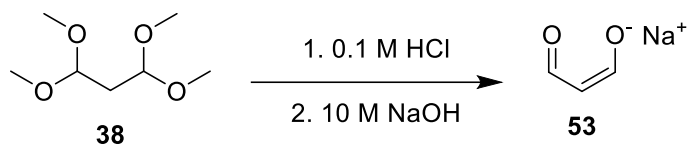
TCCA (9.37 g, 40.32 mmol, 2,10 eq.) is added to a solution of 2,2-dimethylpropane-1,3-diol (**29**) (2.00 g, 19.2 mmol, 1.00 eq.) in 40 mL dry DCM, and the solution is stirred and brought to 0 °C with an ice bath. TEMPO (60 mg, 0.38 mmol, 0.02 eq.) is added, and the mixture is brought to room temperature. The mixture is stirred for 30 minutes, and is then filtered through a celite pad. The filtrate is washed with 15 mL of saturated Na₂CO₃, followed by 15 mL 1 M HCl and 15 mL brine. The organic phase is dried over MgSO₄, and the solvent is removed *in vacuo* to give **30** (1.38 g, 72%).

The sample was not purified any further.

¹H NMR (400 MHz, CDCl₃) δ 9.58 (s, 1H), 5.25 (s, 1H), 4.13 (s, 1H), 1.28 (s, 5H), 1.08 (s, 1H).

¹³C NMR (101 MHz, CDCl₃) δ 200.50, 77.35, 77.03, 76.71, 68.38, 58.76, 53.39, 46.36, 19.55, 18.80, 17.17, 15.37.

6.2.1.2. The synthesis of malonaldehyde sodium salt (**53**).



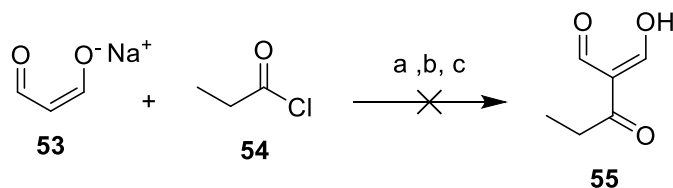
1,1,3,3-tetramethoxypropane (**38**) (4.00 g, 24.36 mmol, 1 eq.) is added to 64 mL 0.1 M HCl at 0 °C. Without stirring, the mixture is kept at 5 °C for 24 hours. The mixture is then rapidly brought to pH 10 with 10 M NaOH, and 6 g activated carbon is added to the mixture. The reaction mixture is then stored at 5 °C overnight. The solids are filtered off, and the solvent is removed *in vacuo* to give **53** (1.57 g, 69%).

¹H NMR (400 MHz, D₂O) δ 8.50 (dd, *J* = 10.1, 0.9 Hz, 2H), 5.16 (t, *J* = 10.1 Hz, 1H).

¹³C NMR (101 MHz, D₂O) δ 192.85, 109.45.

IR (neat): ν_{max} (cm⁻¹) = 3342.81 (m), 2818.37 (w), 2775.75 (w), 1719.27 (w), 1601.80 (s), 1371.03 (s), 1290.42 (w), 1268.89 (m), 1173.88 (m), 1019.53 (w), 813.79 (w), 800.33 (w), 602.80 (w)

6.2.1.3. The synthesis of (E)-2-formyl-3-oxopent-1-en-1-olate (**55**).



Procedure a: Propionyl chloride (**54**) (0.44 mL, 5 mmol, 1 eq.) is added to a solution of DCC (1.14 g, 5.5 mmol, 1.1 eq.) and DMAP (30 mg, 0.25 mmol, 0.05 eq.) in 12 mL dry MeCN at 0 °C. After stirring for 15 minutes, Malonaldehyde sodium salt (**53**) (0.47 g, 5 mmol, 1 eq.) is added, and the mixture is stirred at room temperature for 48 hours. The solids are filtered off, and the filtrate is washed with saturated NH₄Cl solution and brine. The solvent is removed *in vacuo*. No product could be observed in the crude residue, as indicated by the NMR data.

¹H NMR (400 MHz, D₂O) δ 7.92 – 7.83 (m, 1H), 6.78 – 6.70 (m, 1H), 3.43 (qd, *J* = 7.1, 0.8 Hz, 2H), 3.07 (d, *J* = 0.7 Hz, 3H), 2.09 (s, 3H), 1.05 (td, *J* = 7.1, 0.8 Hz, 3H).

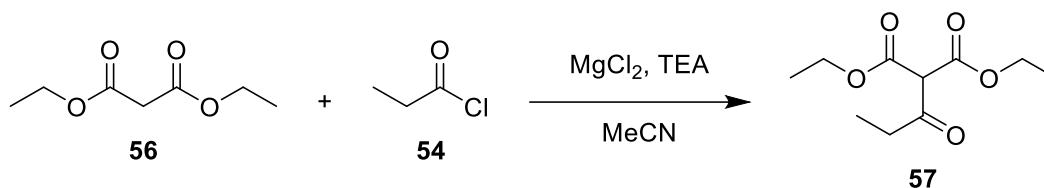
Procedure b: MgCl₂ (0.47 g, 5 mmol, 1 eq.) is added to 5 mL dry MeCN. Malonaldehyde sodium salt (**53**) (0.47 g, 5 mmol, 1 eq.) is added, and the mixture is cooled to 0 °C. Triethylamine (0.69 mL, 10 mmol, 2 eq.) is added, and the reaction mixture is stirred for 15 minutes. Propionyl chloride (**54**) (0.44 mL, 5 mmol, 1 eq.) is added, and the reaction mixture is brought to room temperature and stirred for 15 hours. The reaction mixture is then brought to 0 °C, quenched with 5 M HCl, and the solvent is removed *in vacuo*. No product could be observed in the crude residue, as indicated by the NMR data.

¹H NMR (400 MHz, D₂O) δ 4.63 (s, 1H), 3.05 (qd, *J* = 7.4, 0.9 Hz, 5H), 2.09 (s, 1H), 1.93 (s, 1H), 1.92 (s, 7H), 1.13 (td, *J* = 7.3, 0.9 Hz, 7H), 0.95 – 0.85 (m, 1H).

Procedure c: See procedure b; MgCl₂ was left out. No product could be observed in the crude residue, as indicated by the NMR data.

¹H NMR (400 MHz, D₂O) δ 3.06 (q, *J* = 7.3 Hz, 6H), 2.08 (s, 2H), 2.11 – 2.01 (m, 1H), 1.14 (t, *J* = 7.4 Hz, 8H), 0.91 (t, *J* = 7.6 Hz, 1H).

6.2.1.4. The synthesis of diethyl 2-propionylmalonate (**57**).

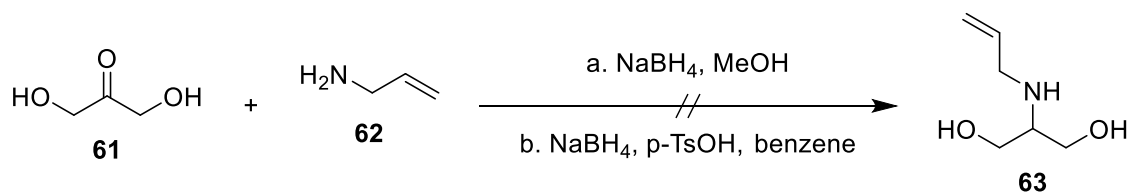


MgCl₂ (2.40 g, 25 mmol, 1 eq.) is added to 25 mL dry DCM. Diethyl malonate (**56**) (3.8 mL, 25 mmol, 1 eq.) is added, and the reaction mixture is cooled to 0 °C. Triethylamine (6.97 mL, 50 mmol, 2 eq.) is added, and after stirring for 15 minutes, propionyl chloride (**54**) (2.18 mL, 25 mmol, 1 eq.) is added. The mixture is stirred at 0 °C, and consequently stirred at room temperature for 15 hours. The mixture is then cooled to 0 °C and quenched with 5 M HCl. The layers are separated, and the aqueous layer is extracted three times with Et₂O. The organic phases are unified, dried over MgSO₄ and the solvent is removed *in vacuo* to yield **57** (4.72 g, 87%).

¹H NMR (400 MHz, CDCl₃) δ 4.26 – 4.10 (m, 4H), 2.59 (qd, *J* = 7.2, 1.0 Hz, 1H), 2.41 (qd, *J* = 7.6, 1.0 Hz, 1H), 2.12 (d, *J* = 1.1 Hz, 10H), 1.88 – 1.78 (m, 1H), 1.25 (dtd, *J* = 7.0, 5.8, 1.0 Hz, 6H), 1.19 – 1.10 (m, 1H), 1.06 (td, *J* = 7.2, 1.1 Hz, 2H).

¹³C NMR (101 MHz, CDCl₃) δ 206.93, 199.53, 183.97, 171.17, 164.65, 99.15, 65.05, 62.21, 61.22, 60.88, 35.30, 30.82, 27.27, 14.01, 13.97, 13.88, 10.94, 7.51.

6.2.1.5. The synthesis of 2-(allylamino)propane-1,3-diol (**63**).



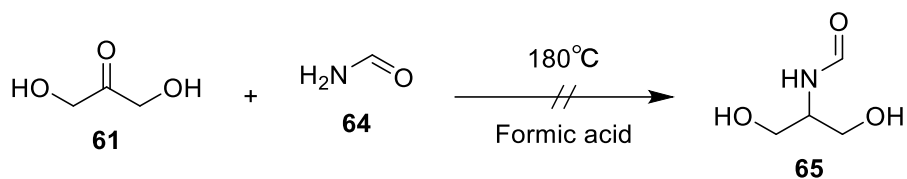
Procedure a: Dihydroxyacetone (**61**) (0.90 g, 10 mmol, 2 eq.) and allylamine (**62**) (0.37 mL, 5 mmol, 1 eq.) are added to 20 ml of dry MeOH. The mixture is stirred at room temperature for two hours, after which it is cooled to 0 °C, followed by the slow addition of NaBH₄ (0.47 g, 12.5 mmol, 2.5 eq.). The reaction mixture is then stirred overnight at 50 °C. The mixture is then allowed to reach room temperature, and 10 mL H₂O is added. MeOH is removed *in vacuo*, and a further 20 mL H₂O is added. The aqueous phase is then extracted three times with EtOAc, and the combined organic phases are washed with brine. The organic phase is then dried over Na₂SO₄, and the solvent is removed *in vacuo*. No product could be observed in the residue, as indicated by the NMR data.

¹H NMR (400 MHz, CDCl₃) δ 5.82 (s, 3H), 5.17 (s, 4H), 5.25 – 5.12 (m, 1H), 5.09 (d, *J* = 9.1 Hz, 1H), 3.73 – 3.53 (m, 2H), 3.47 (s, 2H), 3.50 – 3.25 (m, 1H), 1.16 – 1.04 (m, 1H).

Procedure b: Dihydroxyacetone (**61**) (0.45 g, 5 mmol, 1 eq.), p-toluenesulfonic acid monohydrate (0.04 g, 0.02 mmol, cat.) and allylamine (**62**) are added to 15 mL benzene. The reaction mixture is refluxed overnight, after which the mixture is filtered and the solvent is removed *in vacuo*. The residue is redissolved in 15 mL EtOH, and NaBH₄ (0.19 g, 5 mmol, 1 eq.) is added slowly at 0 °C. The reaction mixture is then stirred for one hour at room temperature. The reaction is quenched by adding 15 mL H₂O and extracted three times with EtOAc. The organic phase is dried over MgSO₄, and the solvent is removed *in vacuo*. No product could be observed in the crude residue, as indicated by the NMR data.

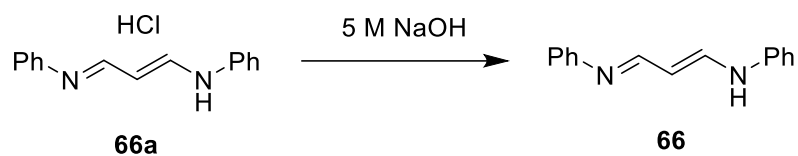
¹H NMR (600 MHz, CDCl₃) δ 5.76 (s, 5H), 5.13 (s, 4H), 5.08 (s, 3H), 5.01 (s, 3H), 3.86 – 3.41 (m, 1H), 3.16 (s, 5H), 2.68 (s, 1H), 2.26 – 1.90 (m, 2H), 1.26 – 1.13 (m, 1H).

6.2.1.6. The synthesis of N-(1,3-dihydroxypropan-2-yl)formamide (**65**).



A mixture of dihydroxyacetone (**61**) (4.00 g, 20 mmol, 1 eq.), formamide (**64**) (9.3 mL, 23.3 mmol, 1.17 eq.) and formic acid (6.2 mL, 16.4 mmol, 0.82 eq.) is heated to 180 °C for 48 hours. The mixture is then cooled to room temperature, and 50 mL H₂O is added. The product is extracted three times with EtOAc, and the combined organic layers are washed with H₂O, saturated NaHCO₃ solution and brine. The organic phase is then dried over MgSO₄, and the solvent is removed *in vacuo*. The residue was a brown slurry, which was not further analysed.

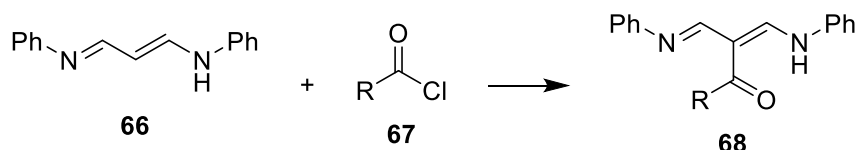
6.2.1.7. The neutralization of malonaldehyde bis(phenylimine) hydrochloride (**66a**).



Malonaldehyde bis(phenylimine) monohydrochloride (**66a**) (2.5 g, 9.6 mmol, 1 eq.) is added to 200 mL H₂O. 44 mL 5 M NaOH is added, and the solution is stirred for 12 hours at room temperature. The solids are then collected through filtration and washed with 50 mL H₂O. The solids are then dried under vacuum to yield **66** (1.73 g, 81%).

¹H NMR (400 MHz, CDCl₃) δ 7.70 (d, *J* = 6.3 Hz, 2H), 7.37 – 7.25 (m, 5H), 7.17 – 6.99 (m, 7H), 5.10 (s, 1H).

6.2.1.8. The synthesis of 2-substituted malonaldehyde bis(phenylimine) (**68**).



Index	R =	Base	Additional reagents	Solvent
a	Propyl	-	-	Toluene
b	t-Butyl	-	-	Toluene
c	t-Butyl	KOtBu	-	Toluene
d	t-Butyl	KOtBu	MgCl ₂	Toluene
e	t-Butyl	KOtBu	LiCl	Toluene

Procedure a: A solution of malonaldehyde bis(phenylimine) (**66**) (22 mg, 0.1 mmol, 1 eq.) in 2.5 mL toluene is cooled to 0 °C, and propionyl chloride (**67a**) (7 μL, 0.1 mmol, 1 eq.) is added dropwise. The mixture is stirred for 24 hours at room temperature. The mixture is filtered, and the solvent is removed *in vacuo*. No product could be observed in the crude residue, as indicated by the NMR data.

¹H NMR (400 MHz, CDCl₃) δ 7.82 – 7.71 (m, 1H), 7.58 – 7.43 (m, 2H), 7.47 – 7.27 (m, 17H), 4.98 (q, *J* = 1.8 Hz, 1H), 4.95 – 4.82 (m, 2H), 4.72 – 4.41 (m, 11H), 4.24 (ddd, *J* = 6.2, 4.8, 1.0 Hz, 1H), 4.13 – 4.02 (m, 3H), 3.53 – 3.35 (m, 10H), 3.25 (ddd, *J* = 10.2, 7.4, 0.9 Hz, 1H), 1.94 – 1.87 (m, 1H).

¹³C NMR (101 MHz, CDCl₃) δ 137.80, 137.52, 137.42, 132.36, 132.26, 131.59, 128.64, 128.57, 128.53, 128.51, 128.47, 128.22, 128.09, 128.07, 128.04, 127.88, 127.84, 108.33, 100.92, 86.67, 83.85, 82.06, 81.98, 81.79, 77.67, 77.32, 77.01, 72.75, 72.72, 72.58, 72.14, 56.10, 55.59, 4.73, 3.20.

Procedure b: A solution of malonaldehyde bis(phenylimine) (**66**) (1.11 g, 5 mmol, 1 eq.) in 30 mL toluene is cooled to 0 °C, and pivaloyl chloride (**67b**) (0.61 mL, 5 mmol, 1 eq.) is added dropwise. The mixture is stirred for 24 hours at room temperature. The

mixture is filtered, and the solvent is removed *in vacuo*. No product could be observed in the crude residue, as indicated by the NMR data.

¹H NMR (400 MHz, CDCl₃) δ 7.55 – 7.41 (m, 2H), 7.34 – 7.26 (m, 1H), 7.24 – 7.04 (m, 1H), 1.30 (s, 5H), 1.30 (d, *J* = 10.0 Hz, 1H), 1.23 (d, *J* = 11.6 Hz, 11H), 1.10 (s, 2H).

¹³C NMR (101 MHz, CDCl₃) δ 173.98, 137.99, 129.83, 129.71, 129.68, 128.93, 124.17, 119.91, 114.24, 41.87, 40.17, 39.57, 28.89, 27.61, 26.97, 26.48.

Procedure c: A solution of malonaldehyde bis(phenylimine) (**66**) (0.43 g, 1.9 mmol, 1 eq.) and KOtBu (0.25 g, 2.2 mmol, 1.2 eq.) in 25 mL toluene is cooled to 0 °C, and pivaloyl chloride (**67c**) (0.23 mL, 1.9 mmol, 1 eq.) is added dropwise. The mixture is stirred for 24 hours at room temperature. The mixture is filtered, and the solvent is removed *in vacuo*. No product could be observed in the crude residue, as indicated by the NMR data.

¹H NMR (400 MHz, CDCl₃) δ 8.29 (dd, *J* = 14.2, 0.5 Hz, 1H), 8.10 (dd, *J* = 9.3, 0.5 Hz, 1H), 7.69 (d, *J* = 6.4 Hz, 2H), 7.56 – 7.38 (m, 3H), 7.38 – 6.99 (m, 20H), 5.27 (dd, *J* = 14.2, 9.2 Hz, 1H), 5.10 (s, 1H), 2.34 (s, 1H), 1.31 (s, 1H), 1.29 – 1.19 (m, 1H), 1.10 (s, 7H).

¹³C NMR (101 MHz, CDCl₃) δ 176.64, 160.65, 151.95, 145.13, 138.80, 137.85, 130.22, 129.70, 129.33, 129.07, 129.01, 128.20, 125.43, 125.27, 123.48, 120.71, 118.13, 113.68, 77.31, 76.99, 76.67, 41.64, 29.07, 27.62, 21.43.

Procedure d: A solution of malonaldehyde bis(phenylimine) (**66**) (1.11 g, 5 mmol, 1 eq.) with MgCl₂ (0.48 g, 5 mmol, 1 eq.) and KOtBu (0.68 g, 6 mmol, 1.2 eq.) in 30 mL toluene is cooled to 0 °C, and pivaloyl chloride (**67b**) (0.61 mL, 5 mmol, 1 eq.) is added dropwise. The mixture is stirred for 24 hours at room temperature. The mixture is filtered, and the solvent is removed *in vacuo*. No product could be observed in the crude residue, as indicated by the NMR data.

¹H NMR (400 MHz, CDCl₃) δ 8.29 (dd, *J* = 14.2, 0.6 Hz, 1H), 8.10 (dd, *J* = 9.3, 0.6 Hz, 1H), 7.71 (s, 2H), 7.57 – 7.38 (m, 4H), 7.42 – 7.00 (m, 17H), 5.34 – 5.21 (m, 1H), 2.15

(s, 1H), 1.30 (d, $J = 0.9$ Hz, 4H), 1.25 (s, 1H), 1.09 (d, $J = 0.6$ Hz, 9H), 1.02 – 0.89 (m, 1H).

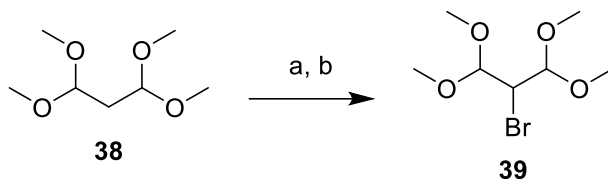
^{13}C NMR (101 MHz, CDCl_3) δ 176.64, 160.66, 151.93, 145.13, 138.78, 130.21, 129.70, 129.33, 129.07, 128.94, 125.44, 124.17, 120.71, 119.90, 118.13, 115.07, 113.67, 77.31, 77.19, 76.99, 76.67, 41.64, 30.91, 29.06, 27.62.

Procedure e: A solution of malonaldehyde bis(phenylimine) (**66**) (1.11 g, 5 mmol, 1 eq.) with LiCl (0.21 g, 5 mmol, 1 eq.) and KOtBu (0.68 g, 6 mmol, 1.2 eq.) in 30 mL toluene is cooled to 0 °C, and pivaloyl chloride (**67b**) (0.61 mL, 5 mmol, 1 eq.) is added dropwise. The mixture is stirred for 24 hours at room temperature. The mixture is filtered, and the solvent is removed *in vacuo*. No product could be observed in the crude residue, as indicated by the NMR data.

^1H NMR (400 MHz, CDCl_3) δ 8.29 (d, $J = 14.2$ Hz, 1H), 8.10 (d, $J = 9.2$ Hz, 1H), 7.71 (s, 3H), 7.55 – 7.41 (m, 3H), 7.40 – 7.27 (m, 8H), 7.27 – 7.19 (m, 3H), 7.19 – 7.00 (m, 12H), 5.27 (dd, $J = 14.3, 9.3$ Hz, 1H), 2.15 (s, 1H), 1.31 (d, $J = 0.6$ Hz, 2H), 1.09 (d, $J = 0.6$ Hz, 9H).

^{13}C NMR (101 MHz, CDCl_3) δ 176.64, 160.66, 151.94, 145.13, 138.78, 130.21, 129.71, 129.36, 129.33, 129.07, 128.94, 125.44, 120.71, 118.13, 113.67, 77.32, 77.00, 76.68, 41.64, 30.91, 29.07, 27.62.

6.2.1.9. The synthesis of 2-bromo-1,1,3,3-tetramethoxypropane (**39**).



Procedure a: 1,1,3,3-tetramethoxypropane (**38**) (4.14 mL, 25 mmol, 1 eq.) and N-bromosuccinimide (4.45 g, 25 mmol, 1 eq.) are dissolved in 20 mL dry chloroform. AIBN (41 mg, 0.25 mmol, 0.02 eq.) is added, and the mixture is slowly heated to 55 °C. Upon reaching the temperature, the reaction starts exothermically. Once the solid N-bromosuccinimide has completely disappeared from the bottom of the flask, the reaction is left to reach room temperature and is cooled to -20 °C overnight. The solids are filtered off, and the filtrate is concentrated *in vacuo*. Whilst the formation of **39** can be detected in the NMR data, it could not be separated from the numerous side products using the described purification method (vacuum distillation), and so a yield could not be determined.

¹H NMR (600 MHz, CDCl₃) δ 9.01 (s, 2H), 4.85 – 4.76 (m, 2H), 4.49 – 4.38 (m, 4H), 3.83 – 3.78 (m, 1H), 3.79 – 3.73 (m, 7H), 3.70 – 3.62 (m, 7H), 3.62 – 3.52 (m, 2H), 3.50 – 3.34 (m, 17H), 3.37 – 3.23 (m, 39H), 2.78 – 2.67 (m, 13H), 2.66 – 2.59 (m, 4H), 1.92 – 1.85 (m, 3H).

Procedure b₁: 1,1,3,3-tetramethoxypropane (**38**) (5.58 mL, 25 mmol, 1 eq.) is added to 7.5 mL dry DCM, and the mixture is cooled to 0 °C. Bromine (1.3 mL, 25 mmol, 1 eq.) is added via a dropping funnel. After complete addition, the reaction mixture is stirred at room temperature until the mixture completely discolours. Then, 15 mL of saturated NaHCO₃ solution is added to quench to reaction. The organic phase is quickly separated from the aqueous phase and washed with 7.5 mL H₂O. The organic phase is dried over Na₂SO₄ and the solvent is removed *in vacuo* to yield **39** (4.019 g, 66%). The sample was used without further purification due to the risk of hydrolysis.

¹H NMR (400 MHz, CDCl₃) δ 4.30 – 4.21 (m, 2H), 3.90 – 3.78 (m, 1H), 3.35 – 3.21 (m, 12H), 3.24 – 3.11 (m, 1H).

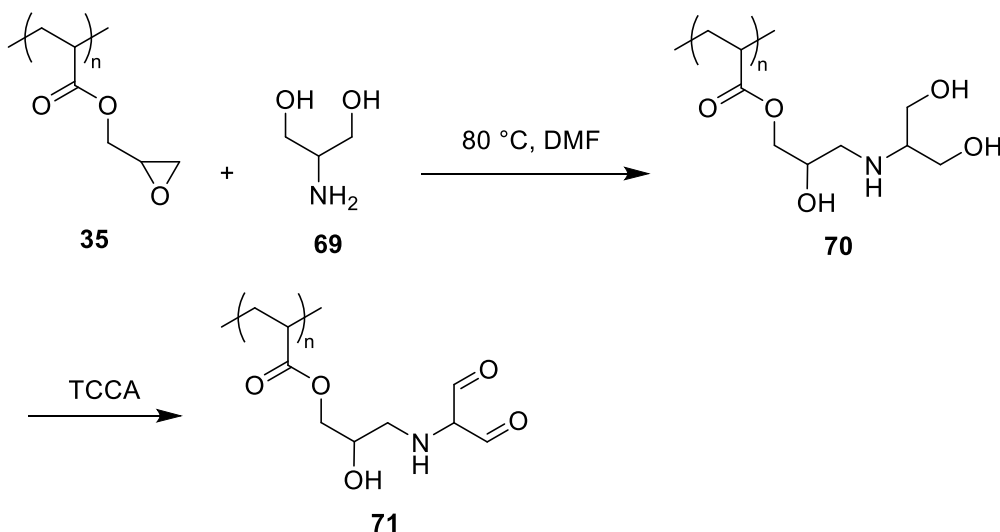
¹³C NMR (101 MHz, CDCl₃) δ 103.29, 103.27, 102.83, 77.65, 77.33, 77.01, 55.52, 55.36, 53.72, 53.68, 52.87, 52.78, 43.59, 30.61.

Procedure b₂: 1,1,3,3-tetramethoxypropane (**38**) (10 mL, 44.75 mmol, 1 eq.) is added to 15 mL dry DCM, and the mixture is cooled to 0 °C. Bromine (2.4 mL, 44.75 mmol, 1 eq.) is added via a dropping funnel. After complete addition, the reaction mixture is stirred at room temperature until the mixture completely discolours. The reaction mixture is then poured into 50 mL dry DCM, slurried with K₂CO₃ (24.7 g, 179 mmol, 4 eq.). After 10 minutes of stirring, the mixture is filtered and poured into an extraction funnel, where 50 mL H₂O is added. The organic phase is removed, and the aqueous phase is extracted twice with DCM. The combined organic phases are washed with brine and dried over MgSO₄. The solvent is then removed *in vacuo* to yield **39** (8.67 g, 79%). The sample was used without further purification due to the risk of hydrolysis.

¹H NMR (400 MHz, CDCl₃) δ 4.36 – 4.30 (m, 2H), 3.93 (dtd, *J* = 6.0, 4.5, 2.7 Hz, 1H), 3.33 – 3.23 (m, 1H), 3.27 – 3.19 (m, 1H).

¹³C NMR (101 MHz, CDCl₃) δ 103.39, 103.01, 101.67, 77.48, 77.16, 76.84, 55.71, 55.53, 55.49, 54.68, 53.82, 52.94, 52.91, 52.40, 43.66, 30.67.

6.2.2.3. The functionalisation of poly(glycidyl acrylate) with serinol (**70**) and subsequent oxidation (**71**).



500 mg of poly(glycidyl acrylate) (**35**) is added to 10 mL DMF. After stirring for 15 minutes at room temperature, serinol (**69**) (638 mg, 7 mmol, ~1.8 eq.) is added. The suspension is heated to 80 °C overnight under light stirring. The suspension is then allowed to reach room temperature, after which the solvent is decanted, and the solids are washed with H₂O to yield **70**.

The conversion rate was not further determined.

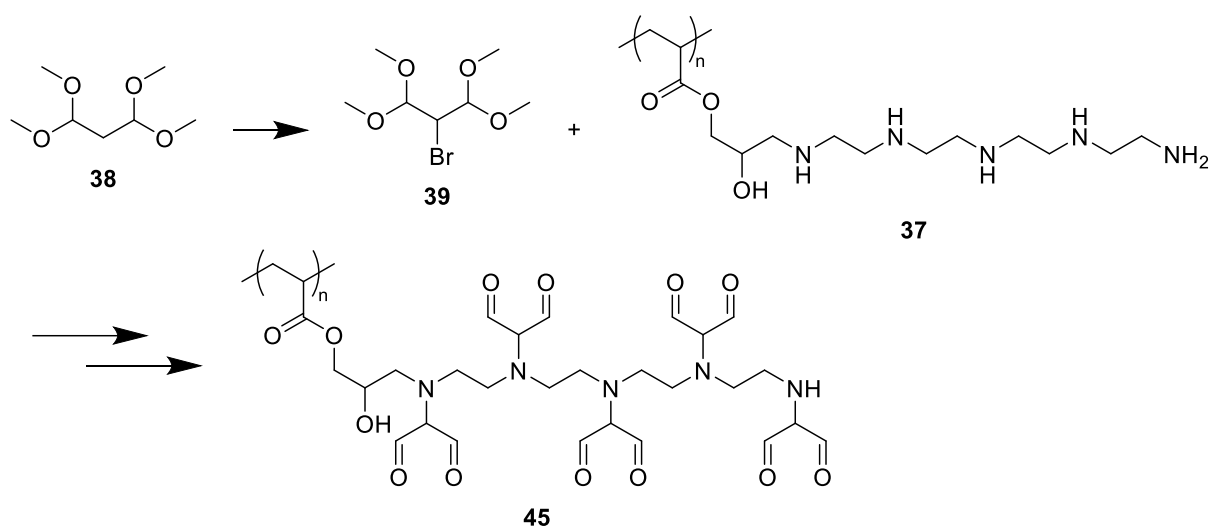
IR (neat): ν_{max} (cm⁻¹) = 3305.40 (s), 2937.17 (m), 2881.50 (m), 2843.90 (m), 1720.64 (s), 1449.40 (w), 1338.48 (w), 1252.30 (w), 1151.54 (s), 1038.23 (m), 989.08 (w), 907.89 (w), 845.44 (w), 750.48 (w)

Subsequently, the wet sample **70** is added to 10 mL DMF. A solution of TCCA (2.00 g, 8.6 mmol, ~2.2 eq.) in 10 mL DMF is added, and the mixture is stirred at room temperature overnight. The solvent is decanted off, and the solids are washed with H₂O and DCM, followed by drying under vacuum to yield **71**.

The conversion rate was not further determined.

IR (neat): ν_{max} (cm⁻¹) = 3211.4 (w), 2956.10 (w), 2901.80 (w), 2789.00 (w), 1710.40 (s), 1448.17 (w), 1402.70 (w), 1326.75 (w), 1143.40 (m), 1078.6 (m), 764.36 (w), 530.84 (w)

6.2.2.4. The functionalisation of poly(TEPA) with 2-bromo-1,1,3,3-tetramethoxypropane (**45**).



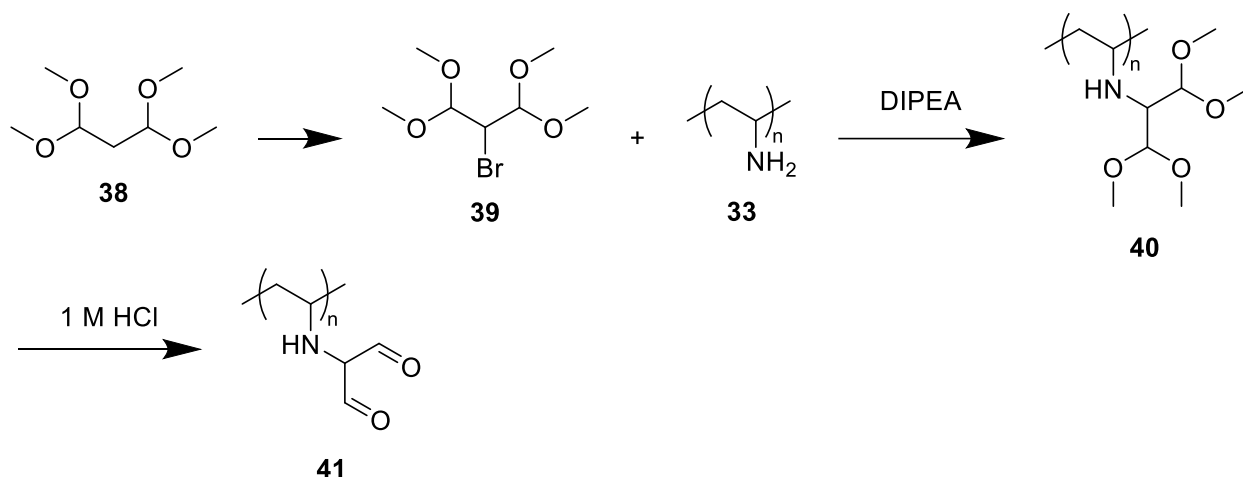
Step 1: 1,1,3,3-tetramethoxypropane (10 mL, 44.75 mmol, 1 eq.) is added to 15 mL dry MeCN. Bromine (2 mL, 44.75 mL, 1 eq.) is slowly added via a dropping funnel at 0 °C. The reaction is allowed to reach room temperature, and the mixture is stirred for one hour. Subsequently, the reaction mixture is poured into a slurry of K₂CO₃ (24.7 g, 178 mmol, 4 eq.) in 50 mL dry DCM. The mixture is stirred for 15 minutes, after which the solids were filtered off.

Step 2: **37** (2.8 g, 1 eq.) is added to the solution, and the suspension is stirred at room temperature for one hour. Subsequently, DIPEA (8.7 mL, 49.9 mmol, 5 eq.) is added, and the reaction mixture is stirred at room temperature overnight. The polymer is then washed with MeCN and H₂O and dried under vacuum to yield **45**.

The conversion rate was not further determined.

IR (neat): ν_{max} (cm⁻¹) = 3222.99 (m), 2940.62 (m), 2830.99 (m), 1721.40 (s), 1657.49 (w), 1602.88 (s), 1451.04 (m), 1401.39 (w), 1266.86 (m), 1156.00 (s), 1061.30 (w), 991.00 (w), 815.27 (w), 748.65 (w)

6.2.2.5. The functionalisation of poly(vinylamine) with 2-bromo-1,1,3,3-tetramethoxypropane (**39**) and subsequently hydrolysis (**41**).



Step 1: **39** is prepared as described in 6.2.2.4, step 1. After filtering off K_2CO_3 , the solvent is removed *in vacuo* and kept dry.

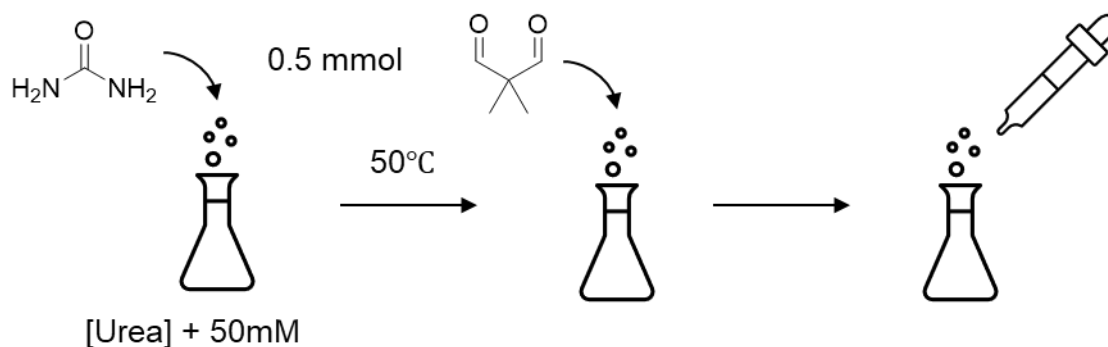
Step 2: 394 mg poly(vinylamine) (**33**) is added to 15 mL dry DMF. DIPEA (1.75 mL, 10.01 mmol, 1 eq.) is added, and the suspension is stirred lightly for 30 minutes. Subsequently, 2-bromo-1,1,3,3-tetramethoxypropane (**39**) (2.53 g, 10.4 mmol, 1.04 eq.) is added, and the mixture is stirred lightly at room temperature overnight. The solvent is decanted, and the solids are washed with DMF and H_2O , and subsequently dried to yield **40**.

IR (neat): ν_{max} (cm^{-1}) = 3252.99 (s), 2926.31 (s), 1651.86 (m), 1589.16 (m), 1440.77 (m), 1385.42 (m), 1190.27 (w), 1118.19 (w), 1057.95 (w), 712.99 (w)

Step 3: **40** is added to 30 mL of 1 M HCl and stirred lightly for 24 hours. The solids are subsequently washed with H_2O until the pH of the aqueous wash is neutral (pH \sim 7). The solids are dried under vacuum to yield **41**.

IR (neat): ν_{max} (cm^{-1}) = 3360.44 (s), 2916.63 (s), 1600.91 (s), 1520.39 (m), 1439.92 (w), 1385.59 (w), 1203.10 (w), 1113.30 (w), 1035.20 (w), 803.70 (w)

6.2.3. General procedure urea-reactivity measurement of small molecules.



^{13}C -labelled urea (31.5 mg, 0.5 mmol, 1 eq.) is dissolved in 16.7 mL PBS, and the solution is heated to 50 °C. Subsequently, 1 equivalent of the compound that is to be tested for its urea reactivity is added, and samples are taken at different time points to determine whether a conversion can be observed in ^{13}C -NMR, indicated by the formation of a product peak. The pH is occasionally checked to ensure that the sample remains neutral.

7. References

1. Legallais, C. *et al.* Bioengineering organs for blood detoxification. *Adv. Healthc. Mater.* **7**, 1800430 (2018).
2. Neiryneck, N. *et al.* An update on uremic toxins. *Int. Urol. Nephrol.* **45**, 139–150 (2013).
3. Castillo-Rodríguez, E. *et al.* Inflammatory cytokines as uremic toxins: “Ni son todos los que estan, ni estan todos los que son”. *Toxins (Basel)*. **9**, 114 (2017).
4. Liu, W.-C., Tomino, Y. & Lu, K.-C. Impacts of Indoxyl Sulfate and p-Cresol Sulfate on Chronic Kidney Disease and Mitigating Effects of AST-120. *Toxins (Basel)*. **10**, (2018).
5. Hippisley-Cox, J. & Coupland, C. Diabetes treatments and risk of amputation, blindness, severe kidney failure, hyperglycaemia, and hypoglycaemia: open cohort study in primary care. *bmj* **352**, (2016).
6. Wilson, P. D. Polycystic kidney disease. *N. Engl. J. Med.* **350**, 151–164 (2004).
7. Bundy, J. D. *et al.* Self-Reported Tobacco, Alcohol, and Illicit Drug Use and Progression of Chronic Kidney Disease. *Clin. J. Am. Soc. Nephrol.* **13**, 993 LP – 1001 (2018).
8. Sarnak, M. J. A patient with heart failure and worsening kidney function. *Clin. J. Am. Soc. Nephrol.* **9**, 1790–1798 (2014).
9. Shankar, M., Narasimhappa, S. & N S, M. Urinary Tract Infection in Chronic Kidney Disease Population: A Clinical Observational Study. *Cureus* **13**, e12486–e12486 (2021).
10. National Kidney Foundation. K/DOQI clinical practice guidelines for chronic kidney disease: evaluation, classification, and stratification. *Am. J. Kidney Dis.* **39**, S1-266 (2002).
11. Stevens, L. A., Coresh, J., Greene, T. & Levey, A. S. Assessing kidney function—measured and estimated glomerular filtration rate. *N. Engl. J. Med.* **354**, 2473–2483 (2006).
12. McCormick, F., Held, P. J. & Chertow, G. M. The terrible toll of the kidney

- shortage. *Journal of the American Society of Nephrology* vol. 29 2775–2776 (2018).
13. van Gelder, M. K. *et al.* Urea removal strategies for dialysate regeneration in a wearable artificial kidney. *Biomaterials* **234**, 119735 (2020).
 14. Locatelli, F. *et al.* Optimal composition of the dialysate, with emphasis on its influence on blood pressure. *Nephrol. Dial. Transplant.* **19**, 785–796 (2004).
 15. Jong, A. J. W. Bottom-up Development of Urea Sorbents for Dialysate Regeneration. (2019).
 16. Feroze, U., Martin, D., Reina-Patton, A., Kalantar-Zadeh, K. & Kopple, J. D. Mental health, depression, and anxiety in patients on maintenance dialysis. *Iran. J. Kidney Dis.* **4**, 173–180 (2010).
 17. Gura, V. *et al.* A wearable artificial kidney for patients with end-stage renal disease. *JCI insight* **1**, (2016).
 18. Pradana, A. R. *et al.* Review: Synthesis of Urea in Several Methods. *Mediterr. J. Chem.* **11**, 146 (2021).
 19. Duranton, F., Jankowski, J., Więcek, A. & Argilés, À. On the discovery of UREA. Identification, synthesis and observations that led to establishing the first uraemic retention solute. *G. Ital. Nefrol.* **33**, 33.S66 (2016).
 20. Vaughan, P. & Donohue, J. The structure of urea. Interatomic distances and resonance in urea and related compounds. *Acta Crystallogr.* **5**, 530–535 (1952).
 21. Alexandrova, A. N. & Jorgensen, W. L. Why urea eliminates ammonia rather than hydrolyzes in aqueous solution. *J. Phys. Chem. B* **111**, 720–730 (2007).
 22. Amtul, Z., Rahman, A.-U., Siddiqui, R. A. & Choudhary, M. I. Chemistry and mechanism of urease inhibition. *Curr. Med. Chem.* **9**, 1323–1348 (2002).
 23. Wang, F. S., Goh, D. L. M. & Ong, H. T. Urea cycle disorder presenting as bilateral mesial temporal sclerosis - an unusual cause of seizures: a case report and review of the literature. *J. Med. Case Rep.* **12**, 208 (2018).
 24. Weiner, I. D., Mitch, W. E. & Sands, J. M. Urea and Ammonia Metabolism and the Control of Renal Nitrogen Excretion. *Clin. J. Am. Soc. Nephrol.* **10**, 1444–

- 1458 (2015).
25. D'Apolito, M. *et al.* Urea-induced ROS cause endothelial dysfunction in chronic renal failure. *Atherosclerosis* **239**, 393–400 (2015).
 26. Singh, L. R., Dar, T. A. & Ahmad, F. Living with urea stress. *J. Biosci.* **34**, 321–331 (2009).
 27. Sumner, J. B. The isolation and crystallization of the enzyme urease. Preliminary paper. in *A Source Book in Chemistry, 1900-1950* 322–327 (Harvard University Press, 2013).
 28. Dixon, N. E., Gazzola, T. C., Blakeley, R. L. & Zerner, B. Letter: Jack bean urease (EC 3.5.1.5). A metalloenzyme. A simple biological role for nickel? *J. Am. Chem. Soc.* **97**, 4131–4133 (1975).
 29. Krajewska, B. Ureases I. Functional, catalytic and kinetic properties: A review. *J. Mol. Catal. B Enzym.* **59**, 9–21 (2009).
 30. Kappaun, K., Piovesan, A. R., Carlini, C. R. & Ligabue-Braun, R. Ureases: Historical aspects, catalytic, and non-catalytic properties – A review. *J. Adv. Res.* **13**, 3–17 (2018).
 31. Walker, V. Ammonia toxicity and its prevention in inherited defects of the urea cycle. *Diabetes, Obes. Metab.* **11**, 823–835 (2009).
 32. Simka, W., Piotrowski, J., Robak, A. & Nawrat, G. Electrochemical treatment of aqueous solutions containing urea. *J. Appl. Electrochem.* **39**, 1137–1143 (2009).
 33. Yao, S. J., Wolfson, S. K., Ahn, B. K. & Liu, C. C. Anodic Oxidation of Urea and an Electrochemical Approach to De-ureation. *Nature* **241**, 471–472 (1973).
 34. Keller, R. W., Yao, S. J., Brown, J. M., Wolfson, S. K. & Zeller, M. V. Electrochemical removal of urea from physiological buffer as the basis for a regenerative dialysis system. *Bioelectrochemistry Bioenerg.* **7**, 469–485 (1980).
 35. Fels, M. Recycle of dialysate from the artificial kidney by electrochemical degradation of waste metabolites: Small-scale laboratory investigations. *Med. Biol. Eng. Comput.* **16**, 25–30 (1978).
 36. Fuchs, J. The Urea-Hypochlorite Reaction. *Chem. Ztg* **83**, 223–226 (1959).

37. Ikematsu, M., Kaneda, K., Iseki, M., Matsuura, H. & Yasuda, M. Electrolytic treatment of human urine to remove nitrogen and phosphorus. *Chem. Lett.* **35**, 576–577 (2006).
38. Lehmann, H. D., Marten, R. & Gullberg, C. A. How to catch urea? Considerations on urea removal from hemofiltrate. *Artif. Organs* **5**, 278–285 (1981).
39. Kameda, T., Horikoshi, K., Kumagai, S., Saito, Y. & Yoshioka, T. Adsorption of urea, creatinine, and uric acid onto spherical activated carbon. *Sep. Purif. Technol.* **237**, 116367 (2020).
40. Kameda, T., Ito, S. & Yoshioka, T. Kinetic and equilibrium studies of urea adsorption onto activated carbon: Adsorption mechanism. *J. Dispers. Sci. Technol.* **38**, 1063–1066 (2017).
41. Yamamoto, S. *et al.* Adsorption of Protein-Bound Uremic Toxins Using Activated Carbon through Direct Hemoperfusion in vitro. *Blood Purif.* **48**, 215–222 (2019).
42. Naguib, M. *et al.* Two-dimensional nanocrystals produced by exfoliation of Ti₃AlC₂. *Adv. Mater.* **23**, 4248–4253 (2011).
43. Mashtalir, O. *et al.* Intercalation and delamination of layered carbides and carbonitrides. *Nat. Commun.* **4**, 1–7 (2013).
44. Mashtalir, O., Lukatskaya, M. R., Zhao, M., Barsoum, M. W. & Gogotsi, Y. Amine-assisted delamination of Nb₂C MXene for Li-ion energy storage devices. *Adv. Mater.* **27**, 3501–3506 (2015).
45. Meng, F. *et al.* MXene Sorbents for Removal of Urea from Dialysate: A Step toward the Wearable Artificial Kidney. *ACS Nano* (2018) doi:10.1021/acsnano.8b06494.
46. Cheah, W. K., Sim, Y. L. & Yeoh, F. Y. Amine-functionalized mesoporous silica for urea adsorption. *Mater. Chem. Phys.* **175**, 151–157 (2016).
47. Cheng, Y.-C., Fu, C.-C., Hsiao, Y.-S., Chien, C.-C. & Juang, R.-S. Clearance of low molecular-weight uremic toxins p-cresol, creatinine, and urea from simulated serum by adsorption. *J. Mol. Liq.* **252**, 203–210 (2018).
48. S. Panda, S., Khanna, P. & Khanna, L. Biginelli Reaction: A Green Perspective.

- Curr. Org. Chem.* **16**, 507–520 (2012).
49. Lin, J. *et al.* Synthesis of partially methyl substituted cucurbit[n]urils with 3a-methyl-glycoluril. *J. Mol. Struct.* **875**, 442–446 (2008).
 50. Baccolini, G., Boga, C., Delpivo, C. & Micheletti, G. Facile synthesis of hydantoins and thiohydantoins in aqueous solution. *Tetrahedron Lett.* **52**, 1713–1717 (2011).
 51. Menor Salván, C. *et al.* Prebiotic Origin of Pre-RNA Building Blocks in a Urea “Warm Little Pond” Scenario. *ChemBioChem* **21**, 3504–3510 (2020).
 52. Jong, J. A. W. *et al.* Reactivity of (Vicinal) Carbonyl Compounds with Urea. *ACS Omega* **4**, 11928–11937 (2019).
 53. Van Slyke, D. D. & Hamilton, P. B. The synthesis and properties of ninhydrin ureide. *J. Biol. Chem.* **150**, 471–476 (1943).
 54. Shapiro, R. & Chatterjee, N. Cyclization reactions of ninhydrin with aromatic amines and ureas. *J. Org. Chem.* **35**, 447–450 (1970).
 55. Jong, J. A. W. *et al.* Effect of substituents on the reactivity of ninhydrin with urea. *Bottom-up Dev. Urea Sorbents Dial. Regen.* **67** (2018).
 56. Kostyanovsky, R. G. *et al.* Pyramidal nitrogen in the crystal of N-[(benzoyl)-(hydroxy) methyl]-N-benzyloxy-N'-(2-bromophenyl) urea. *Mendeleev Commun.* **20**, 167–169 (2010).
 57. Arnold, Z., Buděšínský, M. & Pánková, M. Reactivity of triformylmethane. I. Reactions of triformylmethane with selected types of amino compounds. *Collect. Czechoslov. Chem. Commun.* **56**, 1019–1031 (1991).
 58. Ayala, A., Muñoz, M. F. & Argüelles, S. Lipid peroxidation: production, metabolism, and signaling mechanisms of malondialdehyde and 4-hydroxy-2-nonenal. *Oxid. Med. Cell. Longev.* **2014**, 360438 (2014).
 59. Buděšínský, M., Fiedler, P. & Arnold, Z. Triformylmethane: An efficient preparation, some derivatives, and spectra. *Synthesis (Stuttg.)* **1989**, 858–860 (1989).
 60. Freitag, M. A., Pruden, T. L., Moody, D. R., Parker, J. T. & Fallet, M. On the keto-

- enol tautomerization of malonaldehyde: An effective fragment potential study. *J. Phys. Chem. A* **111**, 1659–1666 (2007).
61. Nowroozi, A. & Raissi, H. Strong intramolecular hydrogen bond in triformylmethane ab-initio, AIM and NBO study. *J. Mol. Struct. THEOCHEM* **759**, 93–100 (2006).
 62. Riggins, J. N. & Marnett, L. J. Mutagenicity of the malondialdehyde oligomerization products 2-(3'-oxo-1'-propenyl)-malondialdehyde and 2,4-dihydroxymethylene-3-(2,2-dimethoxyethyl)glutaraldehyde in Salmonella. *Mutat. Res. Toxicol. Environ. Mutagen.* **497**, 153–157 (2001).
 63. Cgf, K. Oxidative metabolism of exocyclic DNA adducts. in (2008).
 64. Samek, Z., Hapala, J., Fiedler, O. & Arnold, Z. Structure of amidomalonaldehydes and some related compounds. *Collect. Czechoslov. Chem. Commun.* **42**, 1659–1685 (1977).
 65. Tserng, K. Y. & Kalhan, S. C. Gas Chromatography/Mass Spectrometric Determination of [15N]Urea in Plasma and Application to Urea Metabolism Study. *Anal. Chem.* **54**, 489–491 (1982).
 66. Gross, K. C. & Seybold, P. G. Substituent effects on the physical properties and pKa of phenol. *Int. J. Quantum Chem.* **85**, 569–579 (2001).
 67. Gross, K. C. & Seybold, P. G. Substituent effects on the physical properties and pKa of aniline. *Int. J. Quantum Chem.* **80**, 1107–1115 (2000).
 68. De Luca, L., Giacomelli, G. & Porcheddu, A. A very mild and chemoselective oxidation of alcohols to carbonyl compounds. *Org. Lett.* **3**, 3041–3043 (2001).
 69. Pounds, S. *et al.* 11th conference of the central european division e.V. of the international isotope society. *J. Label. Compd. Radiopharm.* **47**, 243–288 (2004).
 70. Reichardt, C., Ferwanah, A.-R. & Yun, K.-Y. Synthesen mit aliphatischen Dialdehyden, XXXVIII. Darstellung und Eigenschaften von Cycloalkylmalonaldehyden. *Liebigs Ann. der Chemie* **1984**, 649–679 (1984).
 71. Gu, L., Zhu, S. & Hrymak, A. N. Acidic and basic hydrolysis of poly(N-vinylformamide). *J. Appl. Polym. Sci.* **86**, 3412–3419 (2002).

72. Pinschmidt, R. K., Wasowski, L. A., Orphanides, G. G. & Yacoub, K. Amine functional polymers based on N-ethenylformamide. *Prog. Org. Coatings* **27**, 209–218 (1996).
73. Witek, E., Pazdro, M. & Bortel, E. Mechanism for base hydrolysis of poly(N-vinylformamide). *J. Macromol. Sci. Part A Pure Appl. Chem.* **44**, 503–507 (2007).
74. Gadgeel, A. & Mhaske, S. T. Synthesis of microporous interconnected polymeric foam of poly (glycidyl methacrylate-co-divinyl benzene-co-butyl acrylate) by using aqueous foam as a template. *Colloids Surfaces A Physicochem. Eng. Asp.* **563**, 193–205 (2019).
75. Muzammil, E. M., Khan, A. & Stuparu, M. C. Post-polymerization modification reactions of poly(glycidyl methacrylate)s. *RSC Adv.* **7**, 55874–55884 (2017).
76. Benaglia, M., Alberti, A., Giorgini, L., Magnoni, F. & Tozzi, S. Poly(glycidyl methacrylate): a highly versatile polymeric building block for post-polymerization modifications. *Polym. Chem.* **4**, 124–132 (2013).
77. National Toxicology Program. NTP Toxicology and Carcinogenesis Studies of Malonaldehyde, Sodium Salt (3-Hydroxy-2-propenal, Sodium Salt) (CAS No. 24382-04-5) in F344/N Rats and B6C3F1 Mice (Gavage Studies). *Natl. Toxicol. Program Tech. Rep. Ser.* **331**, 1–182 (1988).
78. Reber, K. P. & Burdge, H. E. Synthesis and Applications of Tricarbonylmethane Compounds. *Org. Prep. Proced. Int.* **50**, 2–80 (2018).
79. Ma, D.-Y., Wang, D.-X., Pan, J., Huang, Z.-T. & Wang, M.-X. Nitrile biotransformations for the synthesis of highly enantioenriched β -hydroxy and β -amino acid and amide derivatives: a general and simple but powerful and efficient benzyl protection strategy to increase enantioselectivity of the amidase. *J. Org. Chem.* **73**, 4087–4091 (2008).
80. Braunberger, T. L., Nahhas, A. F., Katz, L. M., Sadrieh, N. & Lim, H. W. Dihydroxyacetone: A Review. *J. Drugs Dermatol.* **17**, 387–391 (2018).
81. Liu, F., Gou, S., Li, L., Yan, P. & Zhao, C. Efficient and recyclable catalysts based on simple chiral N 1-alkyl, N2-arylmethyl diamines in the Cu-catalyzed asymmetric Henry reactions. *J. Mol. Catal. A Chem.* **379**, 163–168 (2013).

82. Shao, Z. *et al.* An Advanced Intermediate for the Synthesis of (±)-Pumiliotoxin C and Its Analogues. *Synth. Commun.* **34**, 2031–2038 (2004).
83. Kobayashi, K., Yokoi, Y., Nakahara, T. & Matsumoto, N. Synthesis of 2, 3-dihydro-1H-isoindole-1-thiones via the bromine–lithium exchange between 1-bromo-2-(1-isothiocyanatoalkyl) benzenes and butyllithium. *Tetrahedron* **69**, 10304–10310 (2013).
84. Ciriminna, R., Fidalgo, A., Ilharco, L. M. & Pagliaro, M. Dihydroxyacetone: An Updated Insight into an Important Bioproduct. *ChemistryOpen* **7**, 233–236 (2018).
85. Ji, L. *et al.* Diastereospecific epoxidation and highly regioselective ring-opening of (+)-valienamine: practical synthesis of (+)-valiolamine. *Tetrahedron* **69**, 7031–7037 (2013).
86. Horii, S. *et al.* Synthesis and α -D-glucosidase inhibitory activity of N-substituted valiolamine derivatives as potential oral antidiabetic agents. *J. Med. Chem.* **29**, 1038–1046 (1986).
87. Larget, R. *et al.* Synthesis of novel orthoalkylaminophenol derivatives as potent neuroprotective agents in vitro. *Bioorg. Med. Chem. Lett.* **9**, 2929–2934 (1999).
88. A, W. B. E. G. N. D. R. A. S. R. Alicyclic alkylene polyamine microorganism and algae growth inhibitors. (1977).
89. [JP], T. K. [JP]; S. T. [JP]; K. H. [JP]; T. Y. [JP]; T. Y. Process for producing hydroxyalkyltriethylenediamine compound, and catalyst composition for the production of polyurethane resin using the hydroxyalkyltriethylenediamine compound. (2011).
90. TODORIKI, R., ONO, M. & TAMURA, S. Preparation of 3-Substituted Quinolines. I. Alkylation of Malonaldehyde Dianil Derivatives. *Chem. Pharm. Bull. (Tokyo)*. **31**, 4277–4285 (1983).
91. Jupally, V. R. *et al.* Interstaple dithiol cross-linking in Au₂₅ (SR)₁₈ nanomolecules: a combined mass spectrometric and computational study. *J. Am. Chem. Soc.* **133**, 20258–20266 (2011).
92. Jiménez, A. *et al.* A novel class of cationic and non-peptidic small molecules as

- hits for the development of antimicrobial agents. *Molecules* **23**, 1513 (2018).
93. de Cedrón, M. G. *et al.* Novel polyphenols that inhibit colon cancer cell growth affecting cancer cell metabolism. *J. Pharmacol. Exp. Ther.* **366**, 377–389 (2018).
 94. Fagerström, A., Nilsson, M., Berg, U. & Isaksson, R. New propranolol analogues: binding and chiral discrimination by cellobiohydrolase Cel7A. *Org. Biomol. Chem.* **4**, 3067–3076 (2006).
 95. Bredereck, H., Effenberger, F. & Schweizer, E. H. Synthesen in der heterocyclischen Reihe, I. Neue Synthesen 5-monosubstituierter Pyrimidine. *Chem. Ber.* **95**, 803–809 (1962).
 96. Eisert, B. & Haupter, F. Cyclische Dianilsalze von Malondialdehyden. **939**, 264–271 (1959).
 97. Einsiedel, J. *et al.* Discovery of highly potent and neurotensin receptor 2 selective neurotensin mimetics. *J. Med. Chem.* **54**, 2915–2923 (2011).
 98. Jogula, S., Krishna, V. S., Meda, N., Balraju, V. & Sriram, D. Design, synthesis and biological evaluation of novel *Pseudomonas aeruginosa* DNA gyrase B inhibitors. *Bioorg. Chem.* **100**, 103905 (2020).
 99. Riomet, M. *et al.* Access to N-Carbonyl Derivatives of Iminosydones by Carbonylimidazolium Activation. *Org. Lett.* **22**, 2403–2408 (2020).
 100. Ezawa, T. *et al.* Dynamics in catalytic asymmetric diastereoconvergent (3+ 2) cycloadditions with isomerizable nitrones and α -keto ester enolates. *J. Am. Chem. Soc.* **143**, 9094–9104 (2021).
 101. Hurley, K. A., Heinrich, V. A., Hershfield, J. R., Demons, S. T. & Weibel, D. B. Membrane-targeting dcap analogues with broad-spectrum antibiotic activity against pathogenic bacteria. *ACS Med. Chem. Lett.* **6**, 466–471 (2015).
 102. Lim, S. & Seib, P. A. Preparation and Pasting Properties of Wheat and Corn Starch Phosphates. *J. Food Sci.* **68**, 2136–2140 (2003).
 103. Illy, N. *et al.* Phosphorylation of bio-based compounds: the state of the art. (2015).

8. Table of Figures

Figure 1. Structures of several uremic toxins. From left to right: Urea, uric acid, creatinine, p-cresyl sulfate, indoxyl sulfate.	1
Figure 2. Schematic overview of hemodialysis. Taken from Jong (2019). ¹⁵	3
Figure 3. A schematic overview of a Wearable Artificial Kidney (WAK) device with a dialysate regeneration unit. Taken from Jong (2019).	4
Figure 4. Resonance structures of urea.....	4
Figure 5. Decomposition of urea in an aqueous medium (top) and with urease (bottom).	5
Figure 6. Hydrolysis mechanism of urea by urease. Taken from Kappaun et al. (2018). ³⁰	7
Figure 7. Schematic overview of the interaction between urea and spherical AC, as found by Kameda et al. (2016). ⁴⁰	9
Figure 8. The Biginelli Pyrimidone Synthesis: A multicomponent pyrimidone synthesis from (thio)urea (11), an aldehyde (12) and a β -keto ester (10).....	11
Figure 9. A brief overview of several representative reactions of urea under mild conditions.	12
Figure 10. Keto-enol tautomerism of triformylmethane (left) and malonaldehyde (right).	16
Figure 11. Self-condensation reaction of malonaldehyde (MDA). Taken from <i>Riggins et al. (2001)</i>	17
Figure 12. The reaction of triformylmethane and urea in water according to the research of <i>Arnold et al. (1991)</i>	18
Figure 13. The reaction of malonaldehyde and urea in water according to the research of <i>Tsreng & Kalhan (1982)</i>	18
Figure 14. Hypothesized reaction mechanism between urea and malonaldehyde as proposed by <i>Jong et al. (2019)</i>	19
Figure 15. Synthesis pathway of 30	21
Figure 16. Expected decreasing order of pK _A -values of enolizable MDA-derivatives based on the electron-donating / -withdrawing effect of substituents in the 2-position.	21
Figure 17. Synthesis pathway of 33	22
Figure 18. Synthesis pathway of 37	23

Figure 19. Synthesis pathway of target structures 41 and 45	23
Figure 20. The synthesis of 30	24
Figure 21. Schematic overview of measuring the urea reactivity of compound 30 . ..	25
Figure 22. Qualitative ¹³ C- NMR spectrum over time at pH 7 of 30 . ¹³ C-labelled urea gives a signal at 161.93 ppm, and no product formation can be observed.	26
Figure 23. Qualitative ¹³ C- NMR spectrum over time at pH 1 of 30 . ¹³ C-labelled urea gives a signal at 161.93 ppm; a product peak is formed at 155.68 ppm.	27
Figure 24. Schematic representation of the reaction between a disubstituted MDA-derivative and urea. The lack of a central proton prevents the formation of a stable end-product; instead, it is hypothesized that an unstable di-imine (47) is formed.....	28
Figure 25. Perceived changes during basic hydrolysis by <i>Witek et al. (2007)</i> . Within 5 minutes, both the formation of the first amine groups, as well as the amidine rings (as seen in 51), can be observed. After 90 minutes, the amidine ring signals disappear, while both formaldehyde signals disappear after 240 minutes. The formation of hydroxy signals (as seen in 52) can be observed after 20 minutes.....	29
Figure 26. Attempted C-acylation of 53 . a: DCC, DMAP, MeCN; b: MgCl ₂ , TEA, MeCN; c: TEA, MeCN.....	32
Figure 27. The synthesis of 57	32
Figure 28. The hypothesized reaction between the aldehyde group of 53 and the solvent acetonitrile.	33
Figure 29. Top: Reductive amination of 61 with allyl amine (62). Bottom: Leuckart Amide Synthesis with 61 and fomamide (64).....	34
Figure 30. Reaction scheme of the functionalisation of the central carbon of 66	35
Figure 31. Bromination of the central carbon atom of 38 via the procedure of a) <i>Bredereck et al. (1962)</i> and b) <i>Eisert et al. (1960)</i>	37
Figure 32. The functionalisation of 35 with 69	39
Figure 33. Potential oxidation of the secondary amine, leading to a 1,3-dialdehyde structure with a quarternary central carbon atom (72).	40
Figure 34. Reaction overview of the functionalisation of 37	40
Figure 35. Reaction overview of the functionalisation of 33	41
Figure 36. Schematic overview of the urea-reactivity measurement of the synthesized polymeric structures.	42
Figure 37. Graphical depiction of the change in urea concentration of the supernatant of 41 in PBS at 323.15 K.	42

Figure 38. Graphical depiction of the change in urea concentration of the supernatant of 45 in PBS at 323.15 K.	44
Figure 39. Graphical depiction of the change in urea concentration of the supernatant of 71 in PBS at 323.15 K.	45
Figure 40. Expected decreasing order of pK _A -values of enolizable MDA-derivatives based on the electron-donating / -withdrawing effect of substituents in the 2-position.	46
Figure 41. Hypothesized functionalisation of poly(glycidyl acrylate) (35) with 3-amino-propane-1,3-diol (73), followed by an oxidation step to form polymeric structure 75	48
Figure 42. ATR-IR spectrum of PVAm.....	82
Figure 43. ATR-IR spectrum of poly(glycidyl acrylate).....	82
Figure 44. ATR-IR spectrum of 37	83
Figure 45. ¹ H NMR spectrum of 30 in CDCl ₃	83
Figure 46. ¹³ C NMR spectrum of 30 in CDCl ₃	84
Figure 47. ¹ H NMR spectrum of 53 in D ₂ O.	84
Figure 48. ¹³ C NMR spectrum of 53 in D ₂ O.	85
Figure 49. ¹ H NMR spectrum of 55 (procedure a) in D ₂ O.....	85
Figure 50. ATR-IR spectrum of 53	86
Figure 51. ¹ H NMR spectrum of 55 (procedure b) in D ₂ O.	86
Figure 52. ¹ H NMR spectrum of 55 (procedure c) in D ₂ O.	87
Figure 53. ¹ H NMR spectrum of 57 in CDCl ₃	87
Figure 54. ¹³ C NMR spectrum of 57 in CDCl ₃	88
Figure 55. ¹ H NMR spectrum of 63 (procedure a) in CDCl ₃	88
Figure 56. ¹ H NMR spectrum of 63 (procedure b) in CDCl ₃	89
Figure 57. ¹ H NMR spectrum of 66 in CDCl ₃	89
Figure 58. ¹ H NMR spectrum of 68 (procedure a) in CDCl ₃	90
Figure 59. ¹³ C NMR spectrum of 68 (procedure a) in CDCl ₃	90
Figure 60. ¹ H NMR spectrum of 68 (procedure b) in CDCl ₃	91
Figure 61. ¹³ C NMR spectrum of 68 (procedure b) in CDCl ₃	92
Figure 62. ¹ H NMR spectrum of 68 (procedure c) in CDCl ₃	92
Figure 63. ¹³ C NMR spectrum of 68 (procedure c) in CDCl ₃	93
Figure 64. ¹ H NMR spectrum of 68 (procedure d) in CDCl ₃	93
Figure 65. ¹³ C NMR spectrum of 68 (procedure d) in CDCl ₃	94
Figure 66. ¹ H NMR spectrum of 68 (procedure e) in CDCl ₃	94

Figure 67. ^{13}C NMR spectrum of 68 (procedure e) in CDCl_3	95
Figure 68. ^1H NMR spectrum of 39 (procedure a) in CDCl_3	95
Figure 69. ^{13}C NMR spectrum of 39 (procedure a) in CDCl_3	96
Figure 70. ^1H NMR spectrum of 39 (procedure b ₁) in CDCl_3	96
Figure 71. ^{13}C NMR spectrum of 39 (procedure b ₁) in CDCl_3	97
Figure 72. Crystal structure of the hydrolysis product of 39 (2-bromomalonaldehyde) as determined per X-ray crystallography.	97
Figure 73. ^1H NMR spectrum of 39 (procedure b ₂) in CDCl_3	98
Figure 74. ^{13}C NMR spectrum of 39 (procedure b ₂) in CDCl_3	98
Figure 75. ATR-IR spectrum of 32	99
Figure 76. ATR-IR spectrum of 70	99
Figure 77. ATR-IR spectrum of 71	99
Figure 78. ATR-IR spectrum of 45	100
Figure 79. ATR-IR spectrum of 40	100
Figure 80. ATR-IR spectrum of 41	100

9. Table of Tables

Table 1. A list of uremic symptoms contributing to mortality in ESKD patients.	2
Table 2. Investigated vicinal carbonyl structures with the highest rate constant when reacting with urea at pH 2/7.4 at 50°C as found by <i>Jong et al. (2019)</i>	14
Table 3. Reaction conditions for the functionalisation of 66	35
Table 4. Urea reactivity measurement data of 71 . Measured by Babette Lentferink.	101
Table 5. Urea reactivity measurement data of 45 . Measured by Babette Lentferink.	101
Table 6. Urea reactivity measurement data of 41 . Measured by Babette Lentferink.	102

10. Appendix

10.1. Spectra

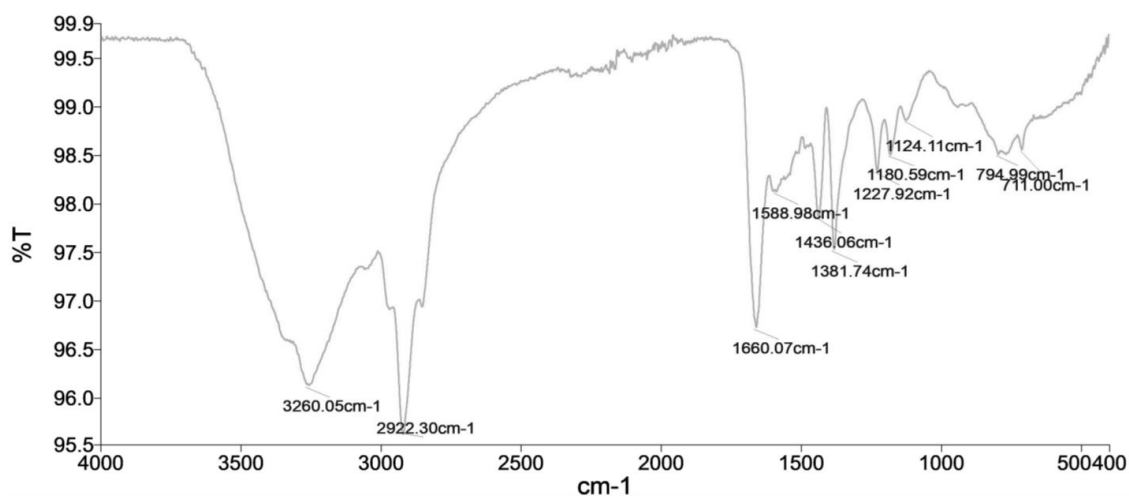


Figure 42. ATR-IR spectrum of PVAm.

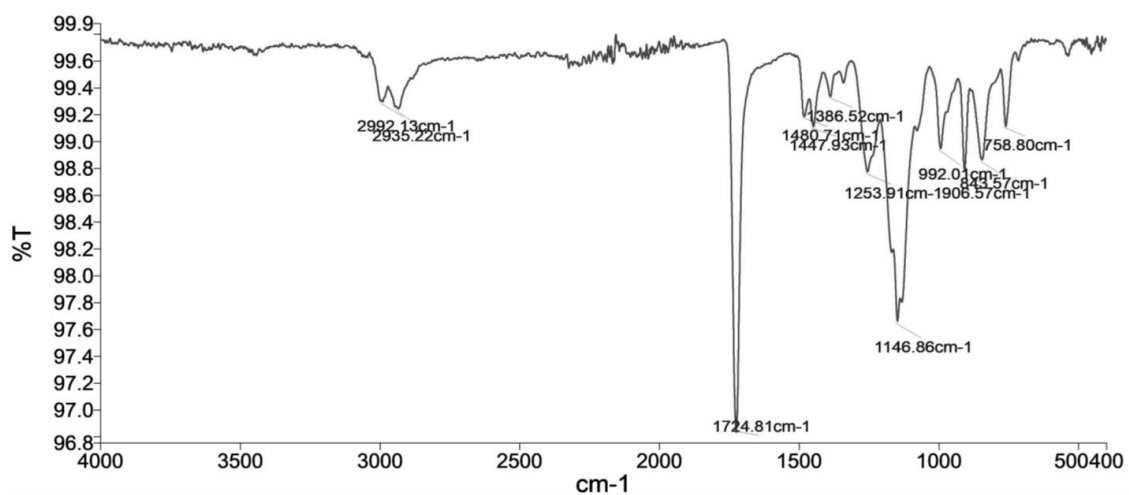


Figure 43. ATR-IR spectrum of poly(glycidyl acrylate).

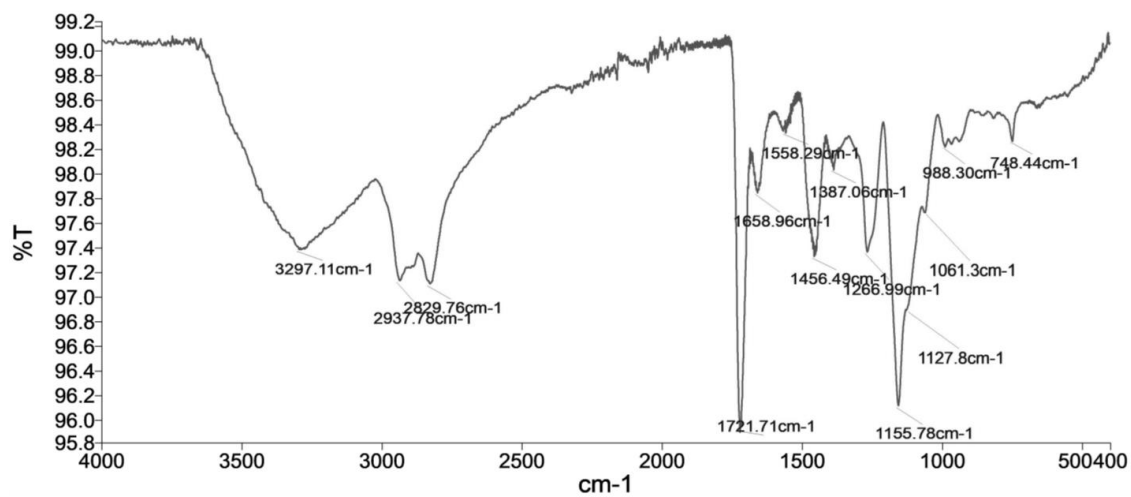


Figure 44. ATR-IR spectrum of **37**.

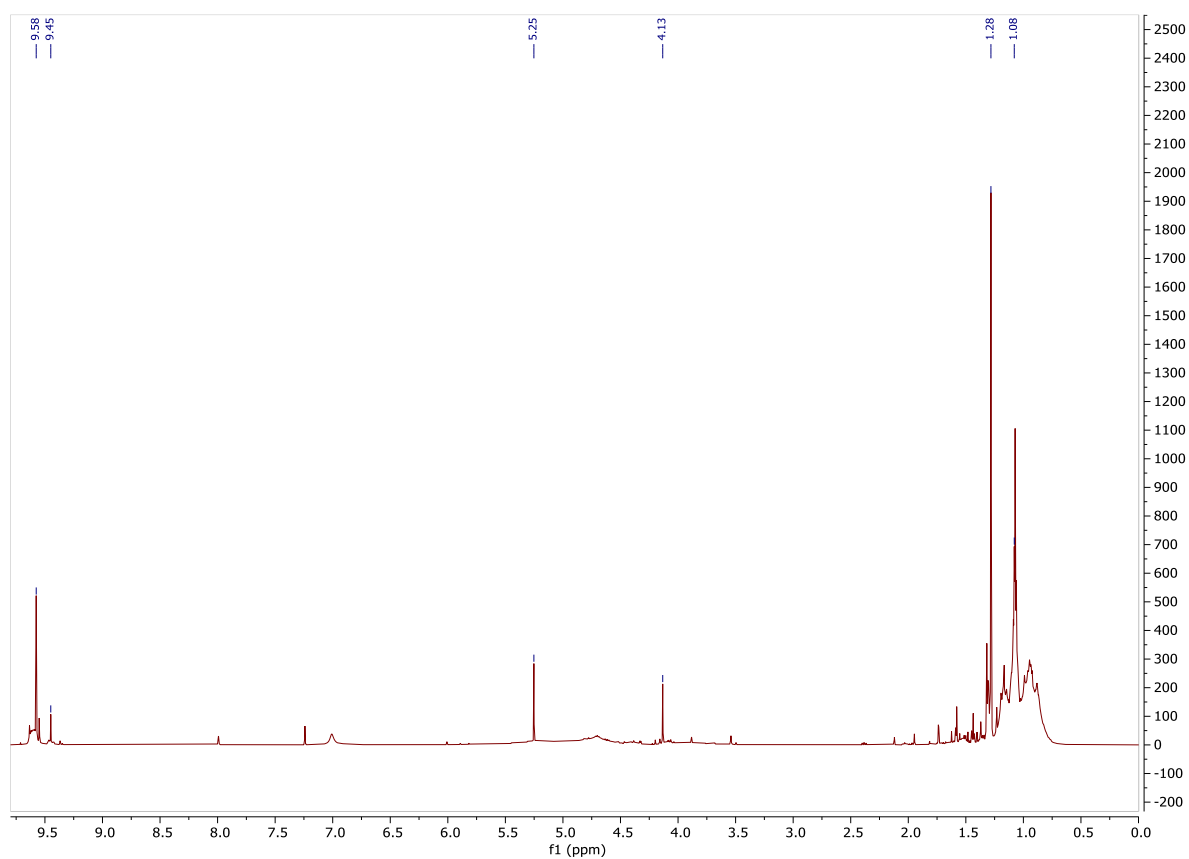


Figure 45. ^1H NMR spectrum of **30** in CDCl_3 .

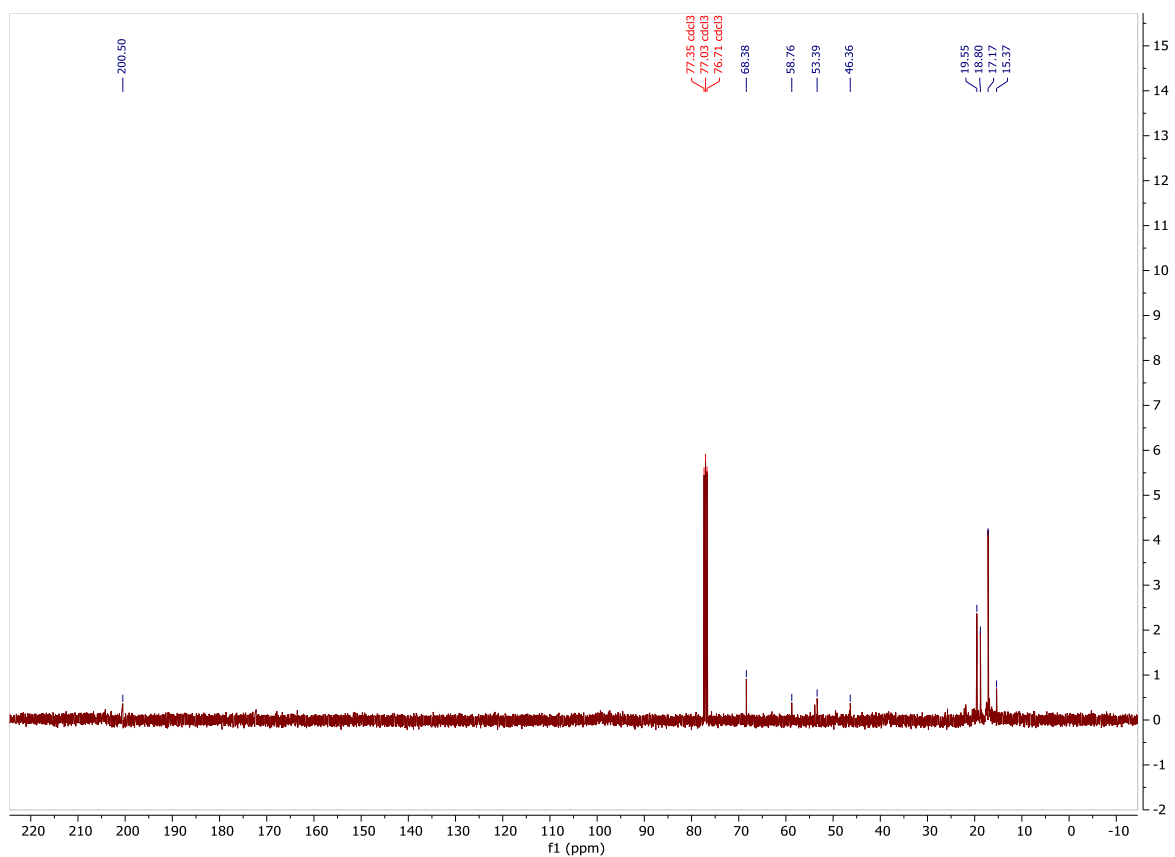


Figure 46. ^{13}C NMR spectrum of **30** in CDCl_3 .

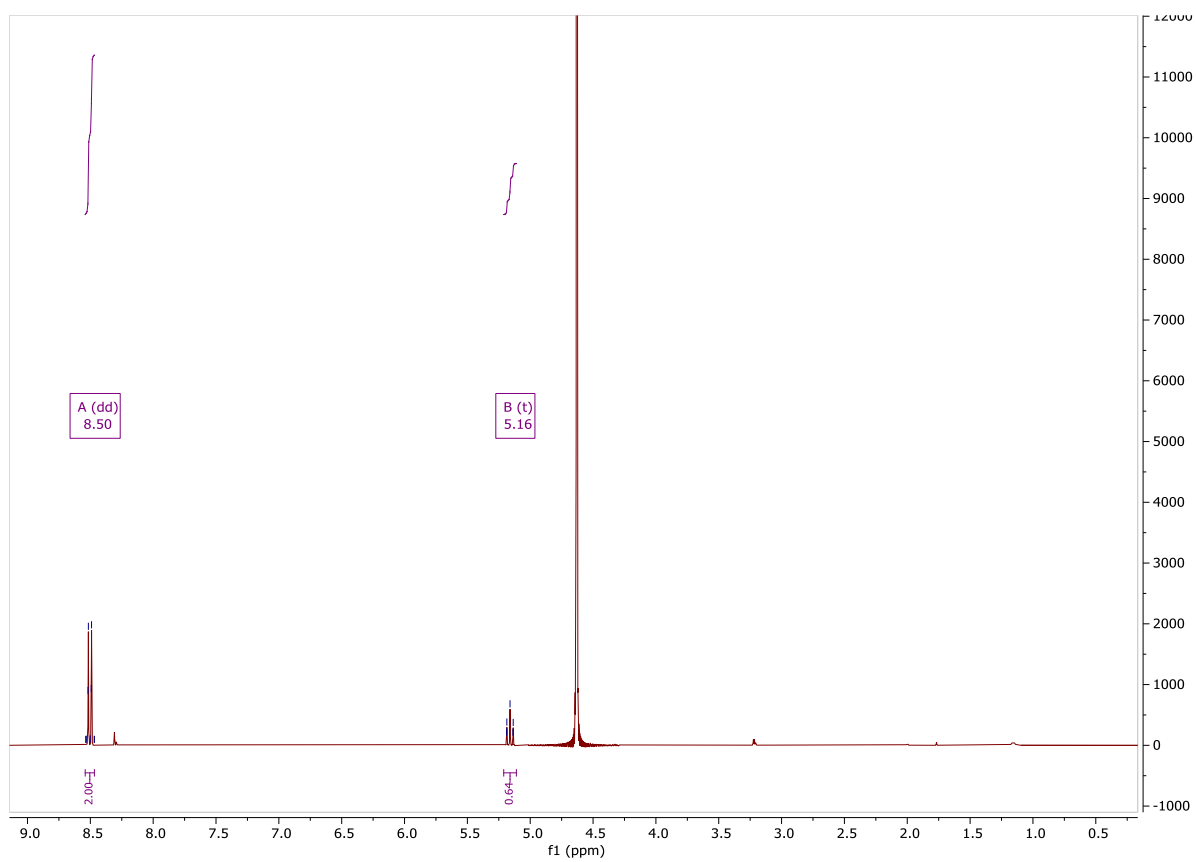


Figure 47. ^1H NMR spectrum of **53** in D_2O .

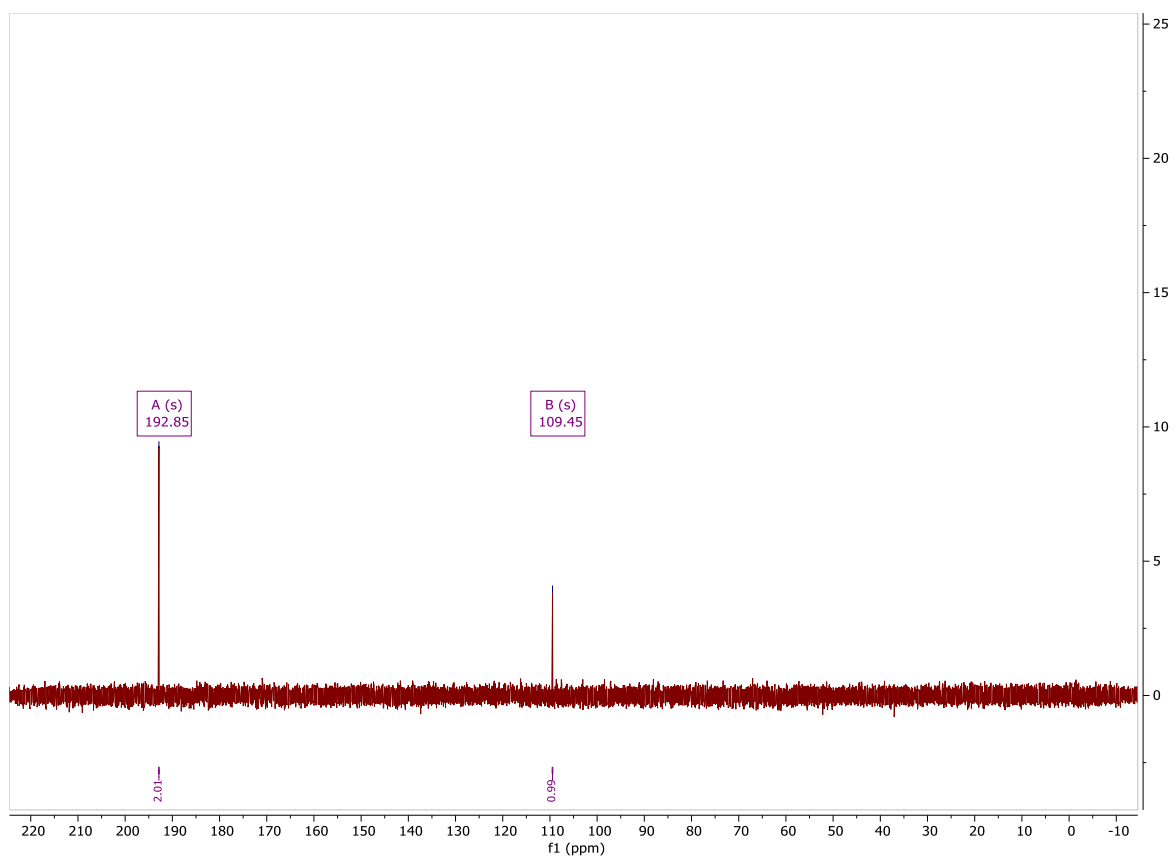


Figure 48. ^{13}C NMR spectrum of **53** in D_2O .

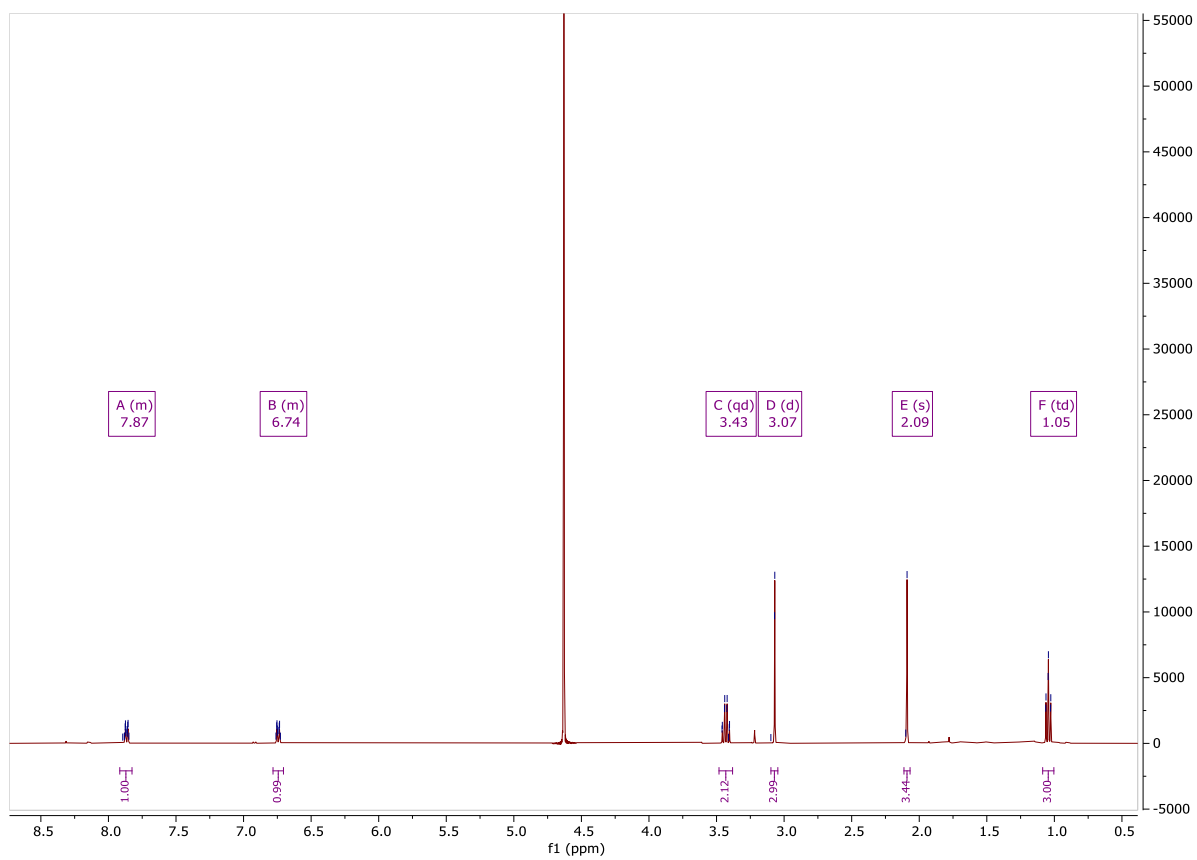


Figure 49. ^1H NMR spectrum of **55** (procedure a) in D_2O .

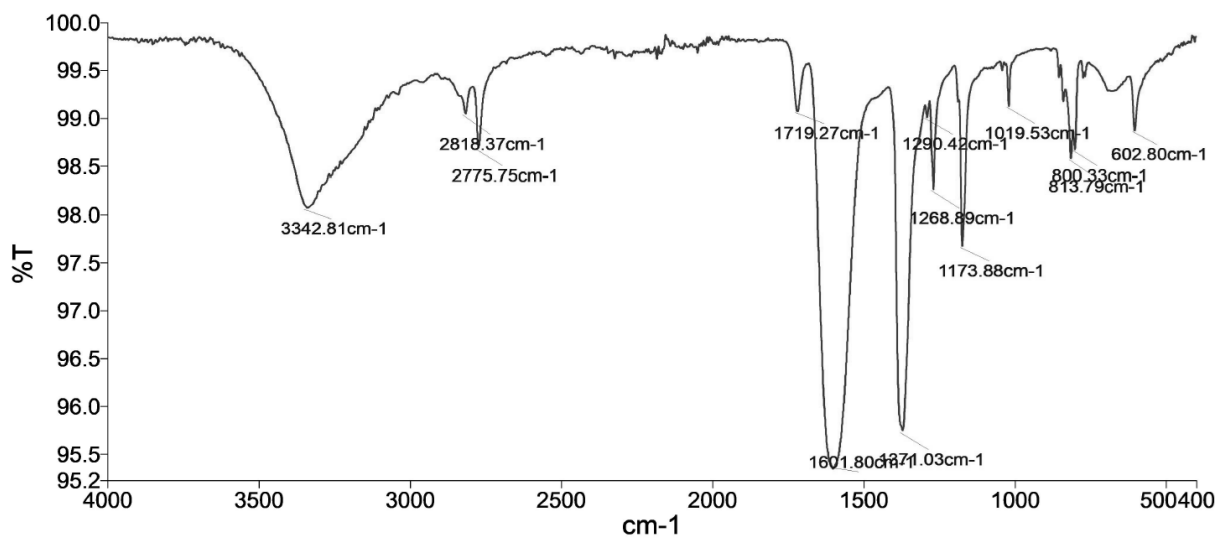


Figure 50. ATR-IR spectrum of **53**.

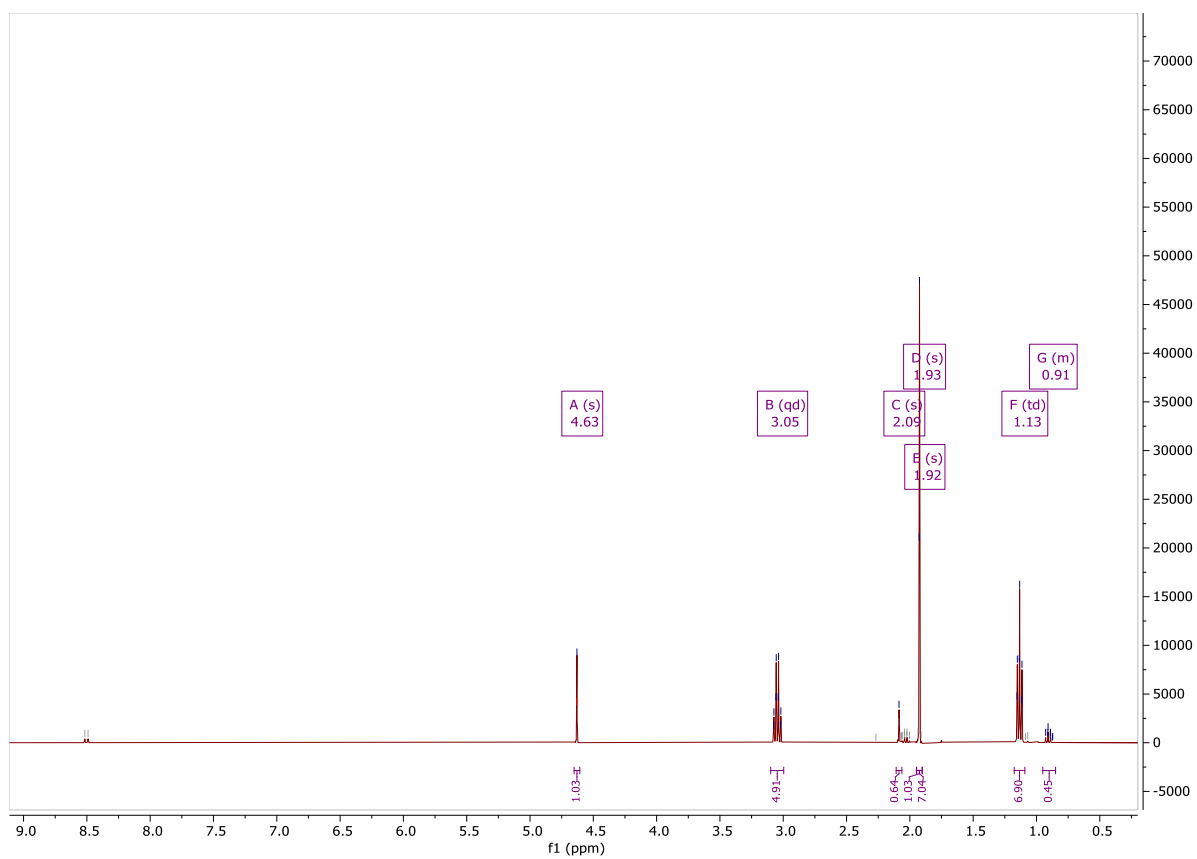


Figure 51. ¹H NMR spectrum of **55** (procedure b) in D₂O.

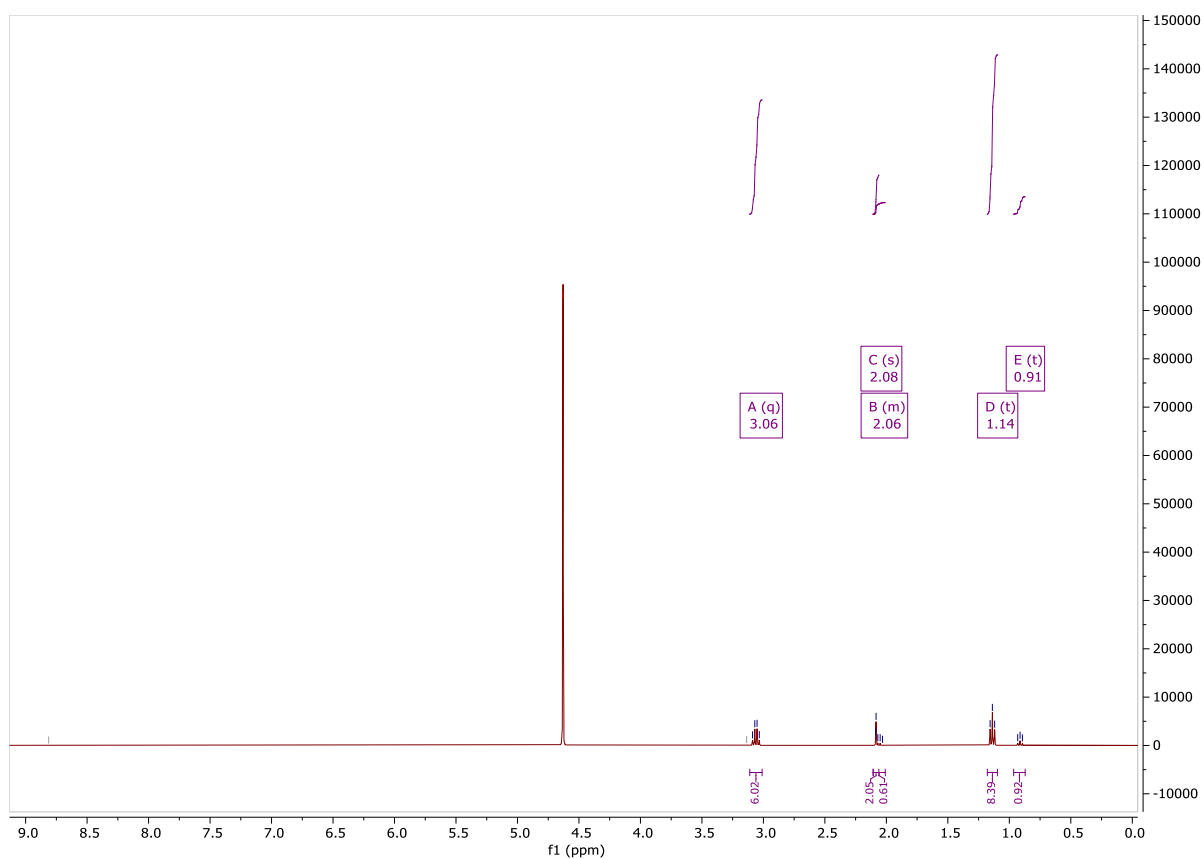


Figure 52. ¹H NMR spectrum of **55** (procedure c) in D₂O.

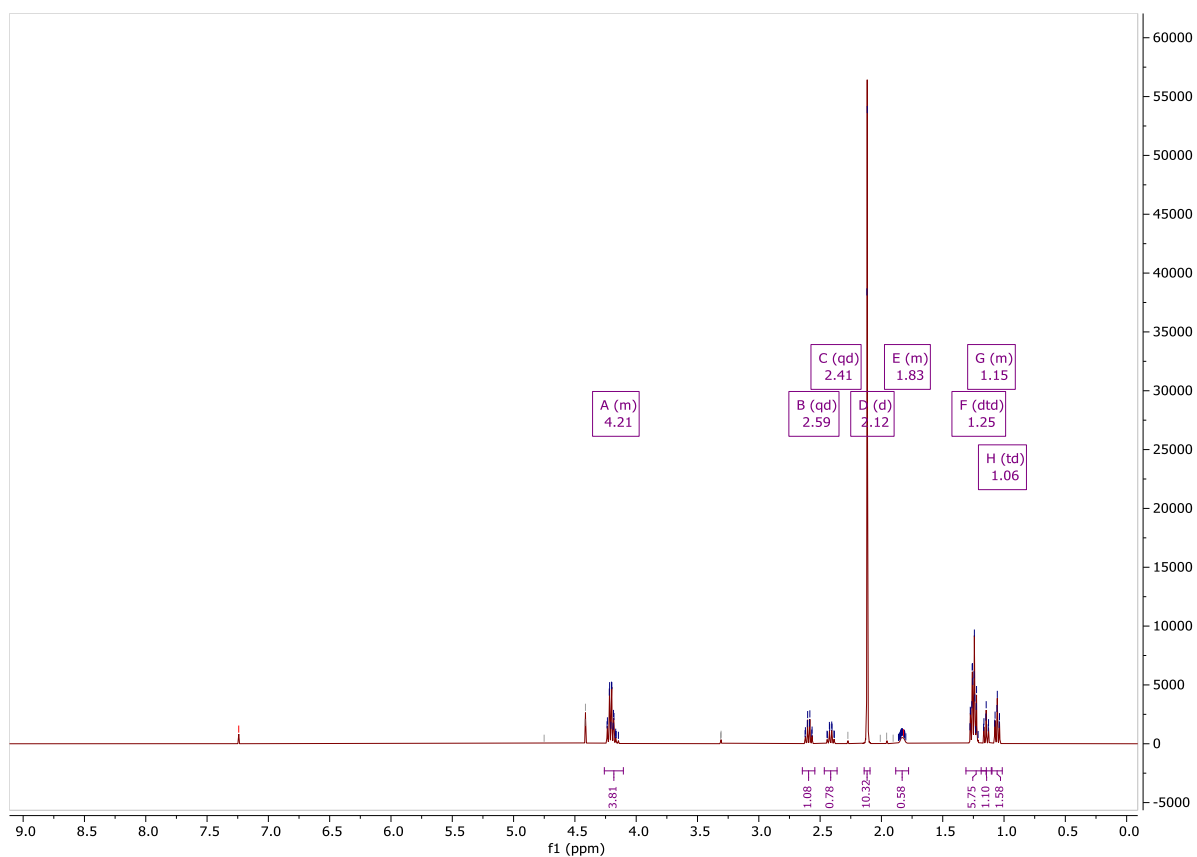


Figure 53. ¹H NMR spectrum of **57** in CDCl₃.

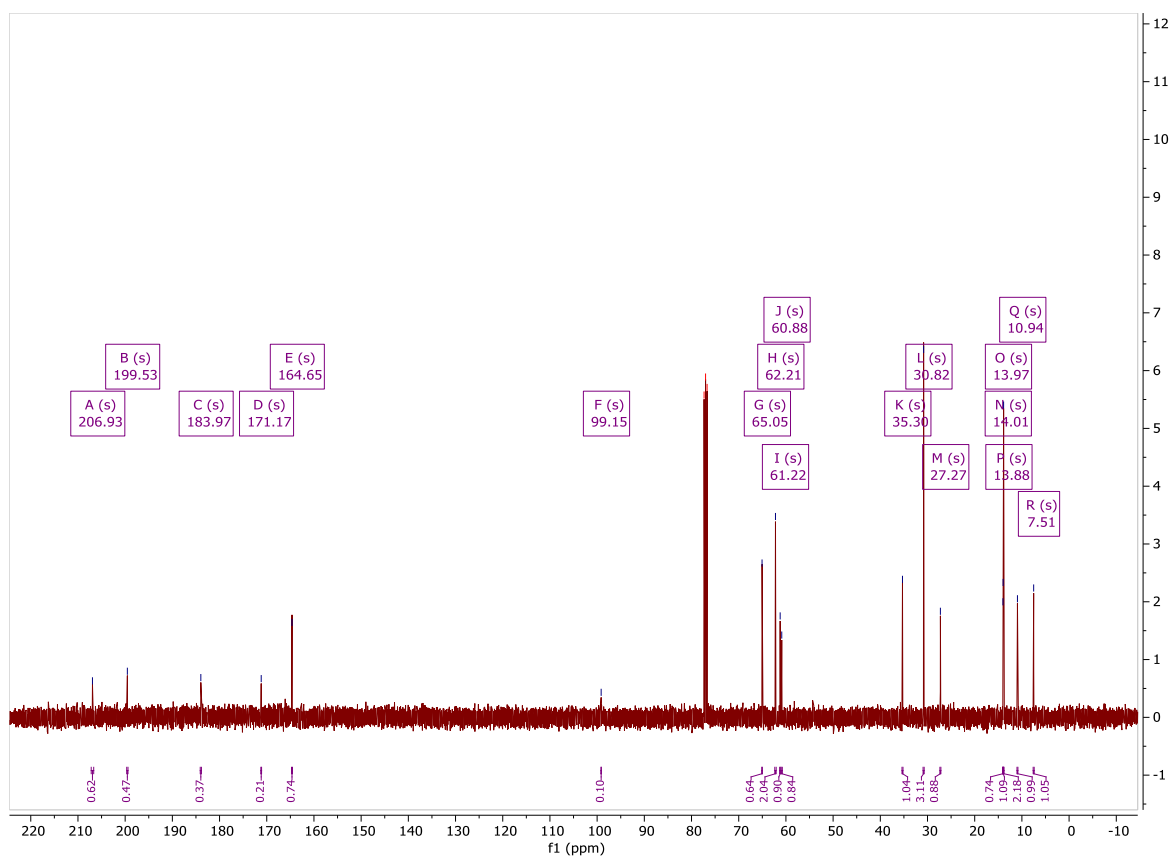


Figure 54. ^{13}C NMR spectrum of **57** in CDCl_3 .

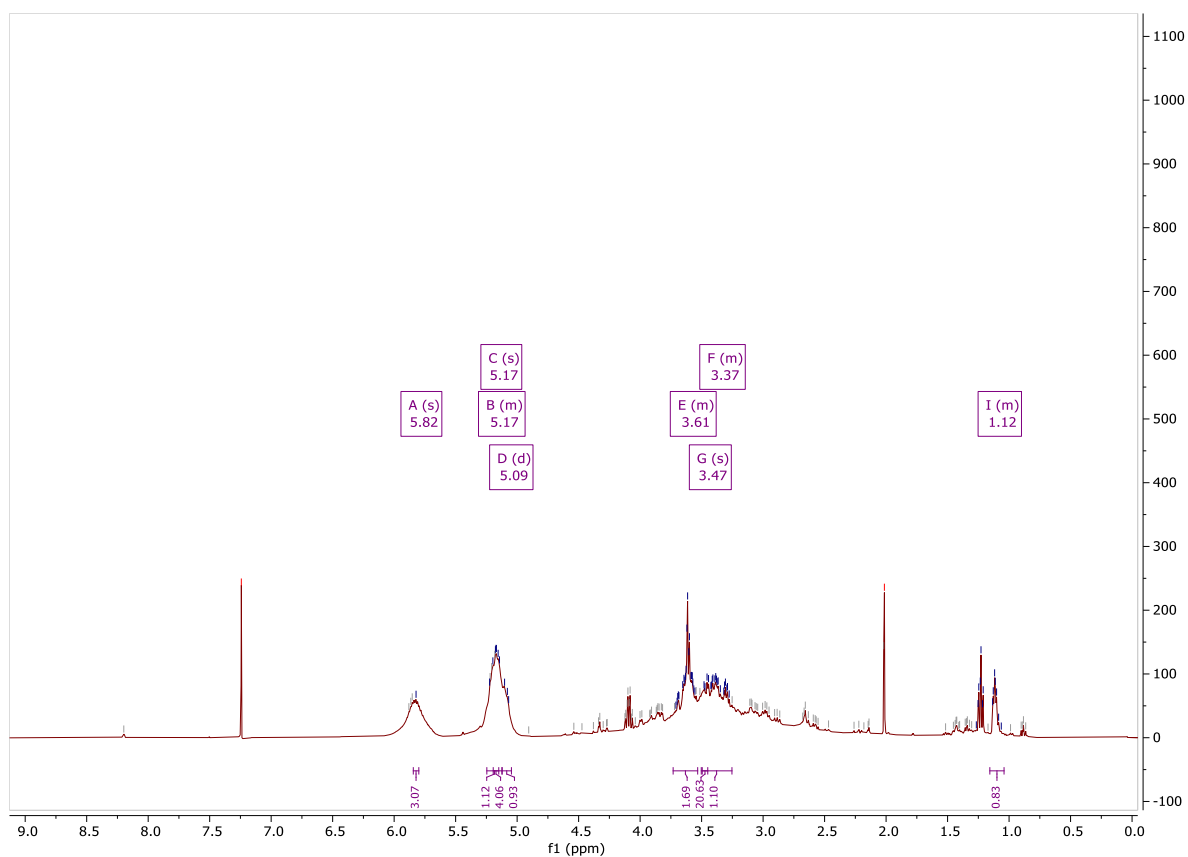


Figure 55. ^1H NMR spectrum of **63** (procedure a) in CDCl_3 .

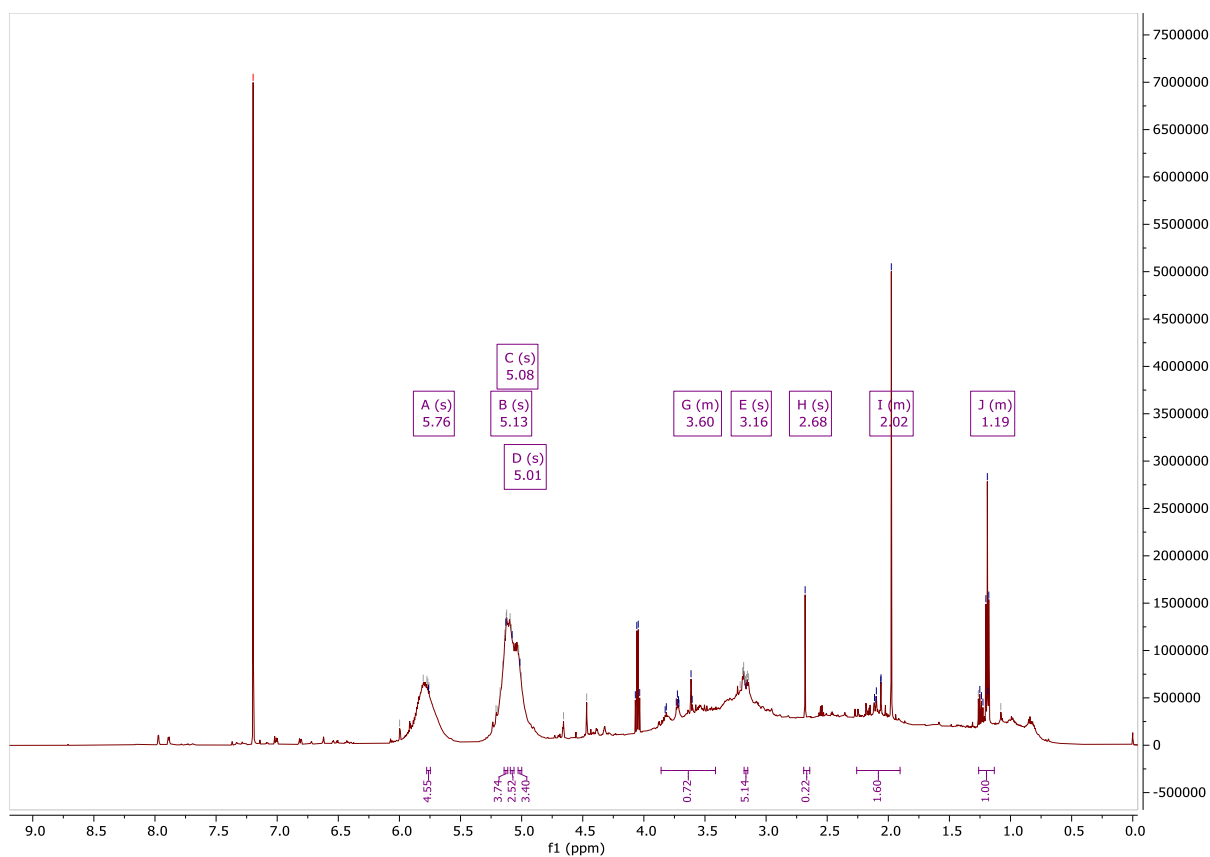


Figure 56. ^1H NMR spectrum of **63** (procedure b) in CDCl_3 .

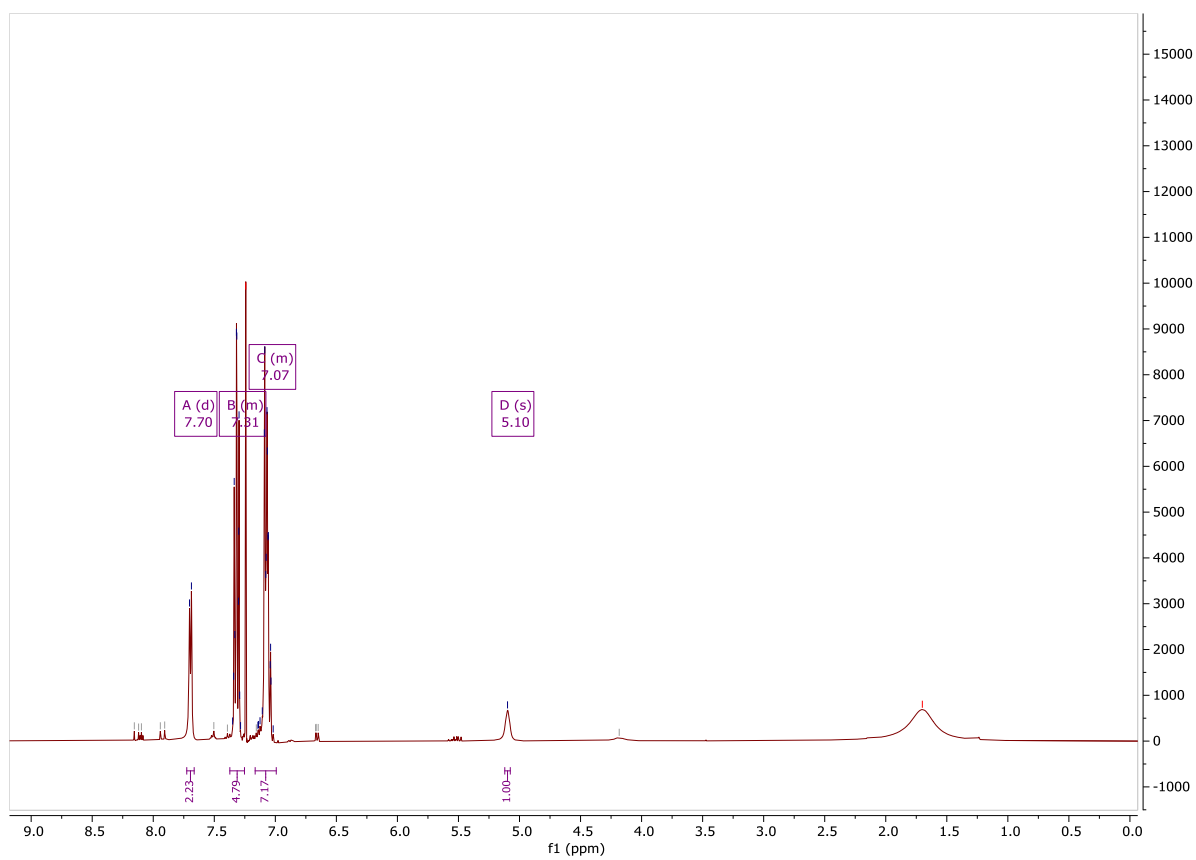


Figure 57. ^1H NMR spectrum of **66** in CDCl_3 .

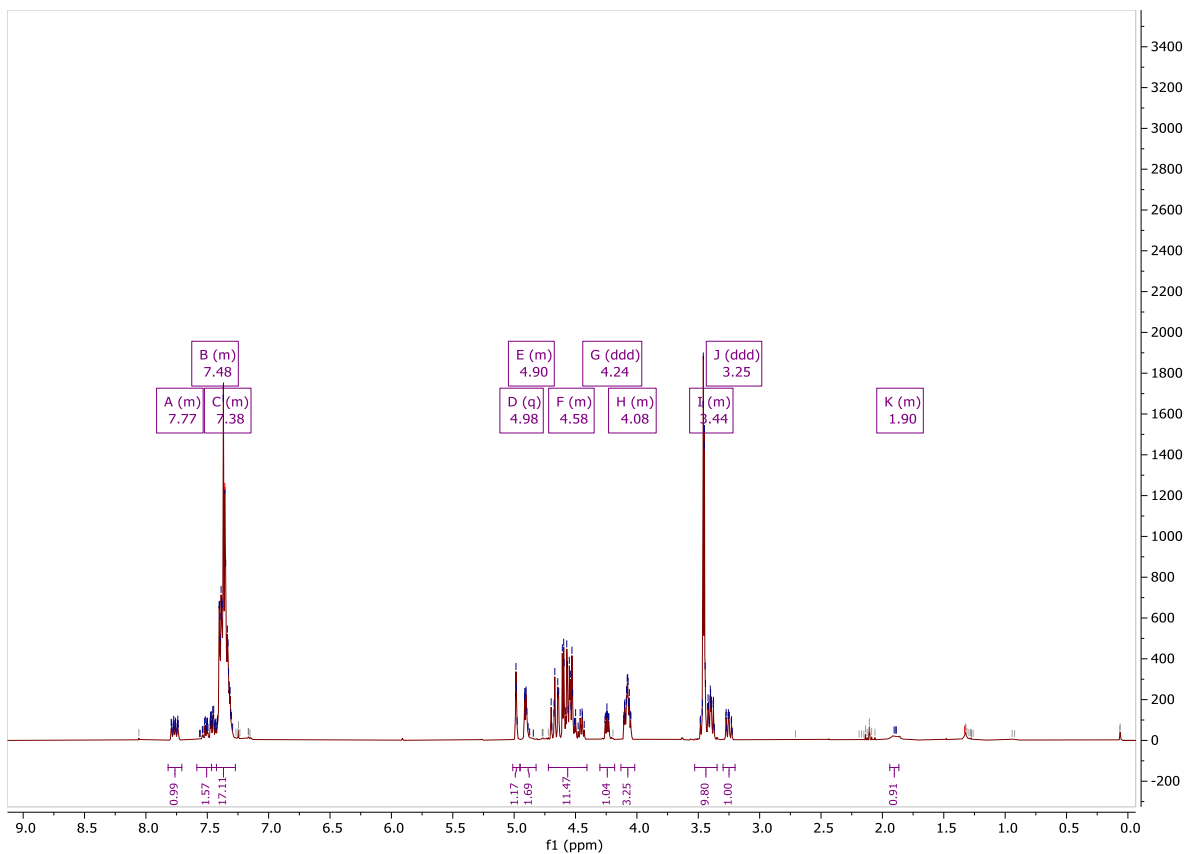


Figure 58. ^1H NMR spectrum of **68** (procedure a) in CDCl_3

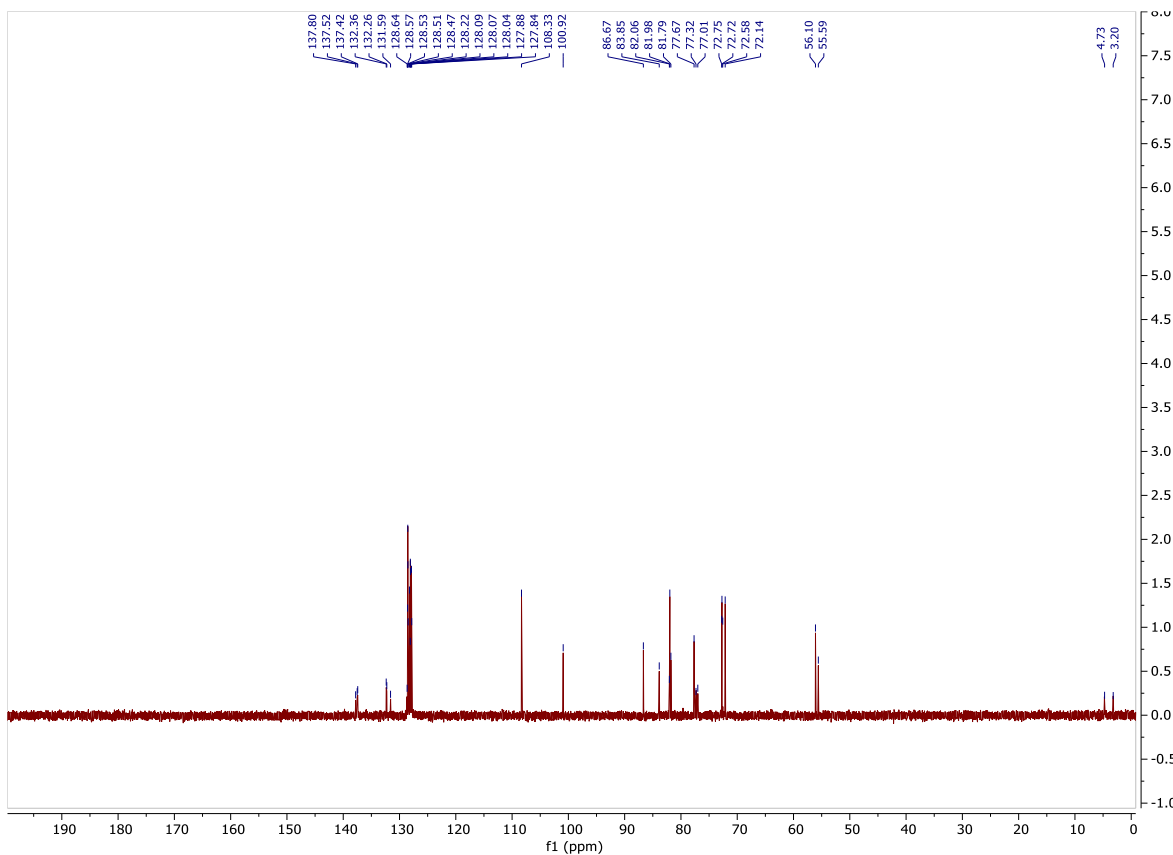


Figure 59. ^{13}C NMR spectrum of **68** (procedure a) in CDCl_3 .

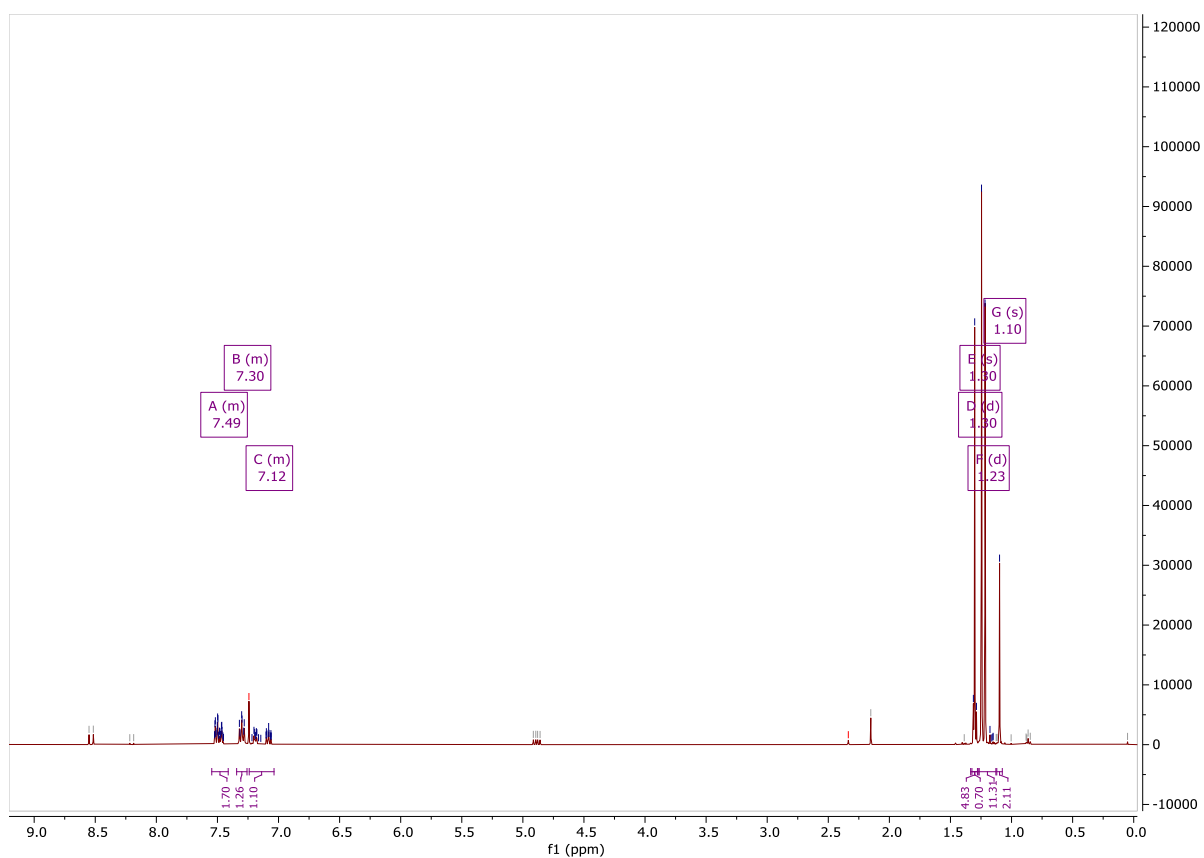


Figure 60. ¹H NMR spectrum of **68** (procedure b) in CDCl₃.



Figure 61. ^{13}C NMR spectrum of **68** (procedure b) in CDCl_3 .

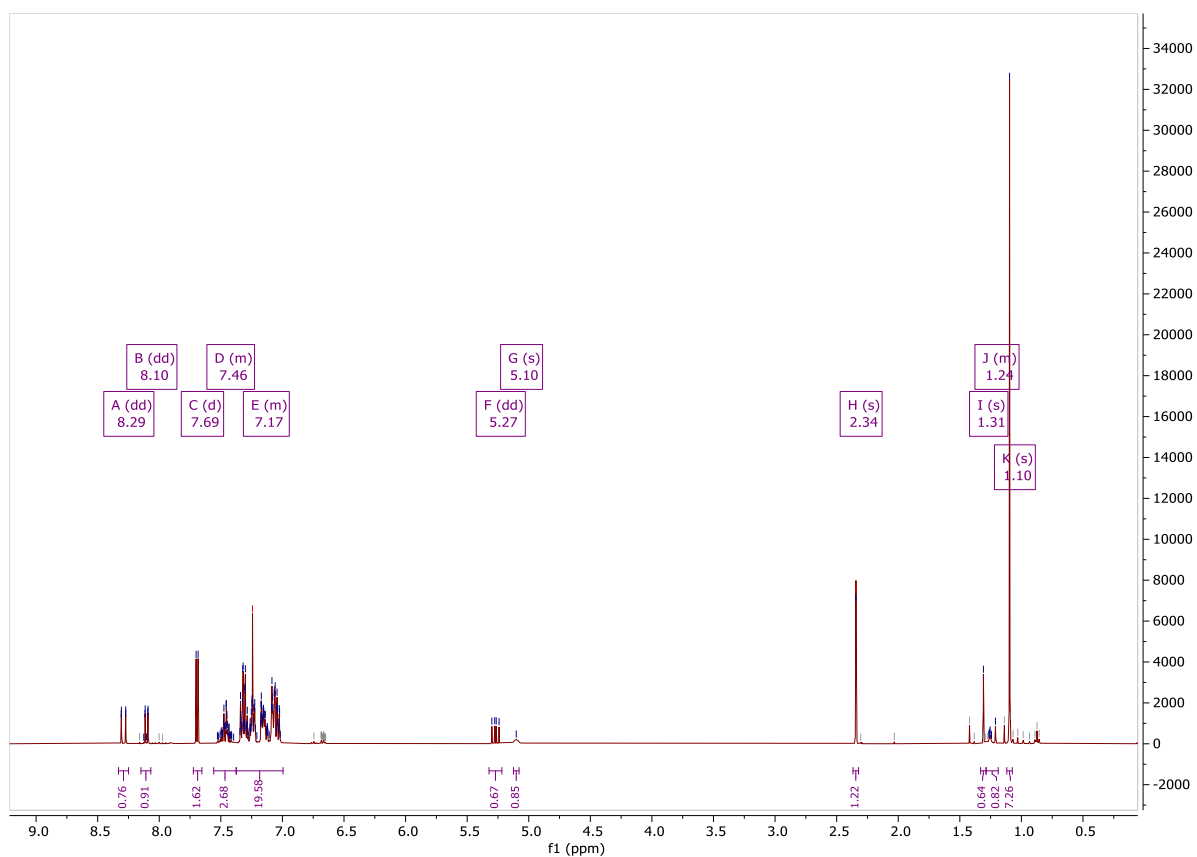


Figure 62. ^1H NMR spectrum of **68** (procedure c) in CDCl_3 .

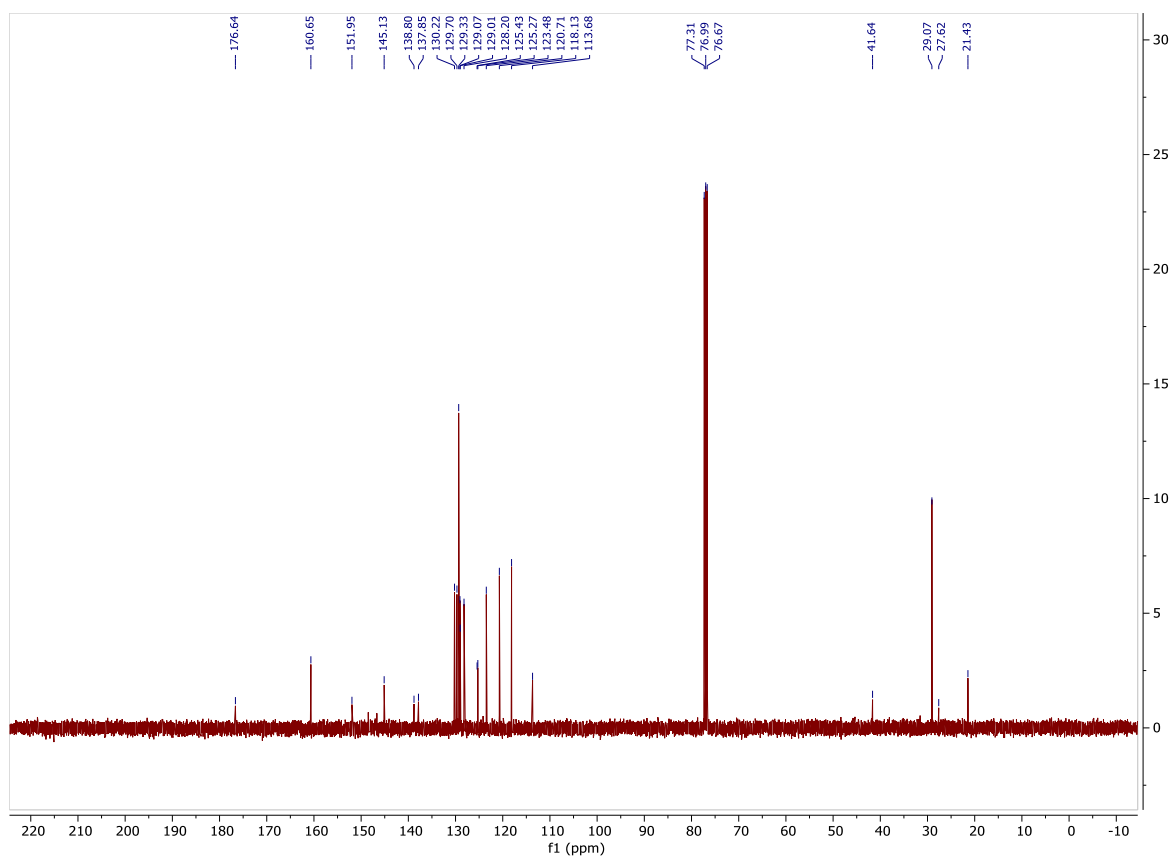


Figure 63. ^{13}C NMR spectrum of **68** (procedure c) in CDCl_3 .

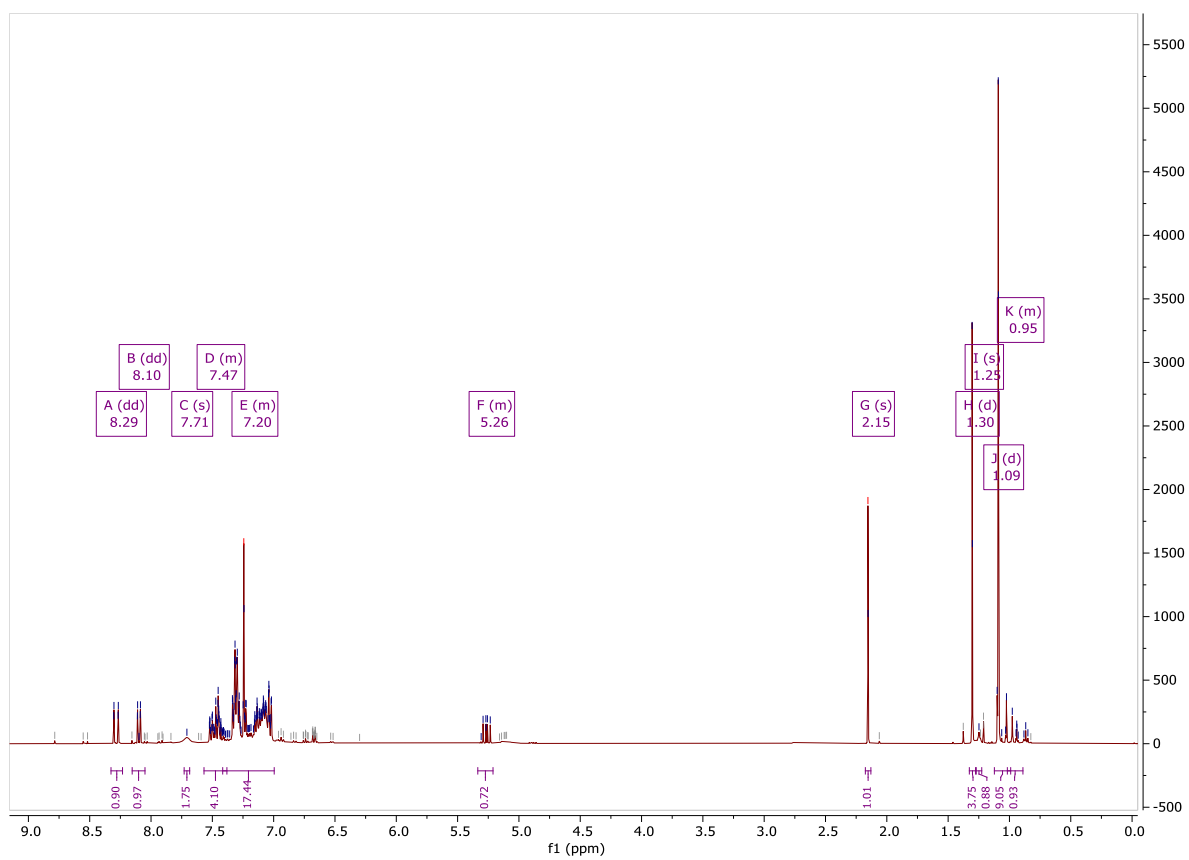


Figure 64. ^1H NMR spectrum of **68** (procedure d) in CDCl_3 .

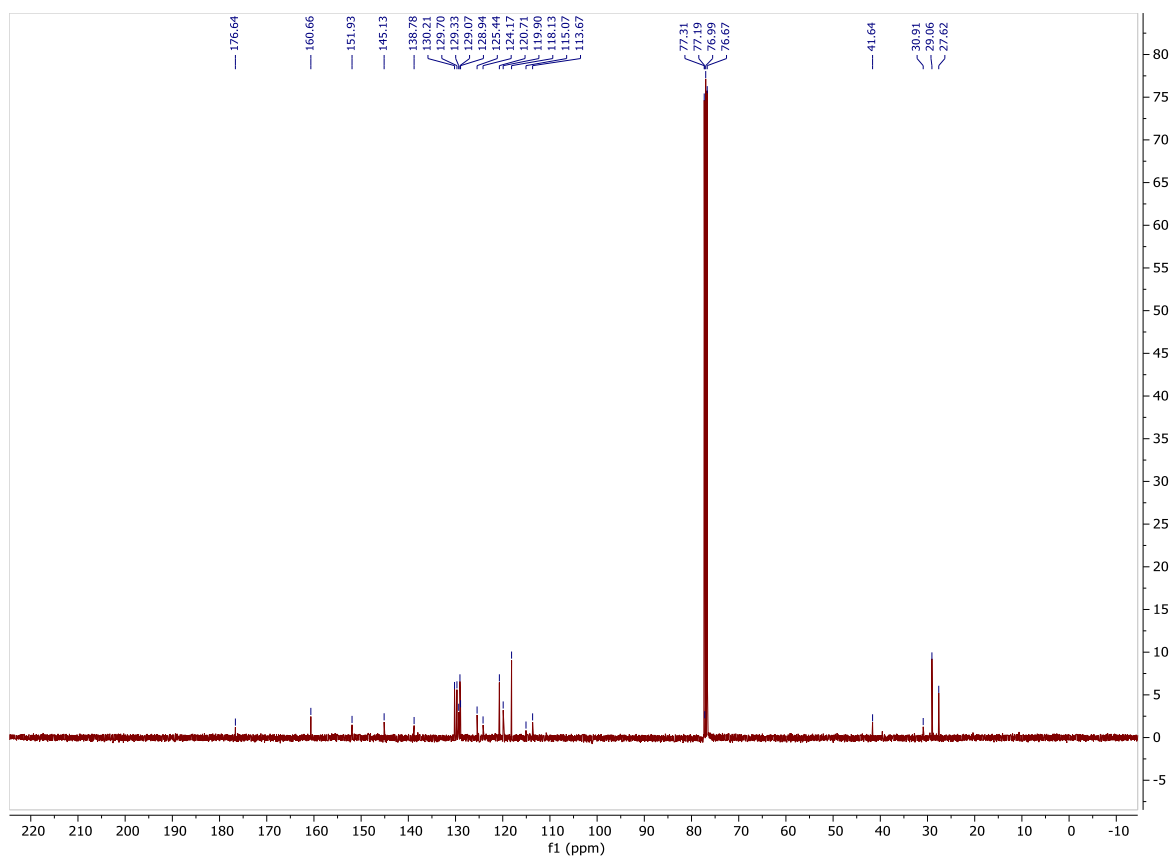


Figure 65. ^{13}C NMR spectrum of **68** (procedure d) in CDCl_3 .

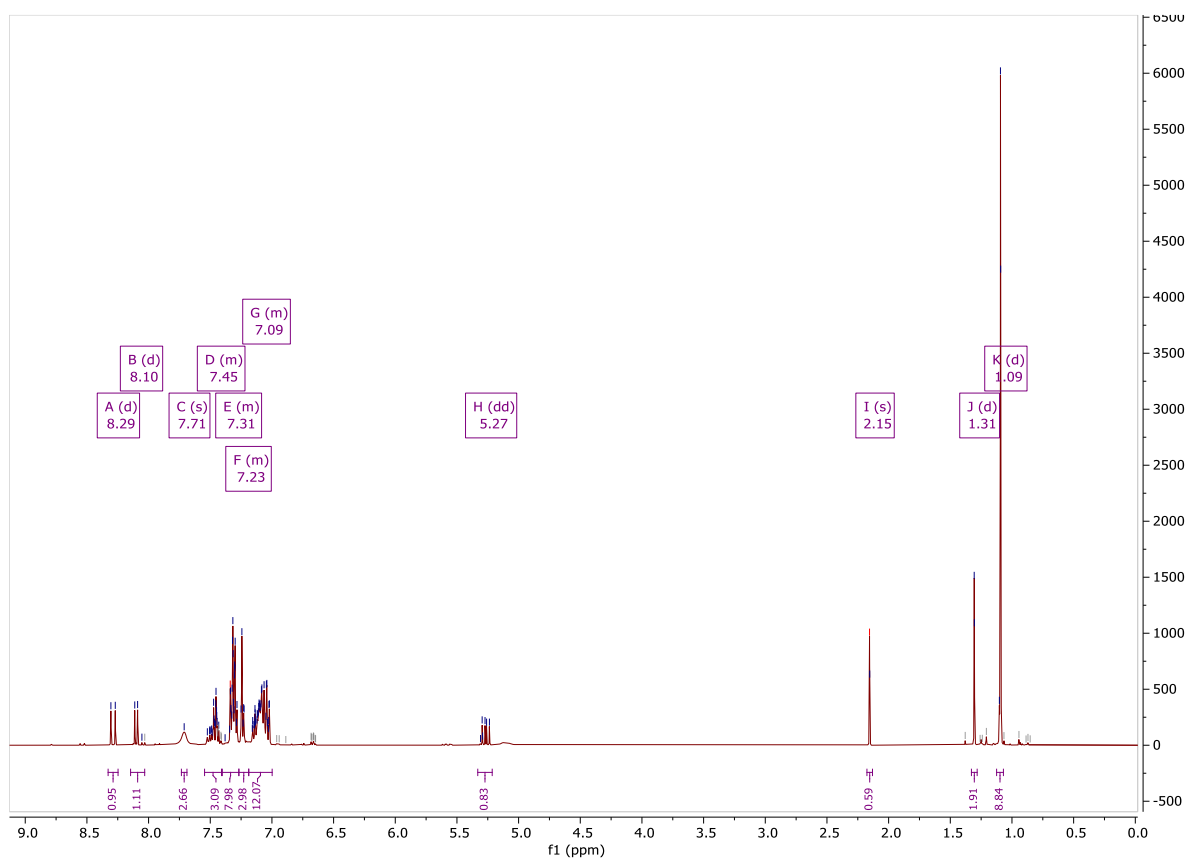


Figure 66. ^1H NMR spectrum of **68** (procedure e) in CDCl_3 .

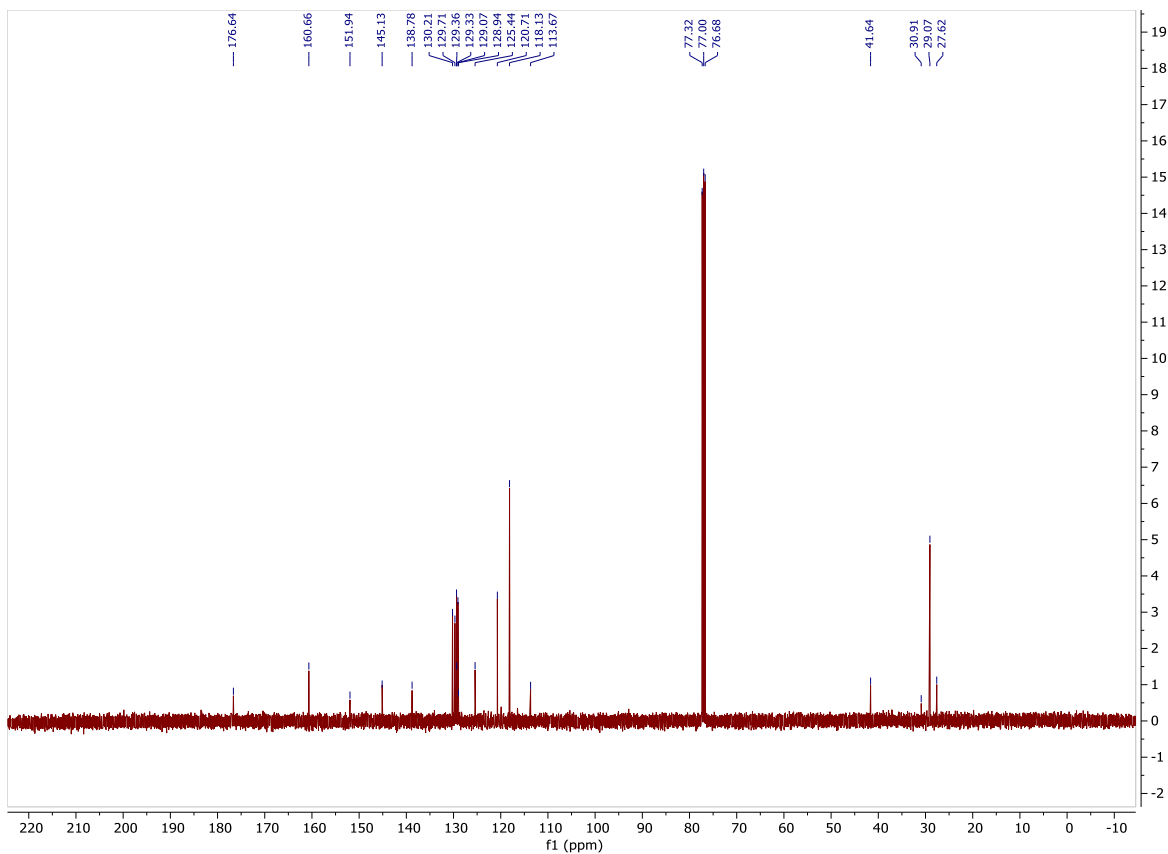


Figure 67. ^{13}C NMR spectrum of **68** (procedure e) in CDCl_3 .

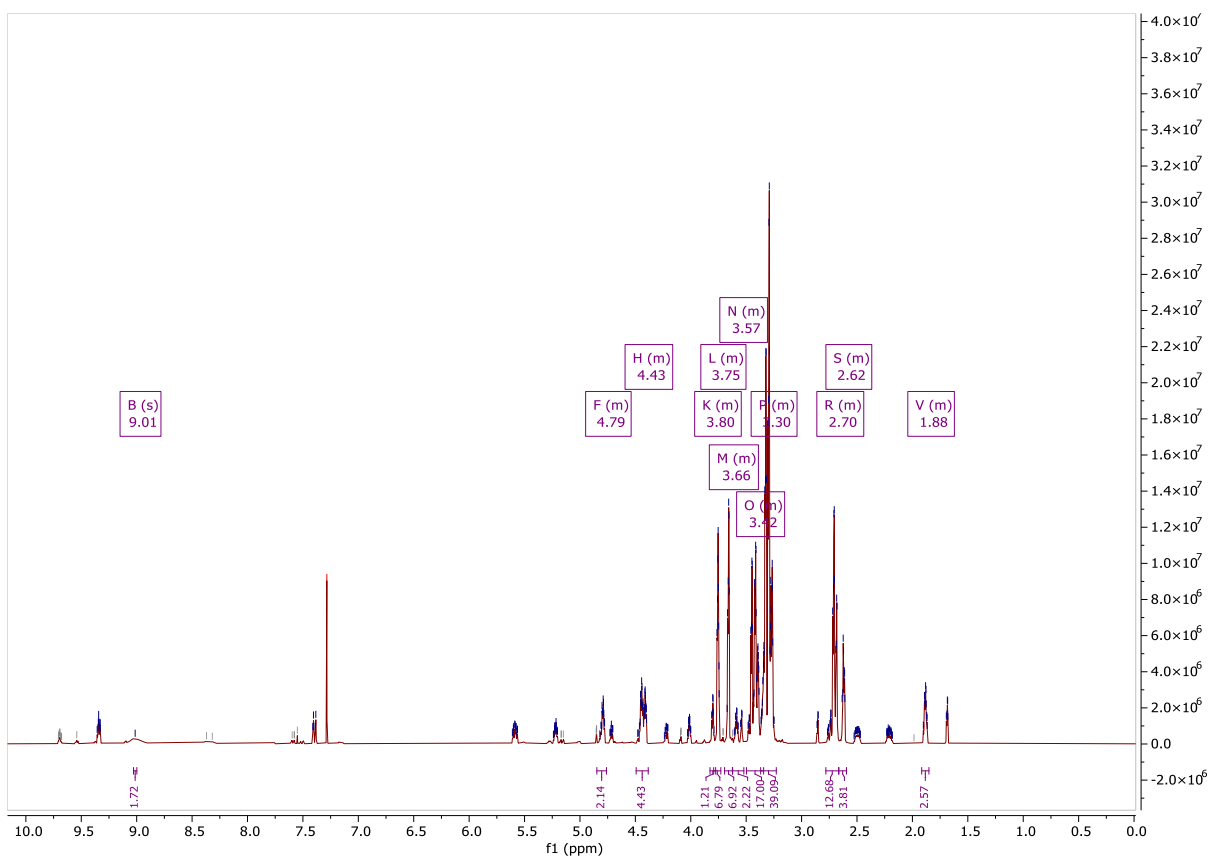


Figure 68. ^1H NMR spectrum of **39** (procedure a) in CDCl_3 .

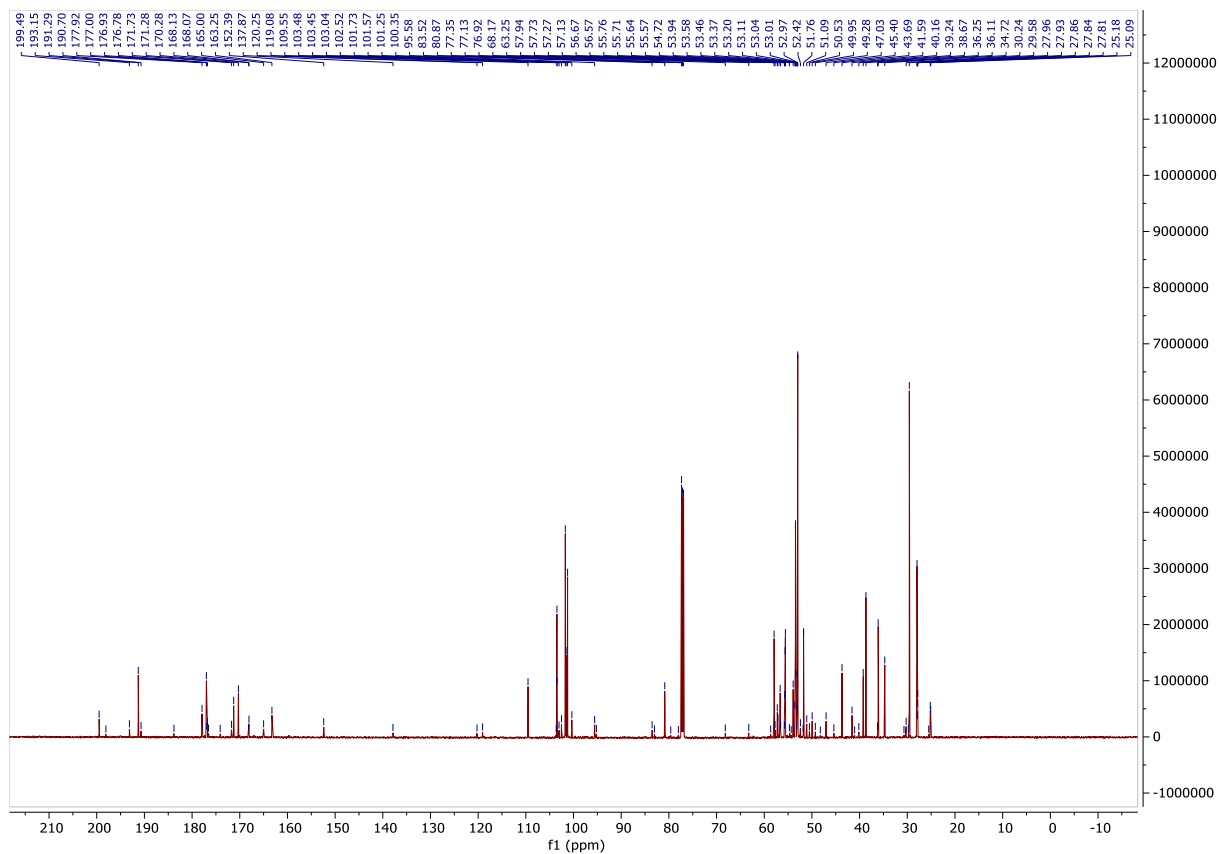


Figure 69. ^{13}C NMR spectrum of **39** (procedure a) in CDCl_3 .

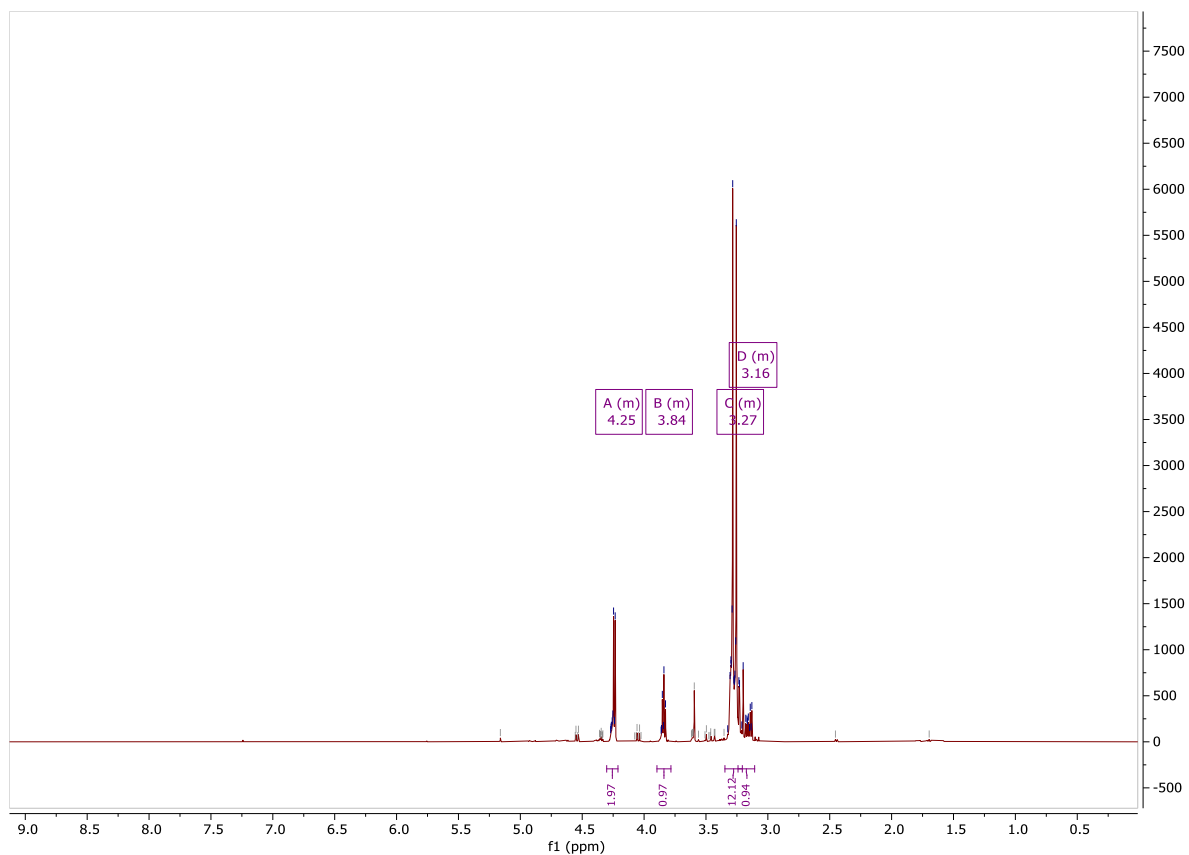


Figure 70. ^1H NMR spectrum of **39** (procedure b₁) in CDCl_3 .

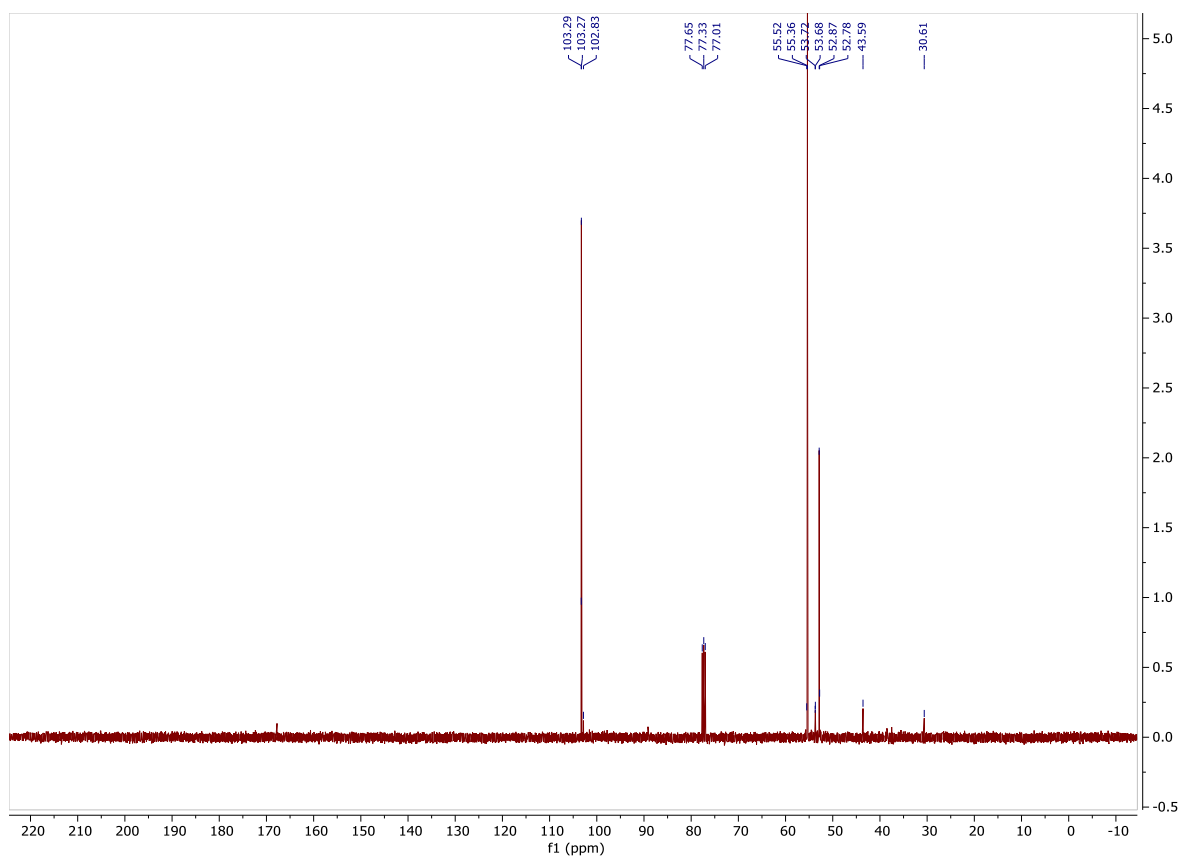


Figure 71. ^{13}C NMR spectrum of **39** (procedure b₁) in CDCl_3 .

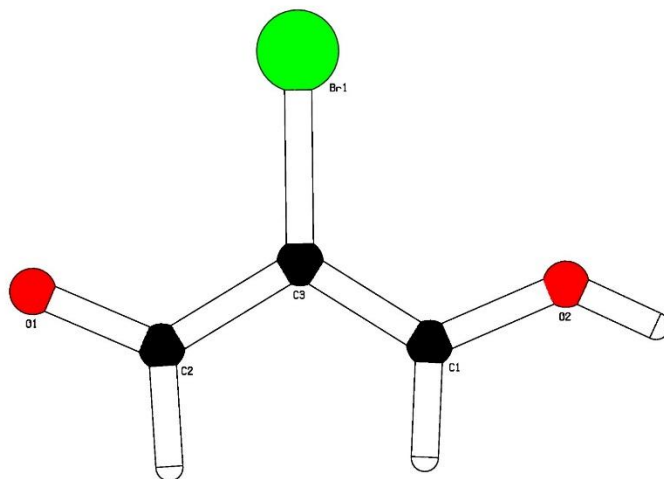


Figure 72. Crystal structure of the hydrolysis product of **39** (2-bromomalonaldehyde) as determined per X-ray crystallography.

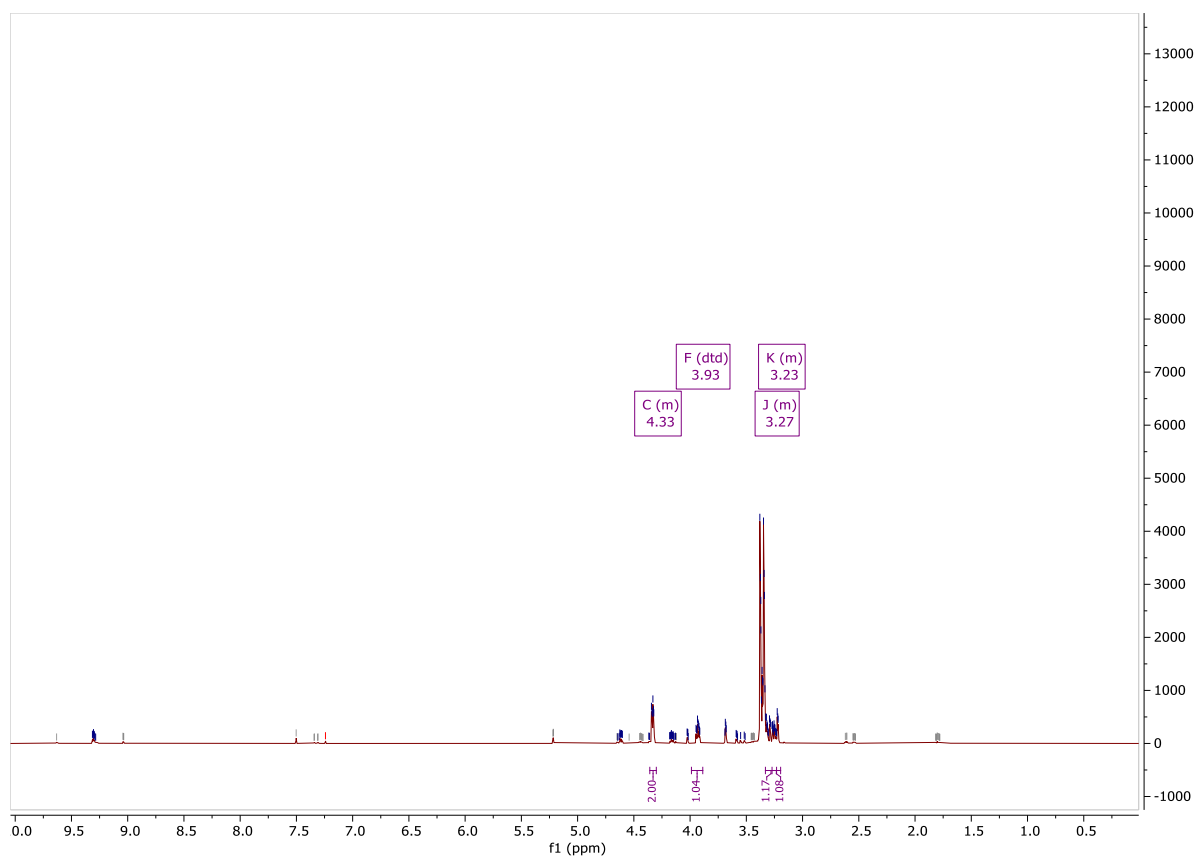


Figure 73. ^1H NMR spectrum of **39** (procedure b_2) in CDCl_3 .

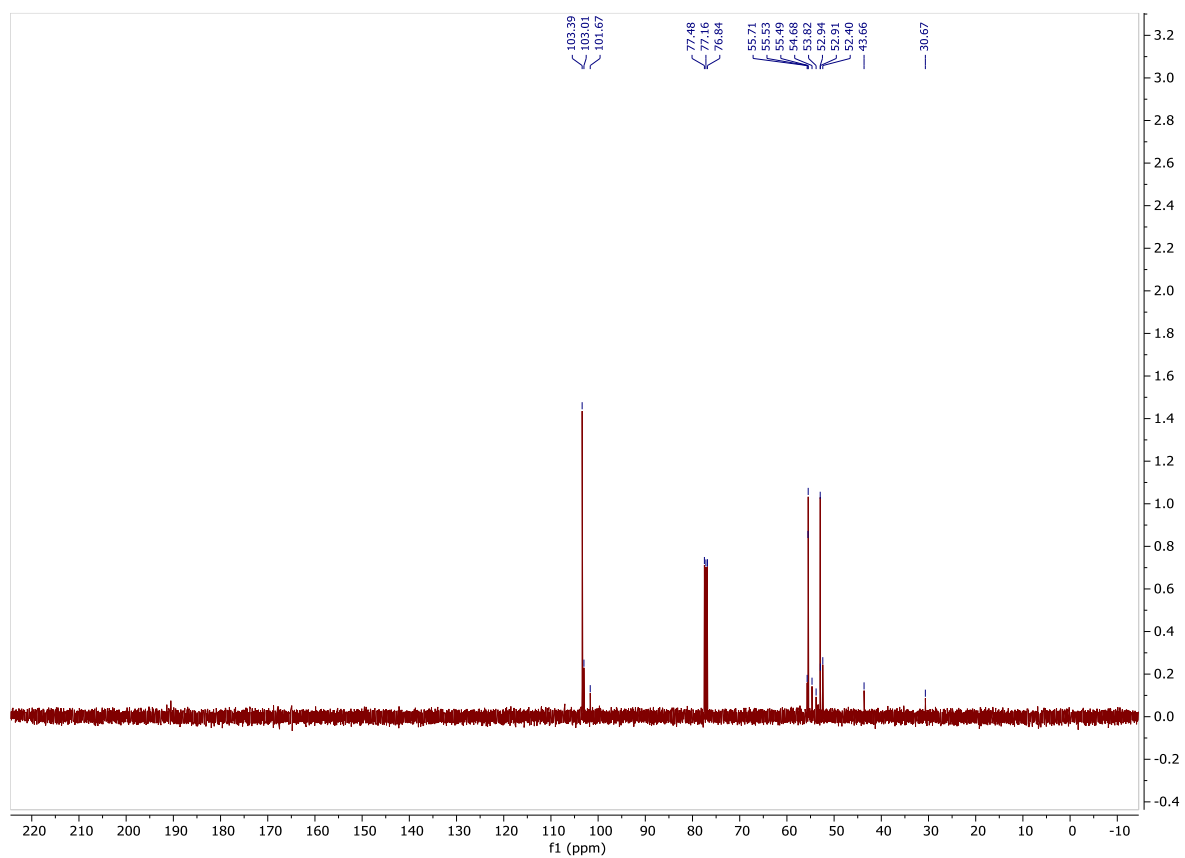


Figure 74. ^{13}C NMR spectrum of **39** (procedure b_2) in CDCl_3 .

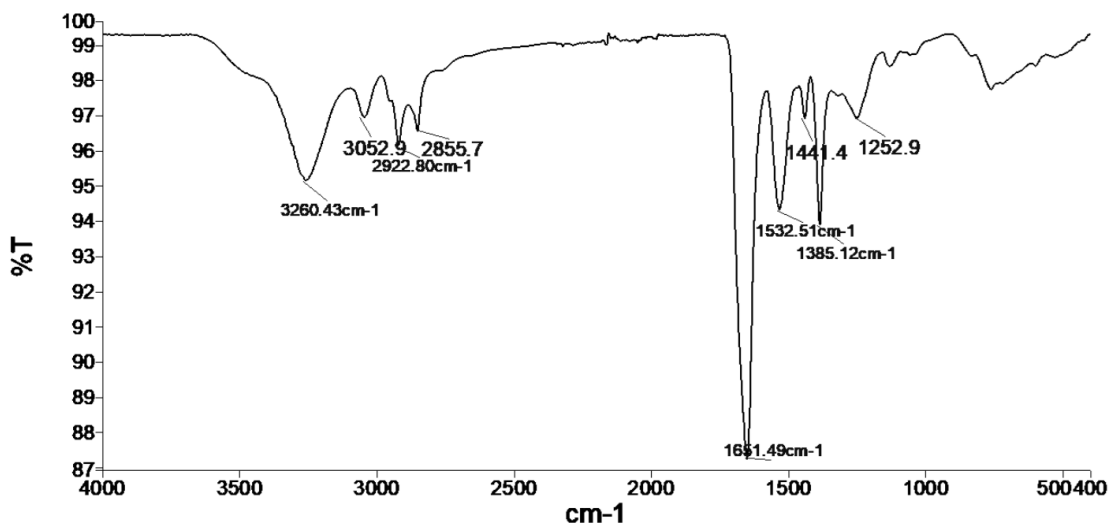


Figure 75. ATR-IR spectrum of **32**.

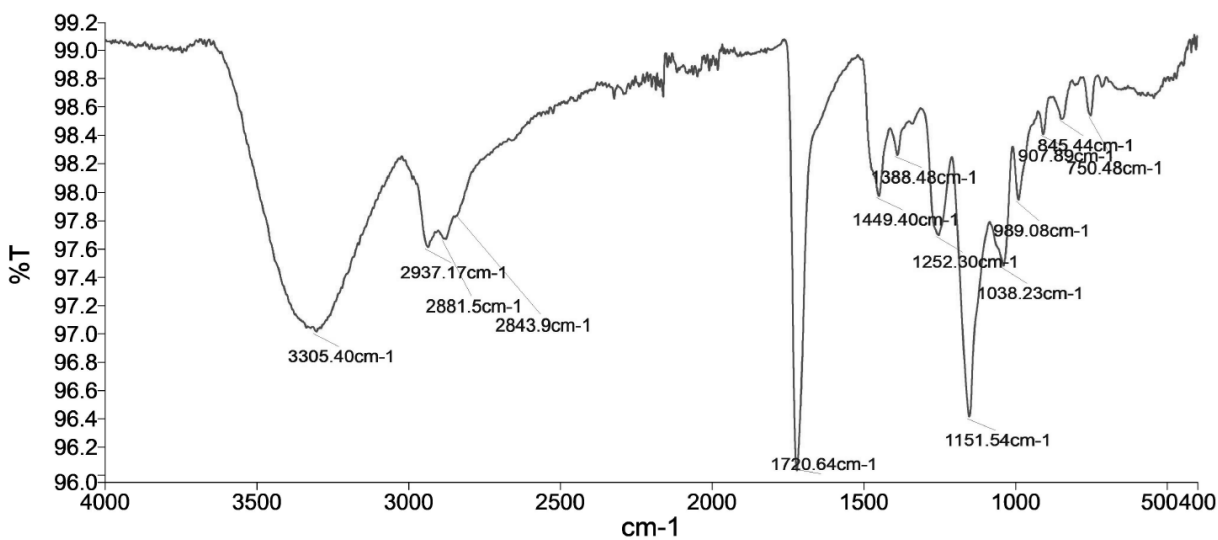


Figure 76. ATR-IR spectrum of **70**.

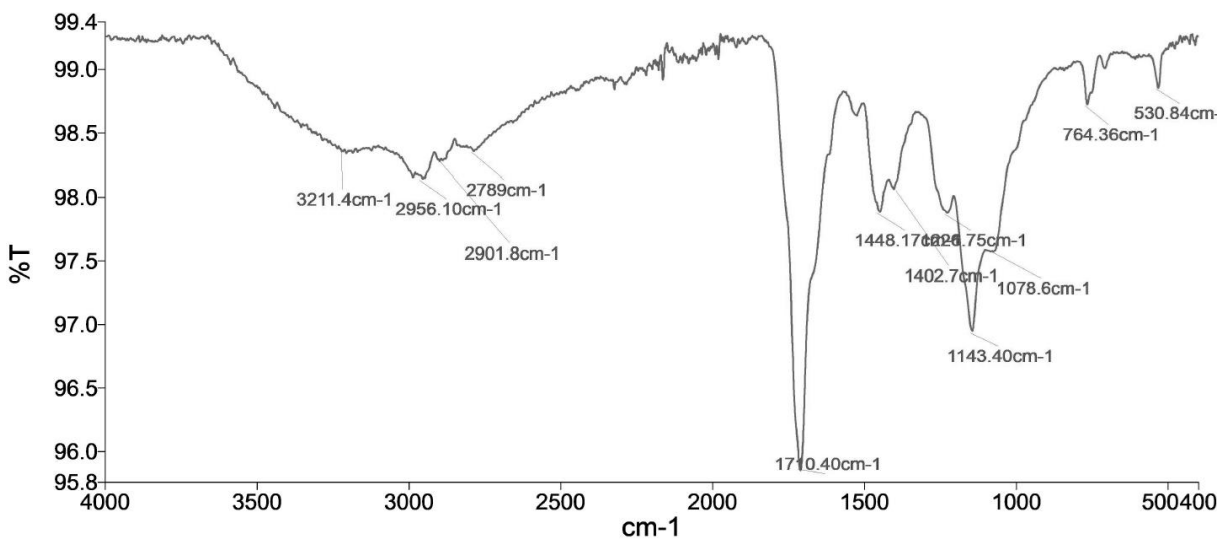


Figure 77. ATR-IR spectrum of **71**.

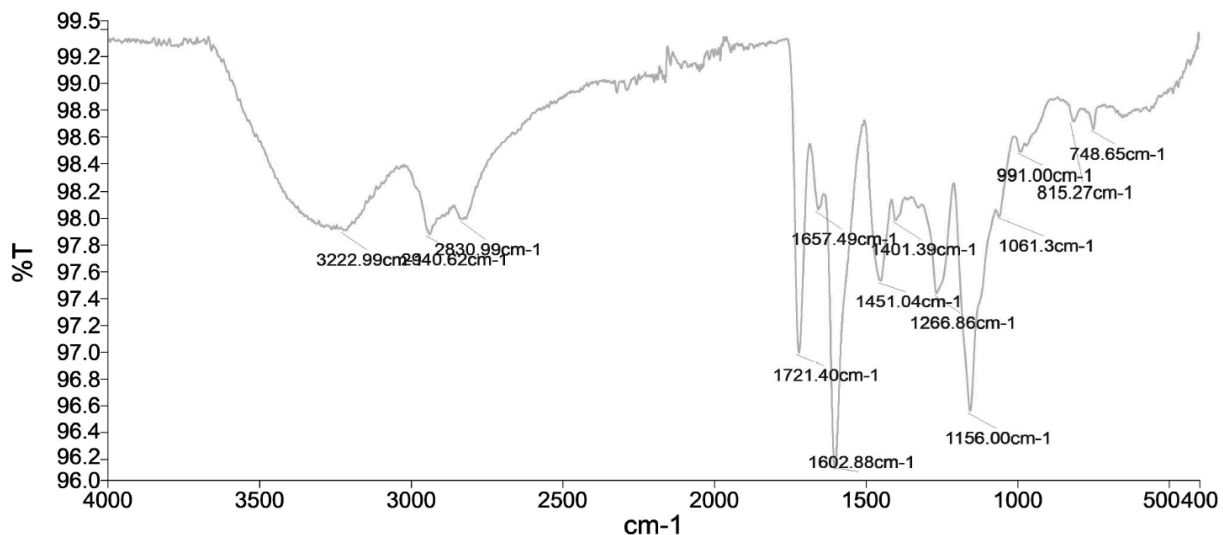


Figure 78. ATR-IR spectrum of **45**.

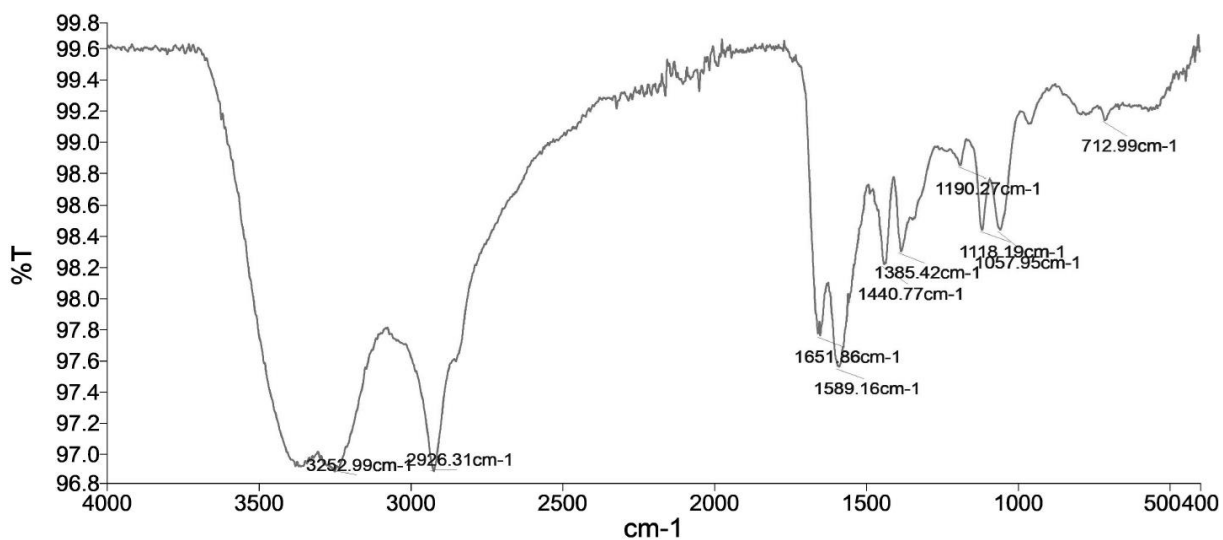


Figure 79. ATR-IR spectrum of **40**.

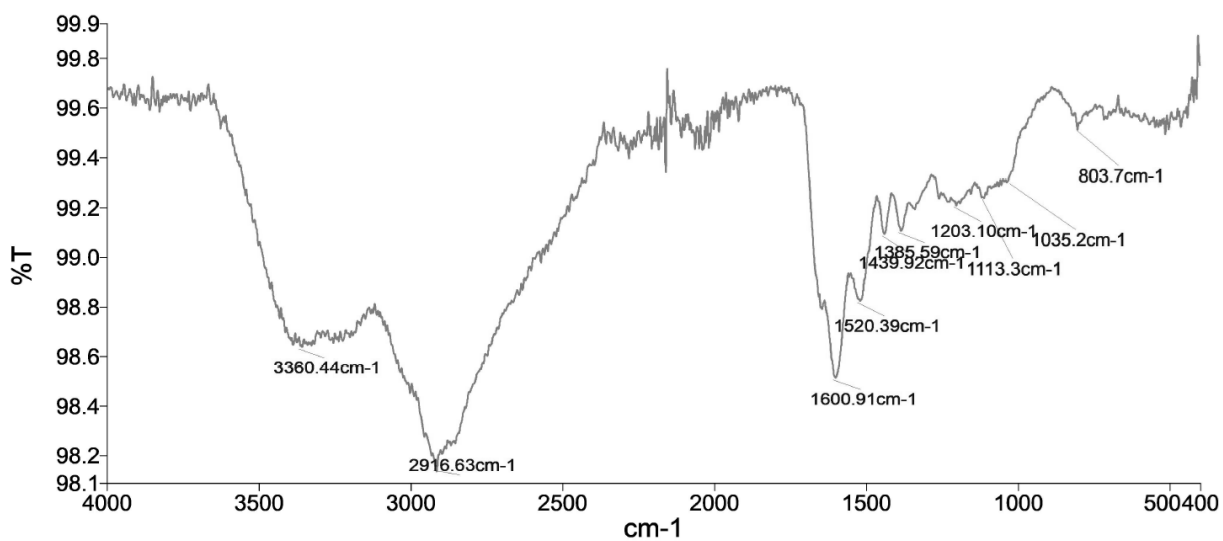


Figure 80. ATR-IR spectrum of **41**.

10.2. Urea reactivity measurements of synthesized polymers.

Each sample was measured twice.

Table 4. Urea reactivity measurement data of **71**. Measured by Babette Lentferink.

Sample	Time [h]	Temperature [°C]	Urea concentration [mM]
1	0.5	70	47.5
	1	70	49.4
	2	70	48.4
	4	70	47.2
	8	70	49.1
	24	70	48.9
2	0.5	70	50.7
	1	70	51.1
	2	70	49.4
	4	70	51.8
	8	70	45.4
	24	70	53.4

Table 5. Urea reactivity measurement data of **45**. Measured by Babette Lentferink.

Sample	Time [h]	Temperature [°C]	Urea concentration [mM]
1	0.5	70	46.6
	2	70	48.2
	4	70	51.2
	8	70	51.1
	24	70	51.5
2	0.5	70	49.1
	2	70	48.3
	4	70	48.5
	8	70	50.6
	24	70	50.3

Table 6. Urea reactivity measurement data of **41**. Measured by Babette Lentferink.

Sample	Time [h]	Temperature [°C]	Urea concentration [mM]
1	0.5	70	50.1
	1	70	50.5
	2	70	45.6
	4	70	49.1
	8	70	49.9
	24	70	49.2
2	0.5	70	47.6
	1	70	50.8
	2	70	43.5
	4	70	43.0
	8	70	50.2
	24	70	50.6

10.3. Urea reactivity measurement with cyclic phosphorous compounds.

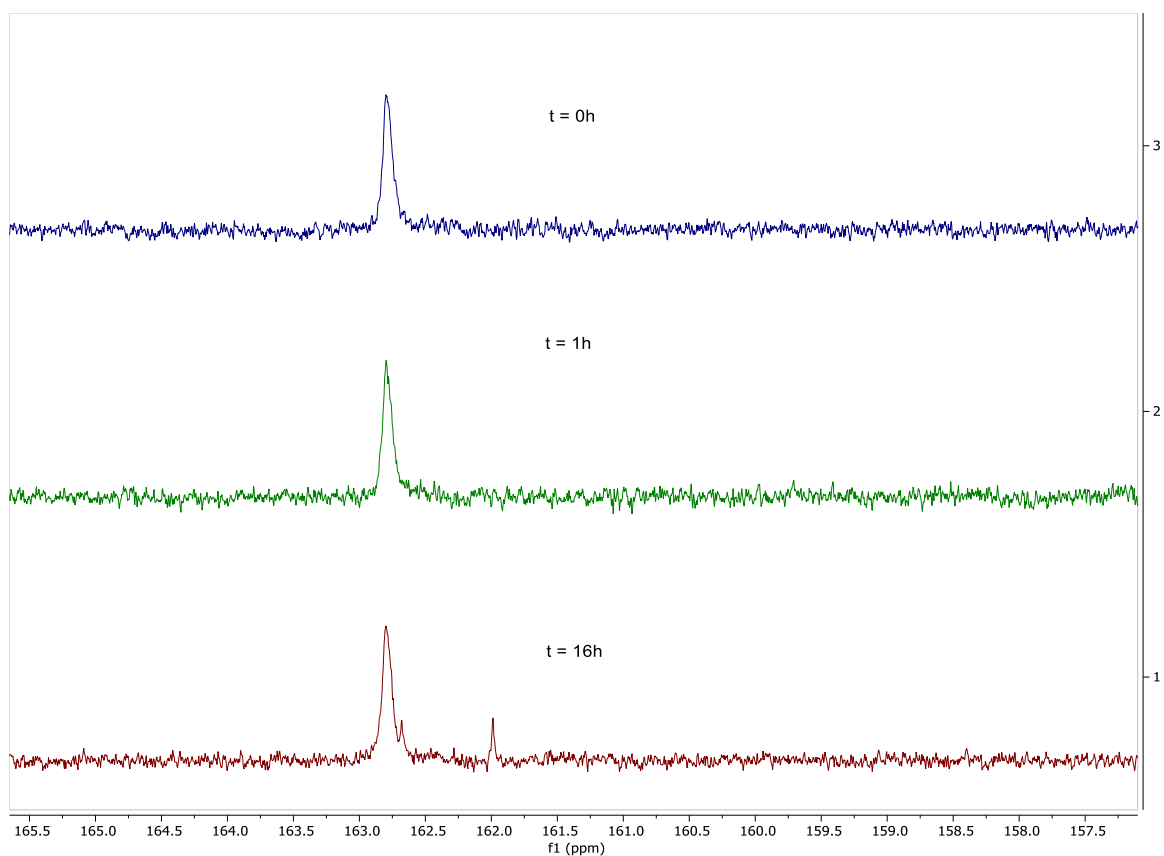


Figure 81. Urea reactivity measurement of phenylglyoxal with ^{13}C -labelled urea and 2.5 eq. sodium trimetaphosphate. The formation of a product peak can be observed at approx. 162 ppm after 16 hours. The measurement was done as described in 6.2.3.